UKD Universitätsklinikum Düsseldorf

HEINRICH HEINE UNIVERSITÄT DÜSSELDORF

Label-free detection of brain tumour cell immunogenicity upon mesenchymal transformation using Raman technology

Inaugural dissertation

for the attainment of the title of doctor
in the Faculty of Mathematics and Natural Sciences
at the Heinrich Heine University Düsseldorf

presented by

Julia Tsiampali

from Kozani, Greece

Düsseldorf, November 2020

from the Department of Neurosurgery of University Hospital Düsseldorf
at the Heinrich Heine University

Published by permission of the
Faculty of Mathematics and Natural Sciences at
Heinrich Heine University Düsseldorf

Supervisor: Prof. Dr. med. Jaroslaw Maciaczyk
Co-supervisor: Jun.-Prof. Dr. Ingrid Span

Date of the oral examination: 11/12/2020

Statutory declaration

“I declare under oath that I have produced my thesis independently and without any undue assistance by third parties under consideration of the ‘Principles for the Safeguarding of Good Scientific Practice at Heinrich Heine University Düsseldorf”.

Julia Tsiampali

Düsseldorf, 04/11/2020

Contents

Summary

Glioblastomas (GBMs) are the most aggressive primary brain tumours in adults and despite strong efforts current therapeutic options have limited impact on glioblastoma stem-like cells (GSCs). GSCs contribute to GBM's progression and chemoresistance and are enriched by epithelial mesenchymal transition (EMT). EMT has been recently correlated with CD73 that has emerged as an interesting target in the treatment of GBMs. However, the role of CD73 in GSC progression remains elusive. This work aims to investigate whether GSC enrichment is dependent on the enzymatic and/or the non-enzymatic activity of CD73 and further to investigate the impact of EMT activator ZEB1 and CD73 inhibition on GSC immunogenicity using Raman spectroscopy.

Chapter 2.1 studies the effect of CD73 inhibition on GSC growth. More specifically, it is shown that the effects on GSC proliferation and clonogenicity were independent from its enzymatic activity but dependent on the CD73 protein level. Selective inhibition of CD73 enzymatic activity by APCP inhibitor affects significantly only on the invasiveness of GSCs, indicating the involvement of adenosine signalling as one of the ways of the invasive regulation. Our results suggested that CD73 and the adenosine receptor A_3 are downstreams of EMT which would be helpful to monitor the invasive properties of GBMs and enhance the anti-EMT therapy.

Chapter 2.2 studies the ability of Raman spectroscopy to discriminate T-cells and monocytes with different phenotypes after incubation with media conditioned by GSCs with ZEB1 and CD73 inhibition. It is shown that discriminatory analysis using linear discriminant analysis (LDA) and support vector machine classification (SVM) yielded sensitivities and specificities of over 70 and 67% respectively upon validation against an independent test set. Principal component analysis (PCA) of the Raman spectra showed that T-cells and monocytes incubated with tumour-conditioned media of GSCs with inhibited ZEB1 and CD73 formed distinct clusters comparing to controls. To further evaluate the effect of ZEB1 and CD73 inhibition of GSCs on T-cells and monocytes flow cytometry analysis was performed and our data suggested that GSCs with ZEB1 and CD73 inhibition can actively influence the phenotype of T-cells and monocytes, explaining the clear separation of clusters in PCA scores of Raman spectra. These findings highlight the use of Raman spectroscopy for the detection of molecular differences in immune and cancer cells.

List of figures

1. Introduction

1.1 Glioblastomas

Glioblastoma (GBM) is the most common and aggressive primary malignant brain tumour that affects adults representing 55.4% of all glioma cases and 47.1% of all malignant central nervous system (CNS) tumours [1, 2]. The median overall survival after the diagnosis is less than two years, with a 2-year survival rate of only 26-33% [3, 4]. Current standard therapy includes maximal possible surgical resection, followed by combined radio-chemotherapy with the alkylating agent Temozolomide (TMZ) and tumour bed radiation [5, 6].

1.1.1 Classification of GBMs

There are two subgroups of GBMs, the primary and the secondary ones displaying unique molecular characteristics and biological features. Primary GBMs are at the vast majority isocitrate dehydrogenase 1 (IDH) wildtype and it is speculated that they can possibly develop *de novo* from transformed neural stem cells or neural progenitor cells. It predominates in patients over 55 years of age [7]. Secondary GBMs are mostly IDH mutant and develop due to the malignant progression of lower grade lesions such as WHO grade II astrocytomas to grade III and in the end to grade IV [7]. Secondary GBMs preferentially arise in younger patients.

According to the molecular classification based on genetic alterations, GBMs are classified into proneural, neural, classical and mesenschymal transcriptional subtypes [8]. Their classification is based on the expression of prolife genes including epidermal growth factor receptor (*EGFR*), neurofilament light (*NEFL*), γ-aminobutyric acid type A receptor alpha-1 subunit (*GABRA1*) and tumour protein 53 (*TP53*). Proneural subtype is characterized by mutations in *IDH1*, *TP53* and platelet derived growth factor receptor alpha (*PDGFRA*) and the patients identified with mutations in these two genes tend to be much younger comparing to the other groups [9]. Neural subtype exhibits expression of neuron markers including *NEFL*, *GABRA1*, synaptotagmin-1 (*SYT1*) and solute carrier family 12 member 5 (*SLC12A5*). The GBM patients with the neural subtype are usually elderly people [10]. The features of the classical subtype include high rates of EGFR alteration as well as lack of *P53* mutation. Mesenchymal subtype is predominantly characterized by *NFI* mutation and it is often accompanied by phosphatase and tensin homolog (*PTEN*) and *TP53* mutations [8]. Interestingly, it has recently been shown that human mesenchymal GBMs were characterized by an increased immune cell presence compared to proneural and classical tumours [11].

1.1.2 Diagnostics

For the presence of GBM, magnetic resonance imaging (MRI), computerized tomography (CT) and positron emission tomography (PET) scans are used in order to produce detailed images of the brain leasion. MRI scan allows to detect accurately high-grade tumours and to distinguish them from normal brain tissue [12]. PET nuclear medicine method provides an insight into the metabolic activity of the examined tissue using radioactively labelled amino acids. For example, it can be helpful in non-invasive grading and differential diagnosis [13]. Furthermore, MRI captures neither the diffusion nature of GBMs nor its intrinsic heterogeneity [14]. In recent years, Raman spectroscopy has been identified as potential modality that can identify the margins of the tumour intraoperatively [15]. Raman spectroscopy is a non-invasive technique that has been used as an alternative to more invasive diagnostic techniques such as biopsy [16].

1.1.3 GBM biology

The progression of GBM is considered to be a consequence of a complex series of molecular mechanisms including activation of oncogenes as well as alterations in tumour suppression genes. These genetic alterations that coincide with progression to GBM include amplification of EGFR, deletion of CDKN2A and mutation or deletion of PTEN [17]. A successful treatment of GBM requires the understanding and the definition of several challenges. These challenges include overcoming the resistant cancer stem cells (CSCs), their interactions with the tumour microenvironment (TME) and the tumour heterogeneity of GBM. GBM cells of an individual tumour may differ in their morphology, genetics and biological behaviour [18]. This heterogeneity is one of the challenges the treatment faces, as some of the tumour cells within an individual tumour may respond differently than other cells to a specific therapy. Although GBMs rarely metastasise outside the brain via haematological and lymphatic vessels, their local invasiveness through normal brain tissue remains one of the main challenges for more effective treatment [19].

1.1.3.1 GBM stem-cells

The GBM's TME is very heterogeneous and it can promote tumour cell growth and the selection of aggressive cells [20]. This subpopulation of GBM cells, known as brain tumour stem-cells (BTSCs), have been identified in many types of cancer including GBM [21]. BTSCs are multipotent and they can trigger tumour initiation. Furthermore, these cells are considered to be responsible for radio- and chemo-resistance, recurrence as well as metastatic and invasive properties of GBMs [21-23]. In brain tumours, CSCs have exhibited characteristics similar to the normal stem or progenitor cells of the tissues of origin, such as expression of CD133 and Nestin [24]. There is recent evidence indicating that the

heterogeneity in GBM that is correlated with the stem-cell phenotype results from intrinsic cancer cell plasticity [25].

1.1.3.2 Epithelial-mesenchymal-like transition in GBMs

A multi-step molecular reprogramming process entitled epithelial to mesenchymal-like (EMT-like) transition controls GBM cell invasion [26]. EMT has been first described in embryonic development and its transcription factors are specialised to coordinate every step of this mechanism [27, 28]. During EMT the cells are undergoing morphological and biochemical changes that allow them to lose their tight connections and interaction with the basement membrane. The cells then obtain a mesenchymal phenotype with high invasiveness and migratory capacities [29]. Even though GBMs lack the epithelial background, the key factors of EMT are involved in increased tumour cell invasion, apoptosis resistance, cell dissemination as well as chemo-resistance [26, 30-32]. The transcription factors orchestrating EMT are the ZEB-, TWIST- and SNAIL-families [33]. The ZEB1 has been described as a key player for metastasis and tumour initiation and it is an important candidate molecule for recurrence of GBM as well as a potential therapeutic target [34-36].

1.2 Immune responses

The immune system is generally divided into two branches; the innate and the adaptive immunity. The first lines of defence include physical and chemical barriers of the innate immune system which help to immediately detect and destroy pathogens with common features. Adaptive immunity can further be divided into humoral and cell-mediated immunity. Innate and adaptive immunity can differ in the timing and duration as well as on the specificity of the response. More importantly, they have different immune cells and mechanisms for the antigen recognition that are involved.

1.2.1 Innate immunity

The innate immune response is composed of phagocytes such as neutrophils, monocytes, macrophages (MΦs), dendritic cells (DCs) and non-cellular components. The cells of the innate immunity play a crucial role in detection and elimination of the pathogens through phagocytosis and the initiation of inflammation. Inflammation is initiated when the innate immune system recognizes common molecular structures of pathogens through pattern recognition receptors (PRRs), such as toll-like receptors (TLRs) and nod-like receptors (NLRs) [37, 38]. The activation of PRRs stimulates phagocytosis and inflammation by activating the gene expression, synthesis and secretion of molecules including cytokines, chemokines and immune receptors [38]. Therefore, the activation of PRRs initiates the early host response to infection and represents an important link to the adaptive immune response [39]. TLRs are type I transmembrane glycoproteins located at the cell surface (TLR1, 2, 4, 5, 6 and 10) or in

intracellular compartments (TLR3, 7, 8 and 9) [40]. TLRs are upstream of the myeloid differentiation factor 88 (MyD88)-dependent signalling pathway and the toll/interferon response factor (TRIF)-dependent signalling pathway, which induce secretion of pro-inflammatory cytokines and type I interferons (IFNs) [41].

Among the families of PRRs there are NLRs that have been identified as cytosolic sensors. NLR proteins are found in the cytoplasm and recognize pathogen products, dead cells, saturated fatty acid-crystals, potassium (K+) efflux and mitochondrial ROS [42, 43]. Inflammatory responses mediated either by NF-κB, MAPK or Caspase-1 activation are the results of NLR protein activation followed by secretion of pro-inflammatory cytokines [44]. Activation of most of the NLR family members results in the assembly of inflammasomes [45]. Inflammasomes are cytosolic molecular platforms that consist of a sensor protein the cytoplasmic NACHT leucine-rich repeat protein 1 (NLRP1), the adaptor molecule apoptosis-associated speck like protein containing a CARD (ASC) and the pro-inflammatory caspases 1 and 5 [46, 47]. Activation of the inflammasome results in the processing and secretion of the pro-inflammatory cytokine (interleukin-1β) IL-1β and pro-IL-18, regulating a pro-inflammatory response.

Most pathogens express on their surface highly conserved and repetitive molecular patterns known as pathogen-associated molecular patterns (PAMPs) [48]. Recognition of PAMPs occurs via PRRs and it initiates a cascade of events resulting in the induction of various inflammatory cytokines, chemokines and type I interferons [49]. The PRRs can also be activated by endogenous damage-associated molecular patterns (DAMPs). DAMPs represent endogenous danger signals as they are released upon cellular stress or tissue injury. This way, they induce potent inflammatory responses by activating the innate immune system during non-infectious inflammation [50].

1.2.1.1 Macrophages and dendritic cells

Monocytes are heterogeneous and represent a large pool of circulating precursors that can differentiate into MΦs and DCs. They play an important role in innate immune responses. They bridge innate and adaptive immunity by phagocytosing antigens and presenting them to B- and T-lymphocytes MΦs can clear the microenvironment of pathogens and antigens by engulfing them via PRRs. MΦs are also essential for development and tissue homeostasis as they can eradicate apoptotic cells and recycle nutrients by digesting waste products from tissues [51]. MΦs contain high levels of lysosomal proteases and rapidly degrade internalized proteins. MΦs can be divided into M1-type (classically activated) and M2-type (alternatively activated), depending on the activation state and functions [52]. M1 MΦs are classically activated by IFN-γ or lipopolysaccharide (LPS) and as a result produce pro-inflammatory cytokines. M1 MΦs produce nitric oxide (NO) or reactive oxygen intermediates (ROI) to protect the host against bacteria and viruses [53]. M2 MΦs are alternatively activated by exposure to cytokines such as IL-4, which can be produced by T-cells during an adaptive immune response or during an innate

immune response by granulates [52, 54]. M2 MΦs are associated with wound healing and tissue repair and produce either polyamines to induce proliferation or proline to induce collagen production [52]. Tumour-associated MΦs (TAMs) are considered to exhibit a M2 population-like profile as they share many functions and surface proteins [55].

DCs were first discovered by Steinman and Cohn in 1973 and are divided in four major populations: classical DCs (cDCs), plasmacytoid DCs (pDCs), Langerhans cells and monocyte-derived DCs [48, 56, 57]. DCs are part of the hematopoietic cell lineage in the bone marrow, from where they migrate to peripheral compartments via the bloodstream [58]. DCs have limited capacity for phagosomal degradation (limited lysosomal acidification and low expression of lysosomal proteases) comparing to MΦs, in order to be able to sustain antigen stability [59]. DCs play the essential role of antigen-presentation to T-cells through the major histocompatibility complex (MHC), therefore, representing a link between the innate and adaptive immunity [59]. When DCs reach their mature state, they present different morphological structures producing cytokines and presenting antigens to $CD4^+$ T-cells [56]. Most importantly, DCs can also present antigens to $CD8^+$ T-cells by cross-presenting exogenous antigens, therefore, they play a key role in generating anti-tumour immunity [60]. cDCs present antigen in secondary lymphoid organs, the lymph nodes and spleen. cDCs are short-lived and replaced by circulating classical dendritic cell precursors. pDCs are long-lived cells and they are present in both lymphoid and non-lymphoid organs. They are characterized by rapid production of type I against viral infections, but they can also present antigens to $CD4^+$ T-cells [61].

1.2.2 Adaptive immunity

The adaptive immune response is activated against specific pathogens or changed body cells and develops after days to weeks. The main characteristics of this immune response are memory and precision. Immunological memory is an important mechanism to rapidly recognize and eliminate pathogens in case of a secondary infection. The components of adaptive immunity are the antigen-specific lymphocytes that have antigen receptors on their surface and through these receptors they recognize and bind antigens [62]. These are the B lymphocytes (B-cells) and T lymphocytes (T-cells) that eliminate pathogens through secretion of antibodies and cytokines. T-cells are generated in the thymus and circulate throughout the body until they recognize their antigen on the surface of antigen presenting cells (APCs), such as DCs.

Once pathogens are phagocytosed by DCs or other APCs they are loaded onto MHC class I or II molecules. Immature DCs are activated by PAMPs and as a result migrate to secondary lymphoid organs, where they present antigens to naïve T-cells. Exogenous antigens are typically loaded onto MHC class II molecules via the endosomal pathway, whereas endogenous antigens are degraded in proteasomes and presented on MHC class I molecules [63]. Antigens presented on MHC class II molecules are recognized by T-cells expressing the cell-surface protein CD4 ($CD4^+$ T-cells) whereas

antigens transported to the cell surface onto MHC class I molecules interact with naïve T-cells expressing the cell-surface protein CD8 ($CD8^+$ T-cells) [64]. These cells consequently differentiate into effector and memory cells [65]. The T-cell receptor (TCR) on both $CD4^+$ helper T-cells and $CD8^+$ cytotoxic T-cells recognizes the peptide-MHC complex presented on the surface of DCs [66]. T-cell activation by DCs requires three signals. The first signal is the interaction between the MHC-antigen complex with the specific TCR. During the second signal activated DCs express a variety of activatory or inhibitory co-stimulatory molecules that bind to ligands on T-cells and provide essential stimuli for T-cell proliferation and survival [67]. The co-stimulatory interactions are CD80/CD28 and CD40/CD40L interactions, while co-inhibitory interactions are the programmed death-1 ligand (PD-L1) and receptor (PD-1), as well as ligand CD80 and its receptor cytotoxic T-lymphocyte-associated protein 4 (CTLA-4). Finally during the third signal a complex cytokine environment of cytokines, such as IL-12 and IFN-γ, is secreted by DCs and other surrounding activated cells, in order to trigger the differentiation of T-cells into effector cells is necessary (Figure 1.1) [67, 68].

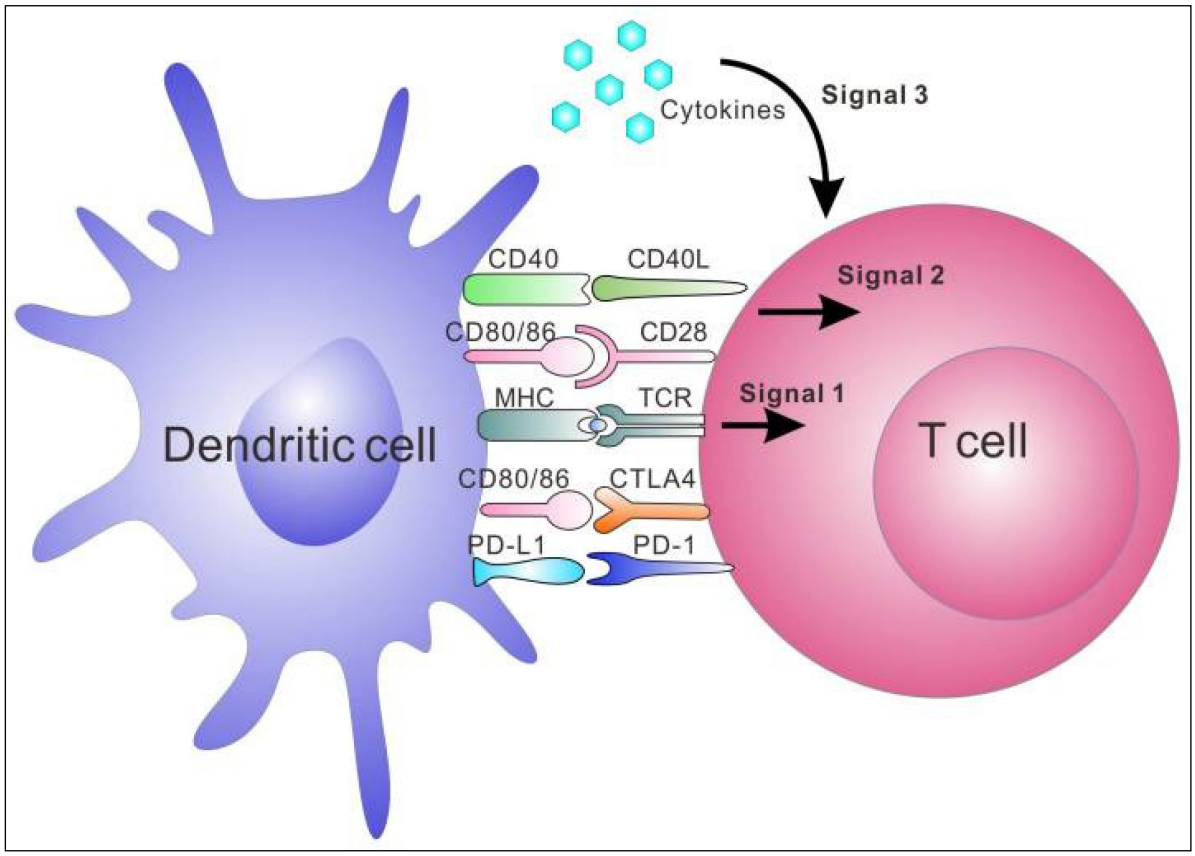

Figure 1.1 T-cell activation by DCs.

There are three signals necessary for T-cell activation/tolerance. DCs present antigenic peptides on MHC molecules to t-cells, which are then recognized via binding of the TCR (signal 1). Activatory or inhibitory molecules on DCs bind to counter-molecules on T-cells (signal 2).

Cytokines, essential for T-cell expansion and differentiation, are released (signal 3). From Wang et al., 2017 [69].

1.2.2.1 T-cells

$CD4^+$ T-cells together with $CD8^+$ T-cells represent the majority of T-lymphocytes. The first step of naïve $CD4^+$ T-cells differentiation is antigenic stimulation through the interaction of TCR and CD4, a glycoprotein, as co-receptor with antigen-MHC II complex of the APCs [70]. DCs are considered to be the most important APCs due to their enhanced ability to stimulate naïve T-cells [71]. $CD4^+$ T-cells are known as T helper (Th) cells due to their role in supporting other immune cells, such as B-cells and cytotoxic $CD8^+$ T-cells (CTLs), for an effective adaptive immune response. Depending on the signal received from DCs, naïve $CD4^+$ T-cells can differentiate into various Th cell subsets. Th cells interact with B-cells and CTLs, through the secretion of cytokines and via the expression of co-stimulatory molecules [72, 73]. $CD4^+$ T-cells differentiate into the following subsets: Th1, Th2, Th9, Th17, Th22, Treg (regulatory T-cells) and Tfh (follicular helper T-cells) [74]. The differentiation of naïve T-cells into Th1 is facilitated by IL-12 and IFN-γ; Th2 by IL-4; Treg by IL-10 and transforming growth factor-β (TGF-β); Th17 by IL-6 and TGF-β; Th9 by IL-4 and TGF-β [70, 75, 76].

$CD8^+$ T-cells, also known as CTLs, recognize antigens presented on MHC class I molecules by APCs and proliferate and differentiate into CTLs after receiving the co-stimulatory signal [77]. CTL effector cells display their cytolytic activity towards target cells by secreting cytotoxic granules, such as perforins and granzymes [78]. Cytotoxic granules are released against the target cell only after recognition of a specific antigen and co-stimulatory receptor, in order to avoid non-specific damage to healthy cells [79]. In addition, cytokines secreted by CTLs, such as TNF and IFN-γ that have antitumor and antiviral functions, trigger the differentiation of $CD4^+$ T-cells into Th1 cells, which will then drive the $CD8^+$ T-cell memory generation [80]. These memory $CD8^+$ T-cells will quickly proliferate and acquire CTL function in case of a secondary infection [78]. Another function of $CD8^+$ T-cells is to destroy the infected cells via Fas/FasL interaction [81].

1.3 The tumour microenvironment (TME)

In addition to cancer cells, the brain TME contains many different non-cancerous cells inside the tumour. These are normal and reactive astrocytes, GSCs, fibroblasts, immune cells, endothelial cells (ECs) and vascular pericytes [82]. It also includes proteins and non-protein biomolecules produced by all the cell types within the TME, which together support tumour growth. The TME in GBMs is characterised by extensive low tumour oxygenation, known as hypoxia, that triggers a complex of tumour cell responses. These responses facilitate migration and invasion of the surrounding parenchyma through activation of multiple molecular pathways such as Wnt/β-catenin, Hedegehog and TGF-β [83]. The expression of these genes changes through biding of hypoxia-inducible factor (HIF) to promoters

of genes containing HREs [84]. Hypoxia is a major problem for GBM patients, as it promotes tumour cell invasion into healthy brain tissue, in order to evade this adverse environment and it is associated with a more aggressive tumour phenotype [85, 86]. The majority of immune cells within brain tumours are tumour-associated macrophages and microglia (TAMs), which can represent 30-50% of the total tumour cell mass in human GBMs [87, 88]. TAMs derive either from the resident microglia and/or bone marrow-derived monocytes [89]. Besides TAMs, T-cells are also found in the GBM parenchyma, though in lower quantities [90].

1.3.1 GBMs immune evasion strategies

Tumours develop strategies to avoid detection and eradication by the immune system. This functional immunosuppression is achieved by modulating the recruitment, expansion and function of tumour-infiltrating leukocytes, such as immune-regulatory myeloid cells, Treg cells, Th17 cells and regulatory B-cells (Breg cells) [91]. The first mechanisms employed by GBM to evade the immune system is an anatomic one, represented by the blood-brain barrier (BBB) [92]. BBB restricts the entry of immune cells into the CNS due to the tight continuous junctions formed between ECs and their low pinocytotic activity [93]. In GBMs, the heterogeneity that characterises the tumour facilitates the immune evasion [94]. This heterogeneity is determined by genetic alterations, exhibiting different phenotypes both morphologically and physiologically, as well as non-genetic programs such as stemness features and interactions with the TME [95]. Therefore, the tumour cells express a wide variety of antigens that can be tumour-specific or tumour-associated [96]. In the TME of GBMs, immunosuppressive cytokines are secreted by tumour cells, microglia and TAMs. Microglia and GBM cells themselves secrete potent immunosuppressive factors, such as IL-6, IL-10, TGF-β and prostaglandin-E. These factors can inhibit T-cell growth, downregulate MHC II on APCs, induce Tregs and lead TAMs towards their M2 immunosuppressive phenotype. Furthermore, the immunosuppressive microenvironment of GBMs downregulates MHC expression and as a result compromises the antigen-presenting ability of microglia [97]. Another strategy for the GBMs to evade immunosurveillance is through the activation of immune checkpoint pathways, that inhibit immune responses against tumours by providing inhibitory signals to T-cells [98]. The most well-studied immune checkpoint molecule involved in GBM immune evasion is PD-L1, which can be induced by microglia and TAMs, that suppresses cytotoxic T-cell proliferation and function and activates Tregs by binding to PD-1 [99, 100]. Microglia and TAMs can also express PD-L1 on their surface [101]. CTLA-4 is another important immune checkpoint molecule, expressed on activated T-cells and Tregs, that interacts with its ligands CD80 and CD86 on APCs to inhibit co-stimulatory T-cell pathways [102]. Interestingly, it has been recently shown that GBM patients with lower CTLA-4 expression had significantly longer overall survival [103]. Additionally, the hypoxic TME activates the immunosuppressive signal transducer and activator of transcription 3 (STAT3) pathway, leading to HIF-1α synthesis. This synthesis subsequently triggers the activation of Tregs and

the production of vascular endothelial growth factor (VEGF) which can inhibit the maturation and function of DCs [92].

1.3.2 EMT status and immune response

The TME contains, apart from the tumour cells, several accessory cell types that can contribute to tumour growth. Such are the angiogenic vascular cells, infiltrating immune cells and cancer-associated fibroblasts [104]. Infiltrating immune cells are cells of both the native and the adaptive immune system. TAMs, subsets of granulocytes, myeloid-derived suppressor cells (MDSCs), DCs, NK cells and mast cells are examples of accessory cells of the innate immune system. The $CD4^+$ T-cells, $CD8^+$ T-cells, Tregs and B lymphocytes are examples of cells of the adaptive immune system, that can infiltrate the TME, leading to tumour associated inflammation [91]. Cancer cells interact in a dynamic crosstalk with immune cells and they exhibit EMT/MET plasticity, in order to adapt to the challenging environment of primary tumour, but also during metastasis [105]. The EMT status of the cancer cells has been described to impact cancer cells' immunogenicity by expressing immunomodulatory cytokines or immune checkpoint ligands affecting the efficacy of the immune response as well as its duration [106]. In lung cancer, the EMT regulatory axis miR-200/ZEB1 controls the T-cell activation repressor PD-L1 expression on tumour cells, even in the absence of IFN-γ, indicating that mesenchymal-like tumour cells are intrinsically capable of immune escape [107]. In breast cancer, it has been shown that tumours coming from more mesenchymal carcinoma cell lines, expressing EMT markers, exhibited low levels of MHC-I, high levels of PD-L1 while Treg cells, M2 MΦ and exhausted $CD8^+$ T-cells were detected in their stroma [108]. In melanoma, SNAIL-induced EMT promoted cancer metastasis through increased invasiveness as well as multiple immunosuppression and immune-resistance [109]. These mechanisms included immunosuppressive cytokines, Tregs, impaired DCs and CTL resistance.

1.4 Glioblastoma therapies

Maximal safe surgery is the initial therapeutic approach for GBMs. Chemoradiation followed by adjuvant TMZ remains the standard therapy for newly diagnosed GBM, but the survival remains poor due to the infiltrative nature of glioma cell towards adjacent tissues [110]. Therefore, new therapies are warranted. Since 2005 there have only been three new treatments approved for GBM including TMZ, bevacizumab and tumour-treating fields (TTFields). TTFields are low-intensity electric fields that target only rapidly dividing glioma cells notably during the phases of mitotic cell division [111]. New diagnostic schemes have been based on the molecular mechanisms of oncogenesis and the molecular subtypes of GBMs [112, 113]. During the past decade, understanding the molecular mechanisms and interactions between tumour cells and immune cells in the TME, has led to a new generation of immunotherapeutic strategies [114]. To date, there is no standard care established for recurrent or progressive GBMs [6].

1.4.1 Chemoradiation therapies

GBM therapy includes surgery followed by radiotherapy and adjuvant therapy with TMZ. The use of radiotherapy is to precisely increase the delivered dose to tumour while sparing normal brain and avoiding local necrosis [115]. TMZ is currently the only chemotherapeutic drug for GBM. Unlike other drugs, it is not completely blocked by the BBB and it has pharmacokinetic characteristics with high oral bioavailability [116]. After oral administration, TMZ is rapidly absorbed and undergoes spontaneous hydrolysis at physiological pH into its active metabolite, 5-(3-methyl triazen-1-yl)imidazole-4-carboxamide (MTIC) [117]. MTIC is directly degraded into methyldiazonium and into an inactive metabolite 5-aminoimidazole-4-carboxamide (AIC) that will finally be excreted by the kidney [117]. TMZ is a lipophilic alkylating agent prodrug with small molecular weight and it generates O6-methylguanine by adding a methyl group to O6-guanine [115]. O6-methylguanine pairs with thymine and results in a mismatch that causes cell death [118]. However, there are GBMs that express O6-methylguanine-DNA methyltransferase (MGMT), which repairs DNA mismatch, making them alkylator resistant. Epigenetic silencing of the MGMT DNA repair gene by promoter methylation compromises DNA repair and has been associated with longer survival in patients with GBM who receive alkylating agents [119, 120]. TMZ is less effective in GBMs lacking MGMT promoter methylation, resulting in a worse outcome for this group of patients [5]. Apart from the DNA interaction, TMZ's anticancer activity is mediated also through alterations of protein post-translational modifications by methylating histone H3 peptide and histone H3 protein [121]. Methylation of the DNA repair protein MGMT is frequent in high-grade glioblastomas but rare in low-grade gliomas [122].

1.4.2 Immunotherapies

In the past decade, exciting breakthroughs in novel immune strategies have been reported, especially the immune checkpoint inhibitors [102]. To date, there are no FDA-approved immune therapies for GBMs as its unique TME and distinctive immune system within the CNS remain a challenge. Current cancer immunotherapies include immune checkpoint inhibitors (ICIs), vaccines (DC and peptide vaccines), chimeric antigen receptor (CAR)-T-cell and viral therapy [123]. Viral therapy aims to increase the immunogenicity of the GBM TME, while oncolytic viruses destroy directly highly proliferative cancer cells and at the same time they trigger the innate immune system leading to cytokine release [124]. Two viral therapies, ASPECT and Toca5, have made it to phase III of the clinical trials [125]. ASPECT showed that patients treated with the virus had a prolongation time to death or re-intervention, however, there was no difference in median overall survival [126]. CAR-T-cell therapy is a newer therapy in oncology and it is currently approved in B-cell lymphoma and leukemia [127, 128]. For the CAR-T-cell therapy, autologous T-cells are collected from a patient's blood, modified so that the extracellular domains contain T-cell activation signal [129, 130]. Upon infusion of the CAR-T-cells

back into the patient, they can mediate targeted lysis of cancer cells that express the associated tumour antigen [129]. The tumour antigens that have been studied the most for CAR targets in GBM are IL-13Ra2, EGFRvIII and Her2 [131]. In DC vaccination monocytes that are isolated from the patient are then activated into immature DCs. Finally these DCs are matured and activated by the tumour lysate and injected back to patient [131]. In peptide vaccination, TAAs are isolated from tumour cells, artificially produced and processed into a HLA-matched vaccine and are finally injected to the patient [132]. The EGFRvIII-targeted vaccine called "rindopepimut" is the only vaccine therapy to have completed evaluation, but it did not display signs of improvement in patient survival rates, when provided with standard therapy in patients with newly diagnosed EGFRvIII mutant GBM [132].

1.4.2.1 Immune checkpoint inhibitors

ICIs represent a form of immunotherapies and they block inhibitory receptors and their ligands that are usually expressed by T-cells and myeloid cells [133]. The negative immune regulatory checkpoint proteins, responsible for the downregulation of T-cell activity, CTLA-4 and PD-1 (or its ligand, PD-L1), are the two major immunotherapy targets of ICIs with human monoclonal antibodies, such as ipilimumab, nivolumab and pembrolizumab [134, 135]. Checkmate 143 was the first phase III trial to evaluate the efficacy of nivolumab +/- ipilimumab comparing to VEGF-inhibitor bevacizumab in recurrent GBM [136]. Although nivolumab did not improve overall survival compared to bevacizumab alone, a small subset of patients did have a durable response, therefore, an analysis of their tumour biomarkers and immune responses could help guiding future trials [136]. Currently, there are several clinical trials of checkpoint inhibitors in combination with other therapies [125]. In this capacity, a large phase III randomized trial (NCT02667587) is testing the effect of nivolumab with TMZ and radiotherapy on MGMT methylated patients. The data of the overall survival is expected to be ready in 2022, despite the fact that the trial did not meet the first endpoint of the Progression-free survival (PFS) [98]. Unfortunately, GBM is a cancer type in which ICIs have not been successful so far.

The resistance of GBMs towards immunotherapy has been correlated with the low immunogenicity, immune privilege of the CNS and immunosuppressive TME [134]. In order to overcome these problems, researchers expanded the application of nanotechnology to enhance the efficacy of cancer immunotherapy [137]. For example, nanoparticles can selectively target IL-13 receptors to tumour cells, minimizing toxic side effects in the healthy tissues [138]. Furthermore, ongoing research is trying to identify new targets that activate or enhance the immune response against cancer cells. As such, the A_2 adenosine receptor (A_2AR) has emerged as an important checkpoint in cancer therapy due to the generation of high levels of immunosuppressive adenosine within the TME that supports immune evasion [139].

1.5 CD73 and extracellular adenosine signalling

Adenosine is an ATP-derived nucleoside, an important component of the nucleic acids DNA and RNA, that regulates a wide range of functions and mechanisms [140]. Adenosine is produced both intracellularly and extracellularly (Figure 1.2). Intracellularly, adenosine is produced from 5′-adenosine monophosphate (5′-AMP) via 5′-nucleotidase. Extracellular adenosine is also the product of the breakdown of precursor nucleotides, mainly from adenosine 5′-triphosphate (ATP) dephosphorylation. It can be further metabolized to inosine and hypoxanthine by the action of adenosine deaminase and to uric acid by xanthine oxidase. Intracellular adenosine can be transported out of the cell by specific bi-directional nucleoside transporters or it can be converted back to 5′-AMP via adenosine kinase and subsequently to ADP and ATP. The extracellular 5′-AMP is produced by degradation of ATP (by ecto-nucleotidase) and cyclic AMP (by ecto-cyclic AMP phosphodiesterase). Stressful conditions such as hypoxia or inflammation are associated with the release of ATP from the intracellular towards the extracellular compartment, leading to increased adenosine levels [141]. ATP is then converted via the ecto-nucleoside triphosphate diphosphohydrolase 1 (CD39) to adenosine monophosphate (AMP). Subsequently AMP is converted via the ecto-5′-nucleotidase (NT5E), also known as CD73, to adenosine. Extracellular adenosine acts as a signalling molecule, once it is released into the extracellular compartment of the cells and the adenosine receptors (ARs) are activated [142]. Inside the cell, adenosine is phosphorylated to AMP by adenosine kinase or degraded to inosine by adenosine deaminase [143]. Therefore, the levels of intracellular adenosine concentrations are maintained through a strict enzymatic control.

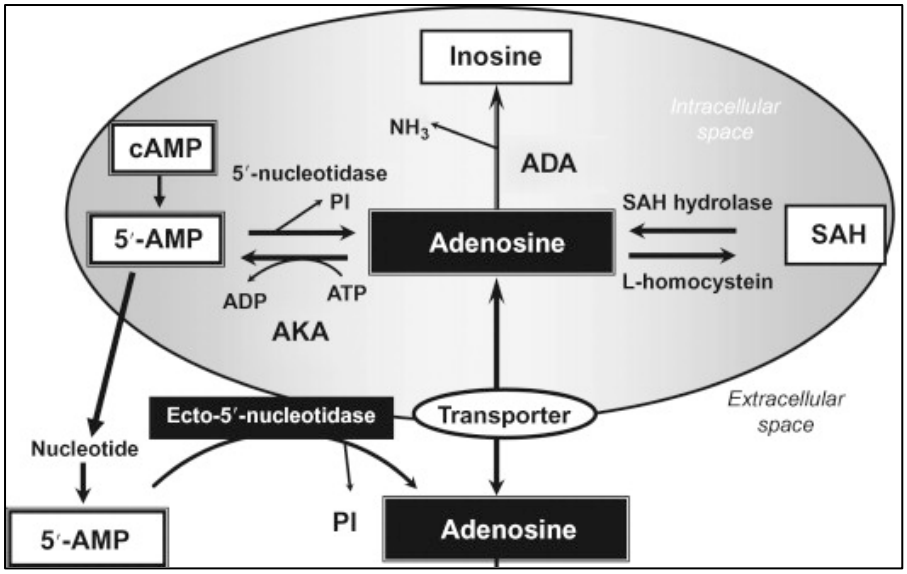

Figure 1.2. Adenosine formation and catabolism.

Adenosine is formed at both intracellular and extracellular sites by AMP and SAH and it is transported across cell membranes by adenosine transporters. After intracellular reuptake, adenosine is converted to AMP by AKA or catabolised to inosine by ADA. Abbreviations: ADA, adenosine deaminase; ADP, adenosine diphosphate; AKA, adenosine kinase; AMP, 5′-adenosine monophosphate; ATP, adenosine 5′-triphosphate; cAMP, cyclic AMP; SAH, S-adenosyl homocysteine. From Morelli et al., 2010 [144].

1.5.1 Purinergic signalling and adenosine receptors

During purinergic signalling, both ATP and adenosine act as extracellular signalling molecules [145]. There are four subtypes of P1 (adenosine) receptors (A_1, A_{2A}, A_{2B} and A_3), a class of purinergic and G protein-coupled receptors. These receptors are expressed by astrocytes, oligodendrocytes and microglia. Moreover, there are seven subtypes of P2X, that are ion channel receptors, expressed by neurons and astrocytes and eight subtypes of the P2Y G coupled to GTP-binding proteins [146]. ARs can differ in their affinity for adenosine, the type of G proteins they recruit and the downstream signalling pathways activated in the target cells [147]. A_1 and A_{2A} are high affinity (activation requires concentration of 0.3-3 nM and 20 nM respectively) whereas A_3 and A_{2B} are low affinity (requires an agonist concentration larger than 1 μM) ARs [148]. However, under hypoxia, the low affinity receptors can be activated by the increased adenosine levels [149]. Activation of ARs via specific agonist or antagonist can alter the proliferation of tumour cells [150].

A_1AR is the most conserved ARs subtype and it is highly expressed throughout the body and the highest levels are present in some CNS regions. It is known to be involved in anti-tumour activity of TAM cells to prevent the development of GBMs [151]. A_2ARs are present in both presynaptic and postsynaptic nerve terminals, mast cells, smooth muscles of human airways and also in the circulating leukocytes [152]. A_{2A}ARs are also found in cancers cells, such as melanoma, lung and breast cancer

cells and they have been correlated with tumour proliferation due to immunosuppression. The first results of A_{2A} receptor activation blockade showed an enhancement in anti-tumour immunity in mouse models [153]. Interestingly, it has been shown that blockade of the A_{2A}R together with CD73, has more potent anti-tumour activity than the blockade of either alone [154]. A_{2B}ARs have been reported with a wide distribution in the lungs, the bladder, the gastrointestinal tracts and the mast cells. Also, it has been found that A_{2B}ARs are overexpressed in various biopsies from patients with different cancers [155]. Furthermore, activation of A_{2B}ARs supported the migration and metastasis of tumour cells by inducing the EMT through activation of the ERK1/2 pathway [156, 157].

A_3ARs are highly expressed in lung and liver, while they are detected at lower density in kidney, testis, heart and the brain [143]. A_3AR is expressed at low levels in normal cells whereas the expression is upregulated in tumour cells [158]. In GBM samples it was reported that among the four ARs, only the expression of A_3AR was significantly upregulated [159]. Interestingly, it has been shown that extracellular adenosine promoted cell migration/invasion in GBMs through A_3AR activation under hypoxia [149]. Moreover, it has been demonstrated that its blockade has a chemosensitizing effect on GSCs [160].

1.5.2 Adenosine and regulation of immune response

The levels of adenosine as well as of ATP are normally very low in extracellular fluids [161]. Upon different conditions and diseases, such as inflammation and cancer, the levels of ATP can be increased through transporter or channel release or direct release through mechanical stress as well as via active vesicular exocytosis [162, 163]. Extracellular ATP can be recognised by immune cells, such as DCs and consequently immune responses are triggered through the activation of inflammasome and the secretion of IL-1β and IL-18 (Figure 1.3) [164]. As a result, NKs, MΦs and T-cells are activated and their proliferation is increased. However, upon inflammation, extracellular ATP is dephosphorylated by CD39 and CD73, leading to the production of high levels of adenosine that creates an immunosuppressive microenvironment [165, 166]. In this case, NKs, MΦs and T-cells uptake adenosine with A_{2A} or A_{2B} receptors leading to inhibition of T-cell proliferation and its cytokine production, decrease of DCs' cytotoxicity and finally inhibition of the T-cell activation by alternative activated MΦs [167].

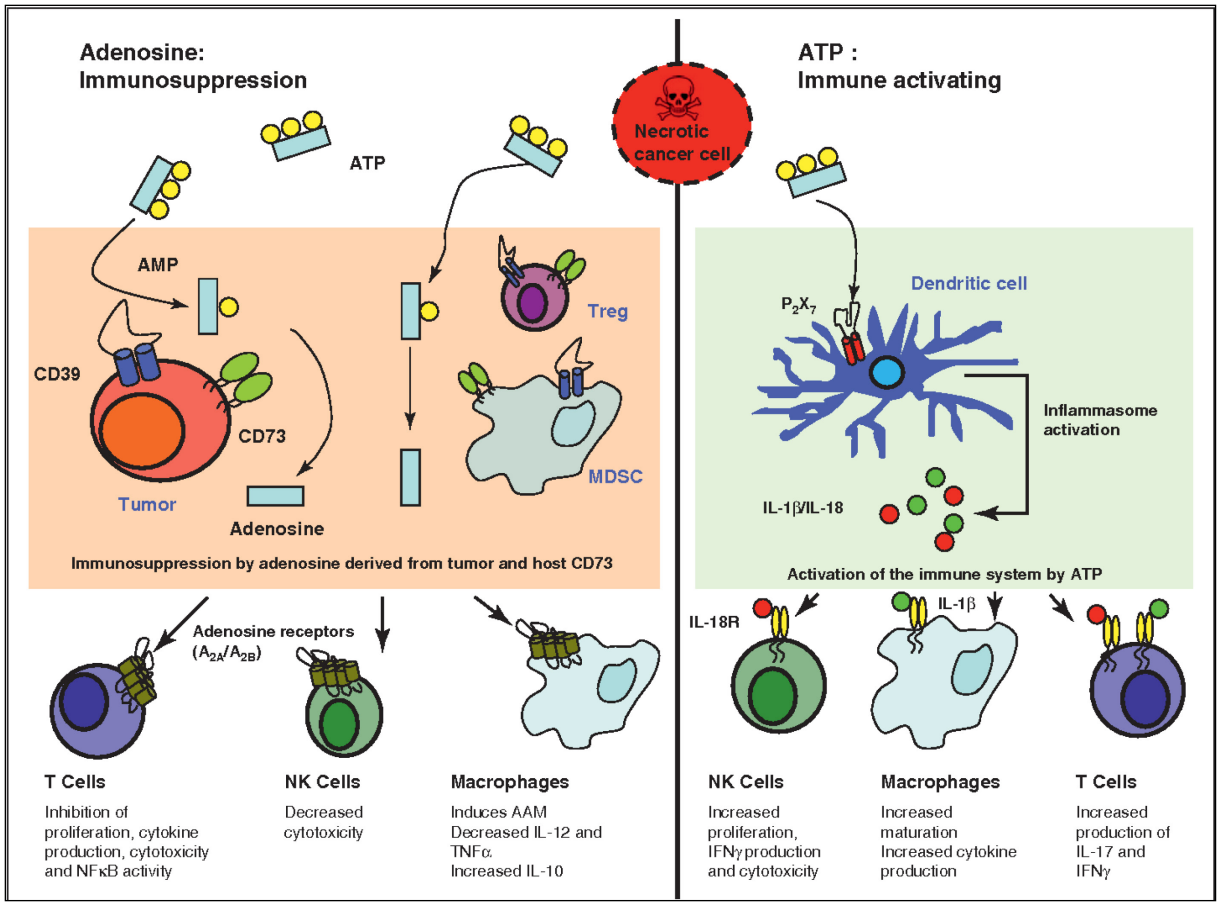

Figure 1.3. ATP immune activation and adenosine immunosuppression.

Extracellular adenosine, produced by the ecto-5′-nucleotidase CD73, causes immunosuppression through binding to the ARs of T-cells, NK cells and macrophages. ATP triggers immune activation via P2X7 receptor on DCs that consequently activate the inflammasome. Abbreviations: AAM, antigen-associated macrophages; AMP, 5′-adenosine monophosphate; ATP, adenosine 5′-triphosphate; IFN-γ, interferon γ; MDSC, myeloid-derived suppressor cells; NK cells, natural killer cells. From Beavis et al., 2012 [167].

1.5.3 CD73 biology and therapeutic potentials of CD73

CD73 is a glycosyl phosphatidylinositol (GPI)-anchored plasma membrane protein and it is expressed in various tissues, including the brain [168]. CD73 consists of two identical 70-kD subunits tethered by a non-covalent link created by its C-terminus (Figure 1.4) [169]. The N and C-terminal domains of CD73 are connected by an α helix, that gives CD73 the capacity to switch between an open and a closed conformation. This change in conformation allows CD73 to induce substrate binding and release during catalytic reactions [169]. A soluble form of CD73 can be shed from the membrane through the hydrolysis of the GPI-anchor and flows in the blood stream as well as other biological fluids maintaining the ecto-5′-nucleotidase activity [170, 171].

CD73 is overexpressed in many types of cancer including GBM [159]. Its expression is significantly influenced by hypoxia [172], other factors such as TGF-β1, IL-6, IFNs type I and Wnt signalling [173]. In various cancer types, CD73 expression has been positively associated with tumour growth, metastasis, angiogenesis, poor prognosis and resistance to chemotherapy [174-177] and it has both enzymatic and non-enzymatic functions in cancer progression [178, 179]. As a nucleotidase, CD73 catalyses the hydrolysis of AMP into adenosine and phosphate, while the extracellular adenosine production plays a master role in cancer immunosuppression, angiogenesis, cell proliferation and chemoresistance.

Along with its enzymatic activity, CD73 functions as a signal and adhesive molecule that controls the tumour cell-extracellular matrix interactions, which may mediate tumour invasion and metastasis [180]. In cervical cancer, CD73 promotes the proliferation and migration of the cells independent of its enzymatic activity [179]. In pancreatic ductal adenocarcinoma, CD73 was found to be upregulated and correlated with poor prognosis and its blockade induced G1 cell cycle arrest through AKT and ERK signalling pathways [181]. Interestingly, CD73 blockade increased sensitivity to TMZ in GBM by decreasing the IC50 value and sensitizing cells to non-cytotoxic drug concentration [174]. Furthermore, CD73 has also functional properties on immune cells such as B-cells, T-cells and NK cells [182]. Notably, in acute myeloid leukemia, CD73 expression on $CD8^+$ T-cells is associated with an increased immune response. Specifically, $CD73^+$ $CD8^+$ T-cells were more functional in contrast to $CD73^-$ $CD8^+$ T-cells that exhibited features of exhaustion alongside high expression of inhibitory receptors, such as PD-1 [183]. CD73's enzymatic activity can be inhibited by APCP (α,β-methylene ADP), a non-hydrolysable analogue of ADP, which is successfully evaluated *in vivo*, however, the efficacy of CD73 blockade was low and its *in vivo* half-life and bio-distribution is not well-understood so far [173]. Anti-CD73 mAbs are the new generation inhibitors that represent an alternative therapy with anti-tumour functions [184]. Recently, positive impact on immune system was reported by blocking CD39 and CD73 ecto-enzymes with mAbs, suggesting that clinical development of these mAbs can be beneficial especially in combination with other ICIs and chemotherapies [185]. All in all, CD73 serves as an essential regulator for the immunity and inflammation as well as for tumour progression and, therefore, it is an exciting target for cancer immunotherapy.

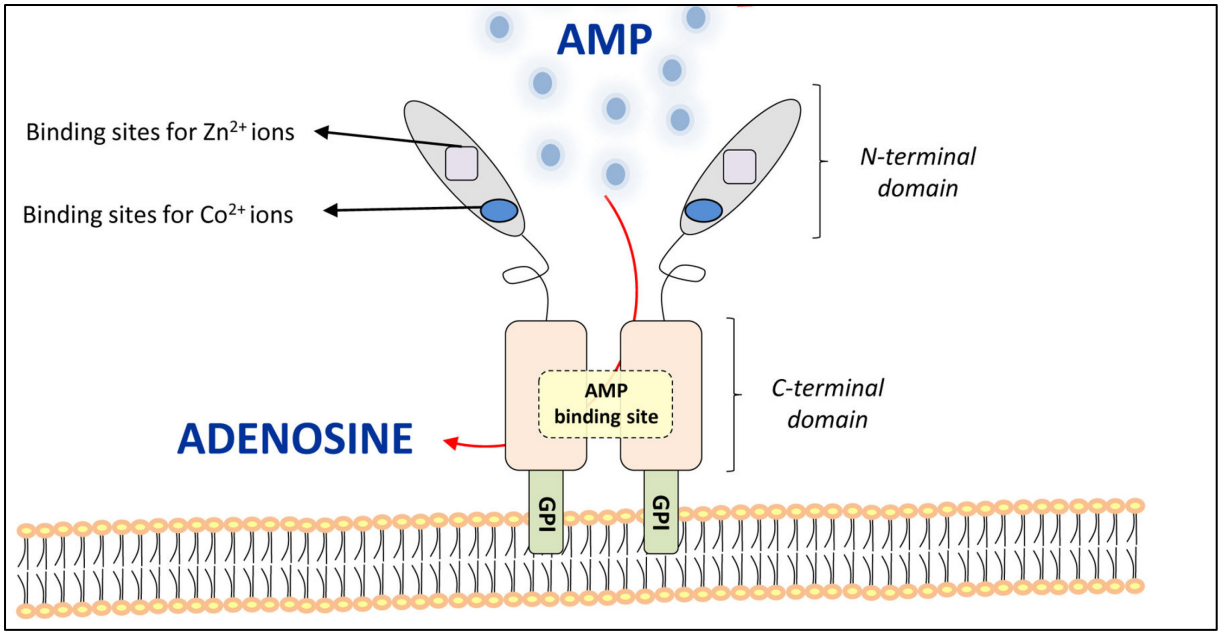

Figure 1.4. Structure of CD73.

Each subunit of the CD73 dimer consists of two structural domains: the N-terminal domain and the C-terminal domain. The N-terminal contains Zn^{2+} and Co^{2+} in their active sites. Abbreviations: GPI, glycosyl phosphatidylinositol. From Antonioli et al., 2016 [184].

1.6 Raman spectroscopy

Given the urgent need for the development of new techniques for cancer diagnosis as well as the intraoperative surgical guidance, Raman technology has been used to assess chemical compositions in cells and tissues [186]. Raman spectroscopy (RS) is a label-free analytical technique that provides sensitive, quantitative and chemically-specific information of a sample. RS principle is based on the interaction of light with the vibrational modes of common molecular bonds in a non-destructive way [187]. The Raman spectra are generated due to the interaction of the photons and the molecules by inelastic scattering [188]. A Raman spectrum shows the Raman intensity versus the Raman shift, which is the difference of frequencies between the Raman scattered and the incident light beam. Between the incident photon and the molecule, energy exchange can occur resulting into two types of Raman scattering; Stokes scattering when the molecule absorbs energy and anti-Stokes scattering when the molecule loses energy [189]. For every type of sample a distinctive spectral fingerprint is obtained, given its distinguished chemical composition and molecular structure [188].

1.6.1 Application of Raman spectroscopy

RS has been a useful tool in a variety of fields, including pharmaceuticals, *in vivo* biomedical studies and cancer diagnosis [190]. In this capacity, RS has been used for endoscopic diagnosis of gastric and

oesophageal cancers [191, 192]. Importantly, Raman-based technology has been applied to improve the accuracy of brain tumour surgery. First attempts of brain imaging were reported three decades ago, when analysing spontaneous Raman spectra for the detection of differences in the concentration of molecules [193]. Later studies have improved the technique and overcame the limitations. As such, near-infrared Fourier transform RS was developed aiming to evaluate low- and high-grade glioma, vestibular schwannoma and central neurocytoma. However, the challenge encountered was the indistinguishable spectra from grey matter [194]. The limitations of the spontaneous and the near-infrared Fourier transform RS overcame with the use of Confocal Raman spectroscopy (CRS), a RS with a confocal microscope, which has been used to obtain spectra with increased signal intensity [195]. CRS technology has two major forms, the Stokes Raman scattering (CARS) and the stimulated Raman scattering (SRS).

RS has been successfully used in GBM biopsy samples, in order to distinguish between vital tumour and necrotic tissue for real-time intraoperative brain biopsy guidance, as necrotic tissues have higher levels than cholesterol [196, 197]. The importance of maximum tumour resection during surgery was underlined, given the fact, that complete tumour resection is crucial for patient life expectancy [198]. Considering that current image modalities used in pre-surgical imaging, such as MRI, do not capture the diffuse nature of GBMs, Raman technology has been described as a tool that can identify the margins of the tumour intraoperatively [16]. RS was used intraoperatively during human GBM surgery to locate cancer tissue in order to target the biopsy locations [199]. Recently, RS has been also applied for the rapid, intraoperative, classification of gliomas by identifying the most common molecular genetic subtypes of diffuse glioma, the IDH1 mutations [200].

1.6.2 Imaging of cancer cells and immune cells

Most common spectral features of cells and tissues are caused by vibrational modes in lipid, protein and nucleic acid molecules [201]. Raman spectra of biological samples present the most important information about the molecules in the fingerprint spectral region [202]. However, spectral differences have also been identified in the region of high-wavenumber Raman spectra corresponding to CH stretching region (2820-3700 cm^{-1}) [203, 204]. A wide range of processes have been examined using RS including fundamental biological processes, such as cell death [205] and mRNA translation during differentiation of embryonic stem cells [206], the induction of double-stranded DNA breaks in dividing cells upon drug-induced apoptosis [207]. Furthermore, cell components have also been assessed by RS such as the nucleus, the endoplasmic reticulum, the Golgi apparatus and mitochondria [208]. Notably, in relation to cancer, RS has been used to characterize different stages in the progression of cancer cells due to their structural changes [209]. The Raman spectra features can present differences in variations in the band intensities and shifts in certain band positions [210, 211].

Most recently, evidence highlights that typical spectral pattern has also enabled to identify T-Lymphocyte subsets, NKs and DCs [212] and can distinguish between activated and non-activated immune cells [213]. RS has enabled the discrimination between $CD4^+$ and $CD8^+$ T-cells, monocytes and B-cells based on the differences of the Raman bands that are identified as CH_2 deformation in lipids (1455 cm^{-1}), adenine/guanine (1585 cm^{-1}) and amide I (1665 cm^{-1}) [214]. Moreover, characterization of classically M1 and alternatively M2 polarized monocyte-derived MΦs has been achieved using RS [215].

1.7 Aim of this work

Despite the research progress in the last decades, understanding how GSCs contribute to tumour progression and chemoresistance has been a challenge. GSCs' invasive properties have been associated with the EMT-like mechanism, that has been correlated with ecto-5'nucleiotidase CD73. It is known that CD73 is expressed in various tumour entities including GBMs and it has both enzymatic and non-enzymatic activities involved in tumour progression. In this respect, it is crucial to elucidate the role of enzymatic and non-enzymatic CD73 activity in GBM progression. The enzymatic activity of CD73 and the EMT-like mechanism have been shown to establish immunosuppressive phenotype in cancer. Therefore, the consequences of CD73 inhibition and EMT-like reprogramming on GBM immunogenicity were evaluated. Given the recent evidence, that RS can be used to detect immune cells, whether Raman scattering was used in order to detect glioma associated neuroinflammation.

This thesis comprises of studies using genetic and pharmacological inhibition of CD73 to identify it as potential target for novel anti-GSC therapies and it examines the label-free detection of GBM immunogenicity using Raman technology. This work is a cumulative thesis and comprises of two chapters of two publications.

Section 2.1 investigates the role of both enzymatic and non-enzymatic activity of CD73 on the maintenance of highly chemo-resistant glioblastoma stem-like cells through genetic interference and pharmacological inhibition. Furthermore, this section includes studies on the effect of pharmacological inhibition of A_3 adenosine receptor on GBM's progression.

Section 2.2 examines the use of Raman scattering for the label-free detection of the molecular signature alterations of GSCs upon ZEB1 and CD73 inhibition. Additionally, this section examines whether Raman technology would sufficiently discriminate alterations of monocytes and T-cells' spectra upon incubation with tumour-conditioned media of the genetically modified GSCs.

2. Publications

2.1 Enzymatic activity of CD73 modulates invasion of gliomas via epithelial-mesenchymal transition-like reprogramming

2.1.1 General Information

Title: **Enzymatic activity of CD73 modulates invasion of gliomas via epithelial-mesenchymal transition-like reprogramming**

Julia Tsiampali[1], Silke Neumann[2], Beatriz Giesen[3], Katharina Koch[1,4], Donata Maciaczyk[2], Christoph Janiak[3], Daniel Hänggi[1] and Jaroslaw Maciaczyk[5,6]

[1] *Neurosurgery Department, University Hospital Duesseldorf, 40225 Duesseldorf, Germany*
[2] *Department of Pathology, University of Otago, 9016 Dunedin, New Zealand*
[3] *Institute of Inorganic Chemistry and Structural Chemistry, Heinrich Heine University Duesseldorf, 40225 Duesseldorf, Germany*
[4] *IUF - Leibniz Research Institute for Environmental Medicine, 40225 Duesseldorf, Germany*
[5] *Department of Neurosurgery, University Hospital Bonn, 53179 Bonn, Germany*
[6] *Department of Surgical Sciences, University of Otago, 9016 Dunedin, New Zealand*

Corresponding Author

Jaroslaw Maciaczyk (Jaroslaw.Maciaczyk@ukbonn.de)

2.1.2 Abstract

Glioblastoma (GBM) is the most aggressive malignant primary brain tumour in adulthood. Despite strong research efforts current treatment options have limited impact on glioma stem-like cells (GSCs) which contribute to GBM formation, progression and chemoresistance. Invasive growth of GSCs is in part associated with epithelial-mesenchymal-like transition (EMT), a mechanism associated with CD73 in several cancers. Here we show that CD73 regulates the EMT activator SNAIL1 and further investigated the role of enzymatic and non-enzymatic CD73 activity in GBM progression. Reduction of CD73 protein resulted in significant suppression of GSC viability, proliferation and clonogenicity, whereas CD73 enzymatic activity exhibited negative effects only on GSC invasion involving impaired downstream adenosine (ADO) signalling. Furthermore, application of phosphodiesterase inhibitor Pentoxifylline a potent immunomodulator, effectively inhibited ZEB1 and CD73 expression and significantly decreased viability, clonogenicity and invasion of GSC *in vitro* cultures. Given the involvement of adenosine and A_3 adenosine receptor in GSC invasion, we investigated the effect of the pharmacological inhibition of A_3AR on GSC maintenance. Direct A_3AR inhibition promoted apoptotic cell death and impaired the clonogenicity of GSC cultures. Taken together, our data indicate that CD73 is an exciting novel target in GBM therapy. Moreover, pharmacological interference, resulting in disturbed ADO signalling, provides new opportunities to innovate GBM therapy.

Keywords: A_3AR, adenosine, CD73, drug targets epithelial-mesenchymal transition, glioblastoma

2.1.3 Introduction

GBM is the most common and most aggressive primary brain tumour with a very poor median overall survival of less than two years [4]. Current treatments for GBM include surgical resection of the tumour, followed by radiotherapy and chemotherapy with temozolomide (TMZ) [216]. A subpopulation of cells, GSCs, characterized by expression of neural stem cell markers and self-renewing capability, contribute to tumour insurgence, progression, recurrence and chemo-resistance [217, 218]. Given that GSCs are resistant to the standard-of-care treatment, refined therapeutic approaches targeting this particular subpopulation are needed.

Epithelial-to-mesenchymal-like transition (EMT) has been identified as one of the mechanisms that governs GBM cell dissemination, disease progression and relapse after treatment [26]. During the acquisition of mesenchymal properties, the cells lose their tight connections and become more invasive gaining stem-cell characteristics [30]. EMT-like changes seem to be crucial for tumour initiation, progression, invasion and therapy resistance in GBM [35]. The transcriptional factor Zinc Finger E-Box Binding Homeobox 1 (ZEB1) is one of the main activators of this molecular switch, together with ZEB2, SNAIL1/SNAIL2 and TWIST1 [31, 33, 219].

Most recently, an ecto-5'-nucleotidase (NT5E) known as CD73 has been shown to regulate EMT, both in ovarian and hepatocellular carcinoma [220, 221]. CD73 is a glycosylphosphatidylinositol anchored cell surface protein, which plays crucial roles in the regulation of adenosynergic signalling [222, 223]. CD73 possesses an enzymatic and non-enzymatic activity [224, 225]. As an enzyme, CD73 catalyses the conversion of adenosine mono phosphate (AMP) to adenosine (ADO) (Figure S1), which is involved in tumour immune escape [226]. In addition to its enzymatic activity, CD73 acts as an adhesive molecule by regulating cell interaction with extracellular matrix components [180, 227]. ADO is also an ubiquitous neuromodulator and upstream regulator of diverse brain functions [228]. It signals through four adenosine receptors (ARs): A_1 (A_1AR), A_2A (A_{2A}AR), A_2B (A_{2B}AR) and A_3 (A_3AR) [229]. Within the tumour microenvironment, high ADO concentrations activate its low affinity receptors A_3 and A_{2B} [230]. In GBM, extracellular ADO has been shown to promote the invasive capacity via A_3AR signalling and modulate EMT-like processes via both the A_3AR the A_{2B}AR [149, 231]. Therefore, CD73 has emerged as an interesting target in the treatment of GBM.

However, the role of the enzymatic and non-enzymatic function of CD73 in GBM progression has not been fully elucidated. Furthermore, it still remains to be clarified how CD73 activity affects the maintenance of highly aggressive and chemo-resistant GSCs. Therefore, we investigated the effect of CD73 modulation on GSCs growth and highlighted its potential as a novel therapeutic target for glioma therapy.

2.1.4 Results

CD73 is expressed in hypoxic areas of GBMs and affects EMT-like reprogramming

When investigating the location of CD73 expression, we found that CD73 was predominantly expressed in hypoxic regions of the brain (Figure 2.1a) such as the pseudopalisades and perinecrotic zone that contain high numbers of invasive cells [232]. Since ZEB1 is a pivotal regulator of EMT in these regions [233] we evaluated the effect of ZEB1 knockdown on CD73 expression. We found that ZEB1 knockdown was associated with a reduction of CD73 expression on the protein (Figure 2.1b) and mRNA level (Figure 1c).

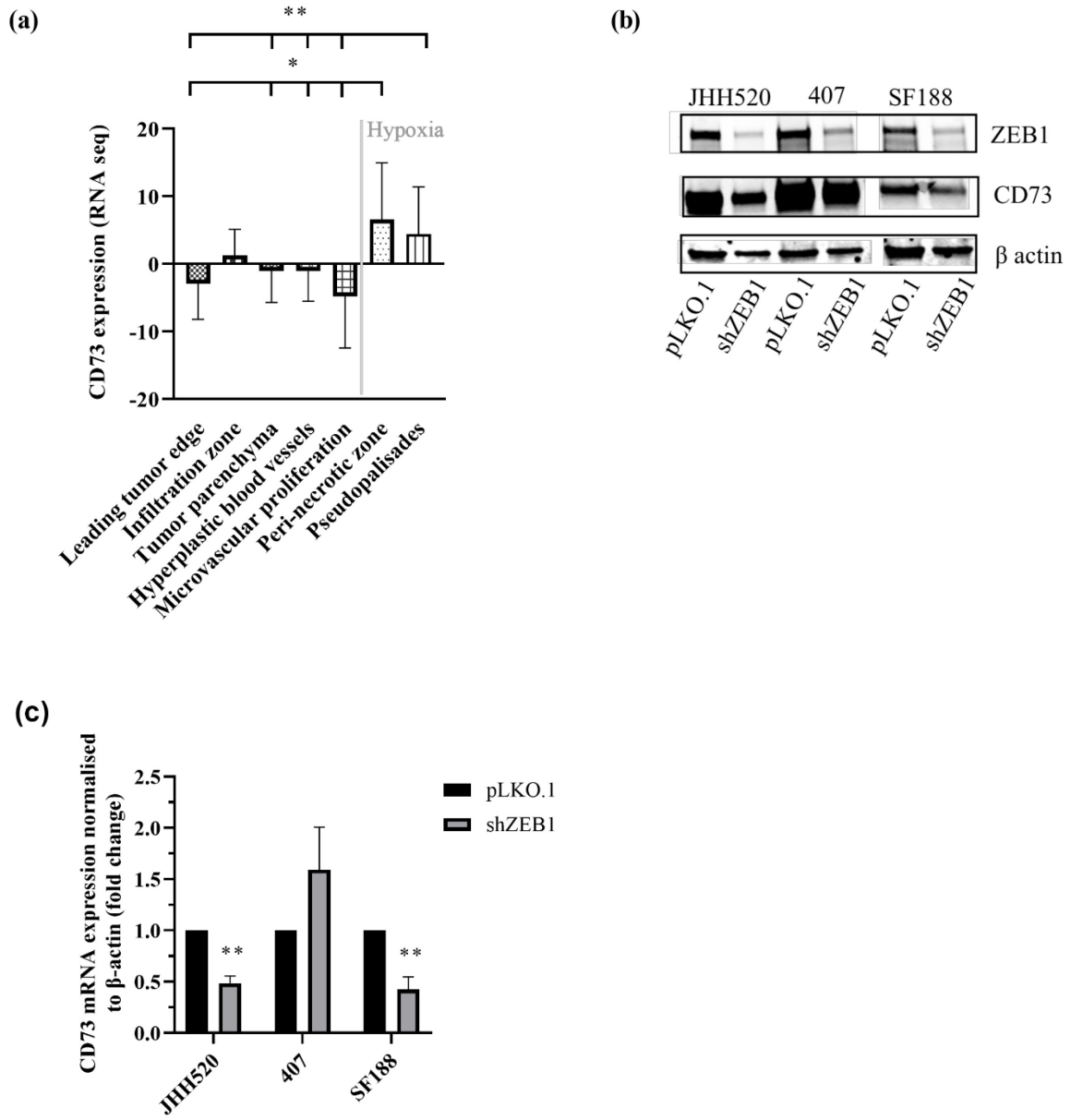

Figure 2.1. CD73 increases in hypoxia and is regulated by EMT

(a) mRNA expression data was retrieved from the IVY Glioblastoma project and analysed for CD73 expression (n=55 samples). CD73 mRNA was increased in the hypoxic pseudopalisades and peri-necrotic areas of GBM samples. Statistical significance was calculated with one way ANOVA. (b) CD73 protein levels upon ZEB1 knockdown were analysed in GSC lines JHH520, 407 and SF188 by western blotting (β-actin, loading control) (c). CD73 mRNA levels were analysed in three GSC lines and found to be decreased in two cell lines (JHH520 and SF188, $p < 0.001$) upon inhibition of ZEB1. Statistical significance was calculated with unpaired t-tests. Results are presented as mean ±SD of three independent experiments performed in triplicate. *$p<0.05$, **$p<0.001$.

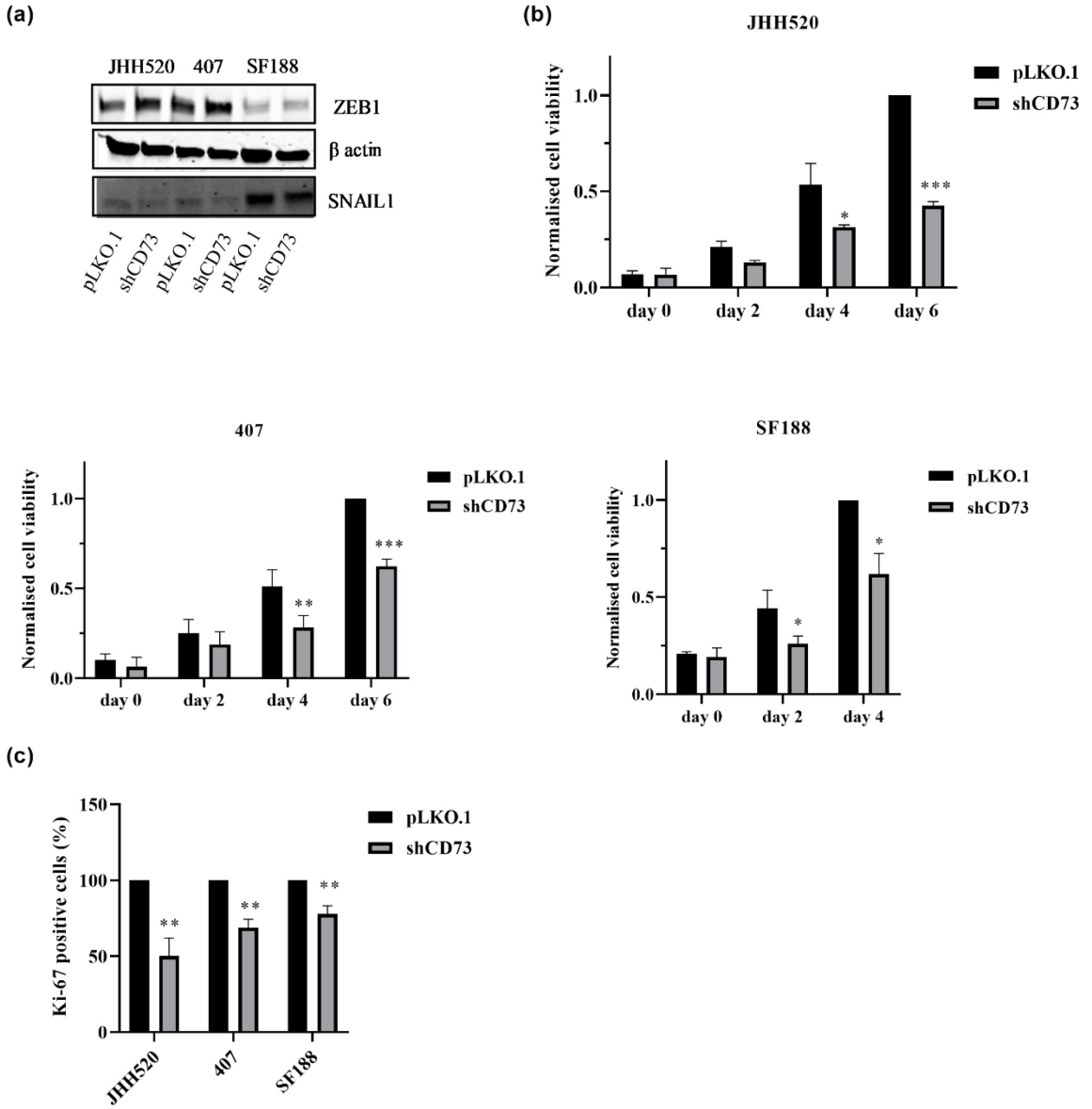

Figure 2.2. CD73 inhibition reduces the viability of GSC cultures and regulates EMT via SNAIL1 protein suppression

(a) SNAIL1 but not ZEB1 was affected by CD73 depletion as assessed by western blotting upon CD73 knockdown. (b) The cell viability and (c) proliferation in CD73 knockdown cells were reduced as compared to control cells (pLKO.1). Statistical significance was calculated with unpaired t-tests. The results are presented as mean ±SD of three independent experiments performed in triplicate. *$p < 0.05$, **$p < 0.005$, ***$p < 0.0001$.

CD73 inhibition reduces the viability, clonogenic and invasive capacities of GBMs

In order to analyse whether CD73 is involved in the maintenance of chemo-resistant GSCs, we established GSC-enriched *in vitro* cultures with suppressed expression of CD73 (JHH520, 407 and SF188) using RNA interference. The knockdown efficiency was confirmed on the mRNA (data not shown) and protein level (Figure 2.10a). When testing the effect of CD73 suppression on EMT activators, we found that CD73 suppression reduced the protein expression of the EMT activator SNAIL1 but not ZEB1 (Figure 2.2a). To investigate the biological effect of CD73 reduction, cell viability of CD73 knockdown and control cells was assessed. CD73 knockdown decreased the viability of all three tested GSC lines (Figure 2.2b, $p < 0.05$). Furthermore, we tested the effect of the CD73 knockdown on the proliferation of all three cell lines by Ki-67 staining, which is a marker of cell cycle progression [234]. Ki-67 was decreased in CD73 knockdown cells indicating a reduced proliferation rate (Figure 2.2c, $p < 0.002$). Similarly, the clonogenic capacity of GSCs was reduced by more than 50% upon CD73 inhibition (Figure 2.3a). Moreover, we tested the invasive properties after CD73 depletion using a modified Boyden chamber assay. We found that CD73 knockdown decreased the number of invading cells by at least 50% in all three cell lines tested (Figure 2.3b). In addition, analysis of matrixmetalloproteinase-2 (MMP-2, an enzyme involved in tumour invasion) mRNA expression showed significantly decreased MMP-2 mRNA transcription upon CD73 inhibition (Figure 2.3c, $p < 0.001$).

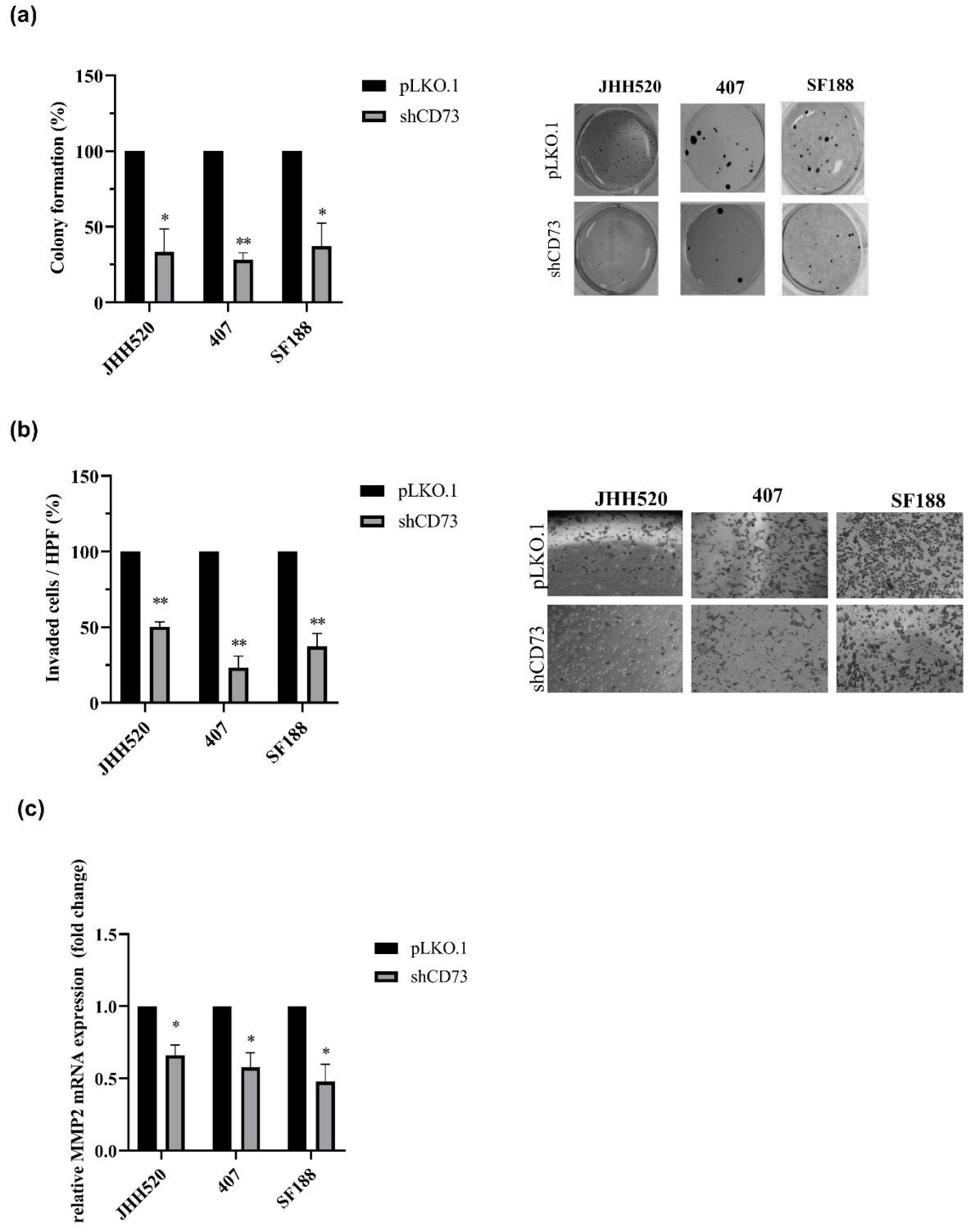

Figure 2.3. CD73 inhibition reduces clonogenicity and invasion of GSC cultures

(a) Knockdown of CD73 reduced colony formation of JHH520, 407 and SF188 cells as assessed by soft agar assays. (b) CD73 suppression decreased the number of invasive cells after 24 h (c) and MMP2 mRNA expression levels compared to control (pLKO.1). Abbreviations: HPF, high

power field. Statistical significance was calculated with unpaired t-tests. The results are presented as mean ±SD of three independent experiments performed in triplicate. *$p < 0.005$, **$p < 0.001$.

The enzymatic activity of CD73 promotes the invasive properties of GSCs

To investigate whether the enzymatic or non-enzymatic activity of CD73 is responsible for maintaining stem-cell characteristics of GSC cultures, we measured changes in the conversion of AMP to ADO upon genetic and pharmacological inhibition of CD73 using HPLC. Further data about the method used and exemplary chromatograms can be found in the Supplementary (Figure 2.8). Reduction of CD73 protein expression led to a decrease of AMP conversion by the cells (Figure 2.4a, $p < 0.001$ for SF188). The pharmacological inhibitor of CD73 enzymatic activity, APCP (10 μM), completely blocked the conversion of AMP to ADO (Figure 2.4a, $p < 0.0001$). In concordance with the CD73 knockdown, it reduced expression of the EMT factor SNAIL1 (Figure 2.4b).

Aiming to determine the role of CD73 enzymatic activity in glioma progression, all three GSC lines were treated with increasing concentrations of the APCP (1-50 μM). The cell viability was evaluated after 2, 4 and 6 days of treatment. Inhibition of CD73 enzymatic activity did not affect the survival of glioma neurospheres (Figure 2.22a). Similarly, inhibition of the enzymatic activity did not reduce the proliferation of GBMs (Figure 2.4c). Moreover, treatment with APCP did not change the clonogenic properties of the tested cell lines 407 and SF188 and it even slightly increased the clonogenic properties of JHH520 by 11. 6% (Figure 2.9c). In contrast, the enzymatic activity of CD73 was crucial for the invasive properties of GSCs (Figure 2.4d). Furthermore, addition of extracellular ADO effectively restored the reduced invasive capacity of glioma cells upon APCP treatment (Figure 2.4d). Taken together, our results indicate that CD73 regulates the invasiveness of GBMs via its enzymatic activity and downstream ADO signalling.

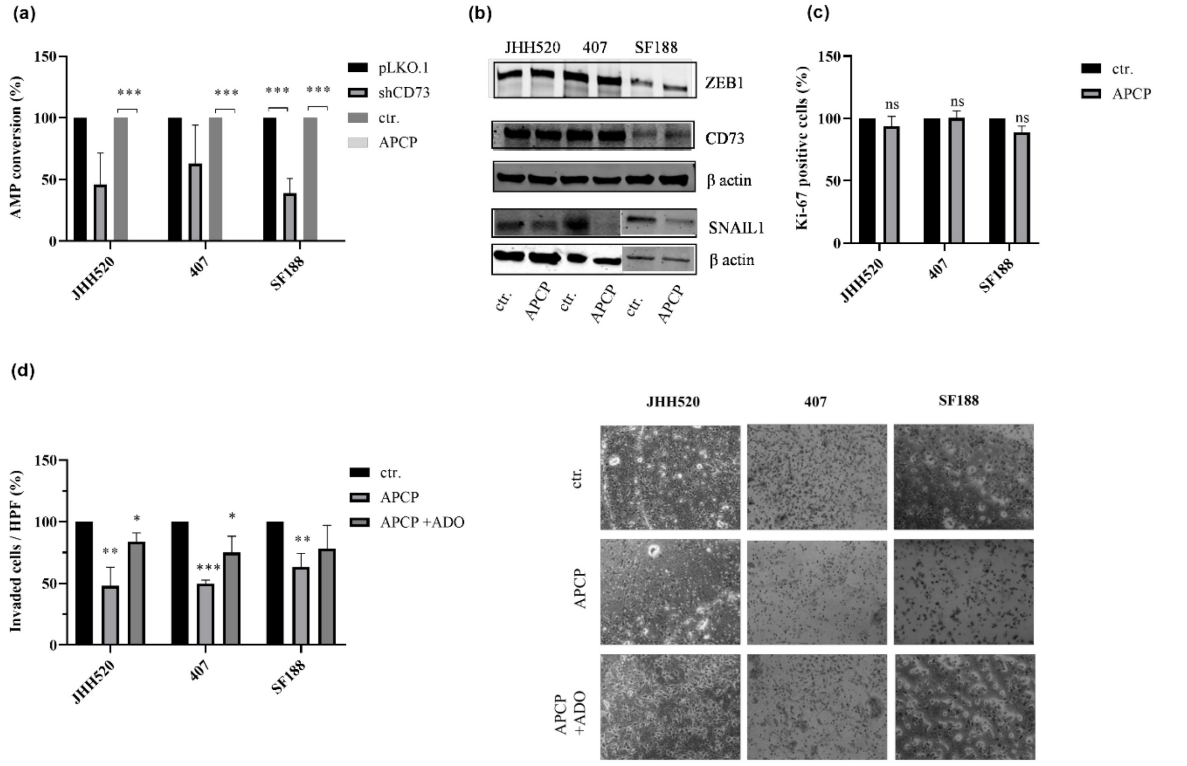

Figure 2.4. CD73 enzymatic activity does not affect GSC proliferation but reduces their invasive properties

(a) The percentage (%) of AMP conversion was measured in empty vector control (pLKO.1) cells, in CD73 knockdown (shCD73) cells, in wild type control (ctr.) cells and 10 μM APCP-treated (APCP) control cells. (b) ZEB1 and SNAIL1 protein expression levels were determined using immunoblotting in APCP (10 μM) for 24 h and untreated control cells (ctr.) (β-actin, loading control). Representative blots are shown. (c) The percentage of the Ki-67 positive cells upon treatment with APCP was not significantly decreased compared with untreated control cells (ctr.). (d) Inhibition of CD73 enzymatic activity with APCP significantly decreased the number of invaded cells after 24 h when compared with untreated cells (ctr.). Addition of 10 μM adenosine (ADO) restored the invasive capacity of APCP-treated cells. Abbreviations: HPF, high power field; ns, not significant. Statistical significance was calculated with unpaired t-tests. Results are presented as mean ±SD of three independent experiments performed in triplicate. *$p < 0.05$, **$p < 0.005$, ***$p < 0.001$.

The phosphodiesterase inhibitor Pentoxifylline supresses ZEB1 and CD73 expression in GSC cultures

The clinically approved compound pentoxifylline (PTX), that is clinically used as vasodilator to increase blood flow and tissue oxygenation [235], has been reported to inhibit dephosphorylation of AMP to ADO via inhibition of 5′-nucleotidase [236]. In addition, due to its properties as a phosphodiesterase inhibitor, PTX increases intracellular levels of the second messenger cyclic adenosine monophosphate (cAMP) that can affect the EMT mechanism [237, 238]. Therefore, we were interested in assessing the effect of this drug on the growth of investigated GSC cultures and ZEB1 protein expression. Treatment with PTX (1 mM for JHH520 and 2 mM for 407 and SF188) decreased the viability of GBMs (Figure 2.5a) and reduced their proliferation (Figure 2.5b). Furthermore, the clonogenic and invasive capacities of GSCs were significantly decreased following PTX treatment (Figure 2.5c-d, $p < 0.0001$). Treatment with PTX (1 mM for JHH520 and 2 mM for 407 and SF188) inhibited ZEB1 and CD73 expression (Figure 2.5e). These data support the use of PTX for targeting GBMs.

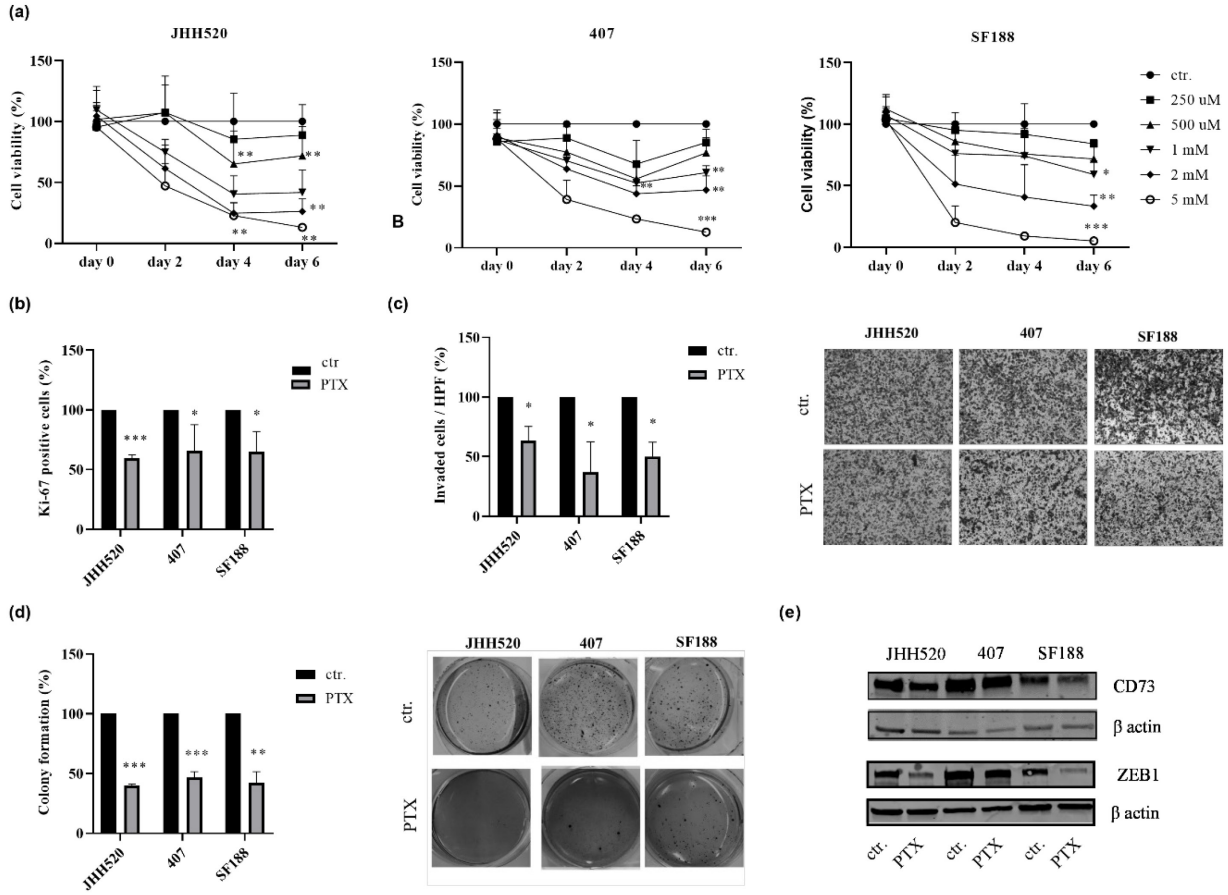

Figure 2.5 PTX inhibits ZEB1 and CD73 expression and reduces the viability of GSCs

(a) GSC lines (JHH520, 407 and SF188) were treated with increasing concentrations of PTX (250 µM - 5 mM) and the percentage (%) of cell viability was assessed comparing to control (ctr.). (b) The percentage of Ki-67 positive cells was reduced in the PTX treated cells (JHH520 1 mM, 407 and SF188 2 mM) compared to untreated cells (ctr.). (c) The invasive capacity of GSCs was also significantly decreased upon PTX treatment (JHH520 1 mM, 407 and SF188 2 mM) cells (ctr.). (d) The clonogenic capacity of cells was assessed by soft agar assays. Treatment with PTX led to a fewer colony formation (JHH520 1 mM, 407 and SF188 2 mM) as compared to untreated cells (ctr.) (e) Lower ZEB1 and CD73 protein expression levels were detected using immunoblotting in PTX treated cells compared to the control cells (ctr.). Abbreviations: HPF, high power field. Statistical significance was calculated with unpaired t-tests. Results are depicted as mean ±SD of three independent experiments performed in triplicate. *$p < 0.005$, **$p < 0.001$, ***$p < 0.0001$.

Pharmacological inhibition of the A_3A receptor effectively targets GSCs

ADO, the product of CD73 enzymatic activity has been shown to promote cell invasion in GSCs via A_3AR [149]. To evaluate the role of A_3AR in GBM growth and EMT modulation, we treated the GSC cultures with the A_3AR antagonist MRS1220. Treatment with increasing concentrations of MRS1220 led to decreased survival (Figure 2.10b, $p < 0.001$). It was further associated with apoptosis as assessed by an increase in cell numbers staining positive for Annexin V (+) and 7-AAD (−) indicating early apoptotic cells and the late apoptotic cells Annexin V (+) and 7-AAD (+) as compared to untreated cells (Figure 2.6a, $p < 0.05$). Furthermore, treatment with MRS1220 decreased the clonogenic and invasive capacities of the glioma cells (Figure 2.6b-c, $p < 0.005$ and $p < 0.05$, respectively). Next, we investigated whether the A_3AR could be the main ADO receptor responsible for GBMs invasive capacities. Therefore, GSCs were treated with the A_3AR antagonist MRS1220 with or without the addition of the inhibitor of CD73 enzymatic activity APCP and ADO. We found that the A_3AR antagonist MRS1220 did not decrease the number of invading cells at the presence of 10 μM APCP and 10 μM ADO when compared with vehicle treated cells (DMSO). However, in paediatric GBM cell line SF188 adding MRS1220 to APCP and ADO significantly decreased the invasion of the cells (Figure 2.6b, $p < 0.005$). To investigate the effect of A_3AR blockade on EMT, we tested the protein expression of EMT markers after treatment with the A_3AR inhibitor MRS1220. We found that blockade of A_3AR reduced ZEB1 expression (Figure 2.6d). Interestingly, blockade of A_3AR decreased both CD73 and SNAIL1 protein expressions in 407. However, the effect of A_3AR blockade on CD73 and SNAIL1 was variable and no common features could be found in the tested cultures (Figure 2.6d). Furthermore, EMT modulation led to a decrease of A_3AR protein expression (Figure 2.6e).

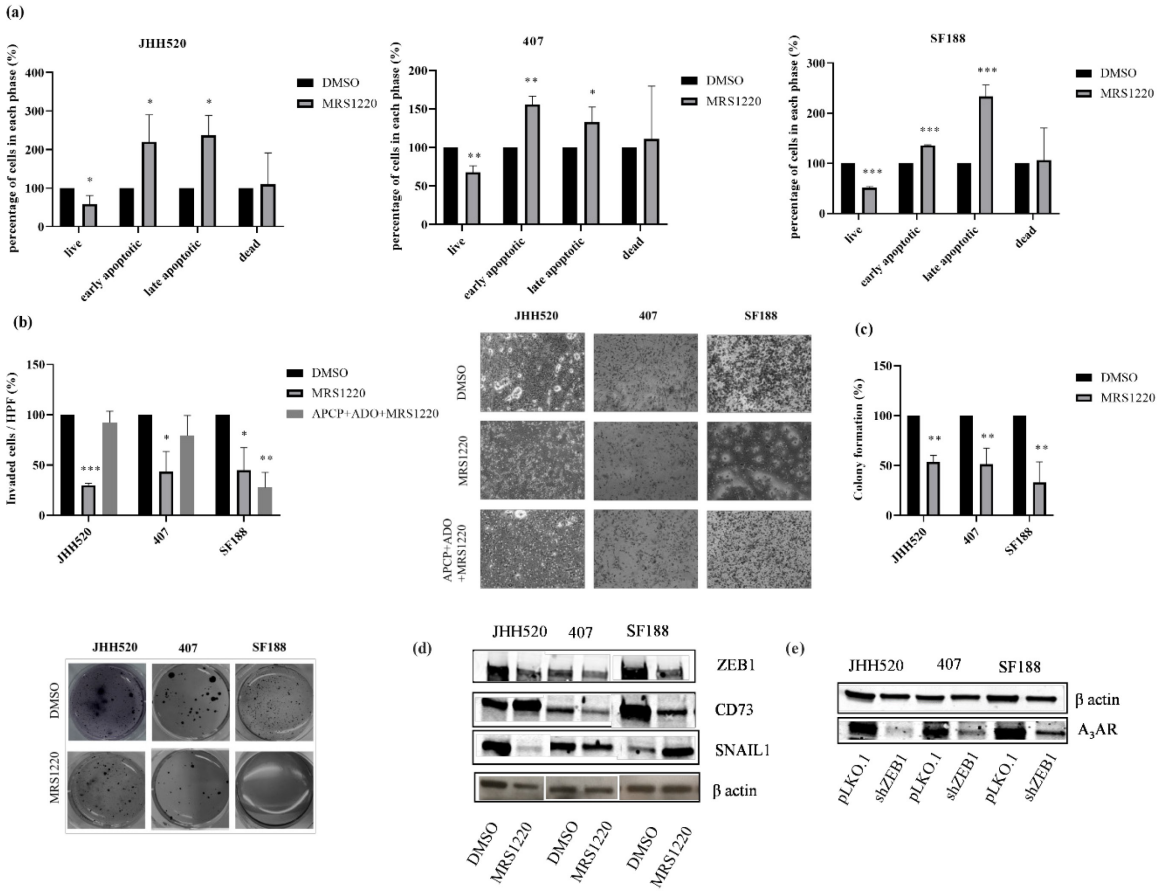

Figure 2.6. Pharmacological inhibition of the A_3A receptor reduces stemness and mesenchymal characteristics in GSCs

(a) Pharmacological inhibition of A_3AR with 10 μM MRS1220 for 24 h induced apoptosis as assessed with the Muse® Annexin V and Dead Cell Kit. Data normalised over the DMSO controls. (b, c) MRS1220 (10 μM) reduced the invasive and clonogenic capacities of GSCs. (d) ZEB1 protein expression levels were decreased in MRS1220 (10 μM) treated cells comparing to the control (DMSO) whereas CD73 and SNAIL1 protein expression levels showed no common features. (e) ZEB1 inhibition decreased the protein expression of A_3AR. Abbreviations: HPF, high power field. Statistical significance was calculated with unpaired t-tests. The results are depicted as mean ±SD of three independent experiments performed in triplicate. *$p < 0.05$, **$p < 0.005$, ***$p < 0.0001$.

2.1.5 Discussion

In this study, we highlight the role of both the enzymatic and non-enzymatic activity of CD73 on the maintenance of highly chemo-resistant GSCs, that are positive for the stemness markers CD133 and SOX2 [239]. Genetic interference of CD73 expression caused a significant suppression of GSC clonogenicity, cell invasion and proliferation [174, 224]. More specifically, we showed that the effects on GSC proliferation and clonogenicity were independent from its enzymatic activity but dependent on the CD73 protein level. However, in contrast to previous findings [174, 179], selective inhibition of CD73 enzymatic activity by APCP had significant effects only on the invasiveness of GSCs. In concordance, addition of the CD73 product ADO efficiently rescued the APCP phenotype. These results indicate that the CD73 enzymatic activity is a possible mechanism contributing significantly to the invasiveness of GBMs. In GBM and breast cancer, CD73 regulates tumour invasion via matrix metalloproteinases (MMPs) by degrading the extracellular matrix (ECM) [174, 180]. Our results also showed decreased MMP2 mRNA expression upon CD73 inhibition, indicating the regulation of invasion via this metalloproteinase, as one of the ways of the possible mechanism. In hepatocellular carcinoma, CD73 promoted invasion of the cells via activating PI3K/AKT signalling [221]. Interestingly, it has also been reported that CD73 promotes invasion and metastasis of head and neck squamous cell carcinoma (HNSCC) by stimulating the adenosine A_3 receptor [177].

We showed, that CD73 protein expression was reduced upon inhibition of the EMT activator ZEB1. Interestingly, both CD73 knockdown and suppression of the CD73 enzymatic activity with APCP reduced the protein expression of the EMT activator SNAIL1 in all three cell lines. Similarly, knockdown of CD73 in HNSCC has been suggested to regulate EMT via SNAIL1 and TWIST1 modulation [177]. These results indicate that there is a reciprocal link between EMT-like processes and CD73 enzymatic activity in GSCs. SNAIL1 has been described to promote invasive and clonogenic capacities in GBM tumours [240]. Thus, the reduced SNAIL1 expression diminishes mesenchymal properties of CD73 knock-down cells, demonstrated by their significantly decreased invasiveness and clonogenicity. Previous studies of our laboratory identified further metabolic enzymes directly correlating EMT-like processes with stemness and chemo-resistance of GSC cultures, which indicates that the metabolic homeostasis is crucial for the maintenance of GSCs and the metabolic enzymes may act as promising targets in GBM therapy [239, 241].

Since the enzymatic activity of CD73 drives the production of immunosuppressive ADO, CD73 has been identified as a novel immune checkpoint target [173, 226]. The clinical approved drug PTX reduced the survival of GSC cultures and the protein expression of ZEB1 and CD73 protein. As expected, treatment with PTX showed a decrease of GSC growth, invasiveness and clonogenicity. It has previously been shown that PTX abolished the radiation-induced G2/M block in GBMs and reduced β-catenin activity in melanoma cells [235, 242]. Interestingly, PTX possess anti-inflammatory properties that are mostly associated with the downregulation of TNF-α synthesis [237]. Taken together,

PTX has been identified as potentially effective compound against GBM. Here we show that its efficacy may at least partially be mediated via EMT activator ZEB1 and downstream CD73.

The A_3AR is an interesting receptor in GBM since it has been shown to promote tumour invasiveness and to increase multiple drug resistance protein-1 (MRP1) expression and GBM proliferation following chemotherapeutic treatment [149, 160]. Indeed, our results indicate the involvement of A_3AR in regulating invasion and clonogenicity of GSCs. Therefore, ADO signalling is a possible mechanism contributing significantly to the promotion of mesenchymal properties of cells. Interestingly, we observed that blockade of the A_3AR in the paediatric GSC line SF188 constantly inhibited the invasive properties of this cell line, whereas the effect in adult-derived JHH520 and 407 cells could be rescued by supplementation with ADO. Importantly, A_3AR inhibitor MRS1220 is an orthosteric inhibitor therefore, given its properties, there are no allosteric changes at the binding site of the receptor and ADO can rescue the effect [243]. This could indicate the importance of further ADO receptors on these cell lines playing a role in promoting invasion and underpin the possible differences between paediatric and adult gliomas.

We also showed that A_3AR is important in regulating EMT via ZEB1. The A_3AR antagonist MRS1220 reduced the protein expression of the EMT activator SNAIL1 in cell lines SF188 and 407 and decreased expression of CD73 in JHH520 cells. In addition, it had been shown that A_3AR blockade in GBM decreased the expression of SNAIL1 under hypoxia [149]. These results indicate that A_3AR regulates EMT globally by affecting the expression of several EMT activators also independent of CD73. Interestingly, treatment of GBM cells with the A_3AR antagonist significantly decreased the viability of the cells by inducing apoptosis. The effect of A_3AR on cell proliferation and apoptosis had been reported to be both positive and negative depending on several factors such as agonist concentration, cell type and tumour microenvironment [143]. In prostate cancer cells, A_3AR activation inhibited PKA-mediated ERK 1/2 activation and subsequent NADPH oxidase activities, resulting in decreased proliferation and invasion of cells [244]. In another study, activation of A_3AR using a selective agonist led to decreased proliferation of melanoma cells through inhibition of the phosphorylation or inactivation of GSK-3β that induced the phosphorylation or inactivation of β-catenin [245]. The greatest challenge is still to understand whether and where selective A_3 agonists or antagonists are the best choice [246]. In view of the data presented here, A_3AR could be an interesting target in GBM therapy.

The exact mechanism of CD73-dependent suppression of EMT activator SNAIL1 and decrease of GSC cell growth, invasiveness and clonogenicity still needs to be elucidated. In human breast cancer, CD73 had a regulatory effect on EGFR expression and phosphorylation, which correlated with tumour growth [247]. It has been shown that CD73 expression was higher in more malignant (higher expression of mesenchymal markers) breast cancer cells and its expression increased significantly in TGF-β-induced EMT cells [248]. The influence of CD73 on EMT could be studied in association with TGF-β, the most common EMT-inducing factor [249, 250]. In colorectal cancer, CD73 downregulated cell growth via

EGFR and the β-catenin/cyclin D1 signalling pathway [251]. However in GBM, the enzymatic activity of CD73 and the production of ADO seems to be involved in the regulation of EMT and invasiveness. In conclusion, our data support the potential role of CD73 as a promising target for GBM therapy. Inhibition of CD73 may efficiently lead to suppression of EMT-like processes and eradication of GSCs in malignant gliomas.

2.1.6 Material and methods

Cell culture

Three human glioblastoma cell lines were used in this study. JHH520 cells were generously provided by G. Riggins (Baltimore, USA), 407 (BTSC-407) by M.S. Carro (Freiburg, Germany) and the paediatric GBM cell line SF188 was provided by E. Raabe (Baltimore, USA). The GSC neurospheres were cultured in Dulbecco's modified Eagle's medium (DMEM) without pyruvate (Gibco), 30% Ham's F12 Nutrient Mix (Gibco), 2% B27 supplement (Gibco), 20 ng/ml human recombinant basic fibroblast growth factor (bFGF, Peprotech), 20 ng/ml human recombinant epidermal growth factor EGF (Peprotech), 5 µg/ml Heparin (Sigma-Aldrich) and 1x Penicillin-Streptomycin (Gibco). HEK293T cells were purchased from American Tissue Culture Collection (Manassas, VA). HEK293T cells were cultured in DMEM with pyruvate (Gibco) plus 10% Fetal Bovine Serum (FBS; Biochrome) and 1x Penicillin-Streptomycin (Gibco).
All cell lines were routinely tested for the absence of mycoplasma contamination and they have been authenticated using STR profiling.

Generation of lentiviral particles

Third generation lentiviral packaging system was used for the generation of the lentiviral particles as previously described [33]. Shortly, HEK293T cells were transfected with the lentiviral target vector and the three packaging plasmids (pMDLgpRRE, pRSVREV and pMD2VSVG) using FuGENE® HD transfection reagent (Promega). Supernatants containing the viral particles were collected after 48, 72 and 96 h post transfection and passed through a 0.45-micron filter before being concentrated using polyethylene glycol and sodium chloride (NaCl). Viral particles were stored at -80 °C until needed. The CD73 knockdown was achieved by cloning shRNA into the pLKO.1 TRC vector (Addgene plasmid) [252]. Plasmids containing shRNA against ZEB1 were created as described previously [26].

Quantitative real time PCR (RT qPCR)

RNA extraction was performed using the RNeasy Mini Kit (Qiagen) following the manufacturer's instructions. RNA concentrations were measured using the Nanodrop2000 spectrometer (Thermo Scientific). Two micrograms of RNA were transcribed into cDNA using the reverse transcriptase M-

MLV (Promega) and random hexameric primers. For each experiment, advanced SYBR Green Supermix (BioRad), 10 ng of cDNA and 10 pmol of each primer were combined and analysed in a CFX Connect Thermocycler (BioRad). The relative expression levels of genes were normalized to the endogenous housekeeping gene β-actin. Calculation of normalized relative gene expression was performed using the supplied software of the CFX Connect Real-Time PCR Detection System (Bio-Rad) The Primer sequences can be found in Table 2.1.

Western blotting

GSCs were lysed in cold RIPA Buffer and the protein concentrations were determined using the DC Protein Assay Kit (BioRad) according to the manufacturer´s instructions. Primary antibodies [CD73, 1/1000, (#ab133582, Abcam); ZEB1, 1/1000 (#HPA027524, Merck); SNAIL1 1/1000 (#3879, Cell Signalling); A_3AR, 1/1000 (#600445); β-actin, 1/1000 (#sc-130657, Santa Cruz)] were diluted in blocking solution containing 5% milk powder in Tris-buffered saline with Tween20 (TBST). The membranes were incubated with the respective primary antibodies overnight at 4 °C. Secondary antibodies [goat-anti-rabbit (#926-32211, IRDye800C LI-COR); goat-anti-mouse (#926-68070, IRDye680RD LI-COR), and goat-anti-rabbit-HRP (#111-035-144, Jackson Immuno Research)] were prepared in blocking solution in a dilution of 1/10000 and the membranes incubated with them for 1 h at room temperature. The band signals were acquired by a luminescence-based system in a LI-COR Odyssey CLx Imager (LI-COR) or by film-based system in a Super Signal West Pico Chemiluminescent Substrate (Thermo Scientific). Band quantification was performed using the Image Studio Lite Software version 2.1.

Cell viability, proliferation and cell death assays

GSCs were seeded at a density of 2 x 104 cells/ml and treated with inhibitor of CD73 enzymatic activity adenosine 5'-(α,β-methylene)diphosphate (APCP) or phosphodiesterase inhibitor pentoxifylline (PTX) at the following concentrations: 5 μM, 10 μM, 20 μM and 50 μM for APCP and 1 mM for PTX or vehicle (H20). Cells were treated with 1 μM, 5 μM, 10 μM, 20 μM and 50 μM of A3AR antagonist MRS1220 or vehicle (DMSO). The viability of the glioma cells was assessed using the Thiazolyl Blue Tetrazolium Bromide assay (MTT, Sigma Aldrich) according to the manufacturer's instructions. The absorbance was measured at 570 nm (reference 650 nm) using a Paradigm ™ multiplate reader (Beckman Coulter).

The percentage of the proliferating cells was determined based on Ki-67 expression using the Muse® Ki-67 Proliferation Kit (Merck Millipore) according to the manufacturer´s instructions. Briefly, pLKO.1 and shCD73 cells or cells cultured in medium containing 10 μM APCP or vehicle (H20) were collected. The cells were then fixed and incubated with Ki-67-PE antibody for 30 min at room temperature. Cells were then analysed using the Muse cell analyser (Merck Millipore).

The MUSE Annexin V & Dead Cell Kit (Merck Millipore) was used in order to measure the percentage of apoptotic cells, according to the manufacturer's instructions. Briefly, cells cultured in medium containing 10 μM MRS1220 or vehicle (DMSO) for 24 h were collected. They were then diluted with PBS containing 1% FBS to a concentration of 2 x 105 cells/ml. An aliquot of 100 μL of this single cell suspension was mixed with 100 μl of Annexin V/ dead reagent and kept in the dark for 20 min at room temperature. The analysis of the cells was performed using the Muse cell analyser (Merck Millipore).

Invasion assay

The invasive capacity of glioma cells was assessed using a modified 24-well Boyden Chamber assay. The inserts were coated with growth factor-reduced Matrigel (BD, Flanklin Lakes) and were incubated for 1 h at 37 °C. An aliquot of 4 x 10^4 cells was re-suspended in 500 μl DMEM (Life Technologies) and placed on top of each insert membrane. The bottoms of the wells were filled with 800 μl DMEM media with 10% FBS. After a 16 h incubation period, the non-invaded cells on the upper surface of the membrane were removed carefully with cotton swabs. The filters of the inserts were fixed in ice-cold methanol for 10 min, washed with PBS and stained with Haematoxylin for 5 min. The invasive capacity of the cells was evaluated by taking 5 pictures per well and counting the stained cells using the ImageJ Program. For the drug treatment experiments, cells were pre-treated for 24 h with 10 μM APCP with or without ADO or 10 μM MRS1220 in standard culture conditions before assessing their invasiveness.

Clonogenicity assay

The clonogenic capacity of glioma cells was measured by performing soft agar assays as described previously [34]. A six-well plate was coated with 1.5 ml of 4% agarose (Gibco) in DMEM to form the bottom layer. The top layer consisted of 0.6% agarose containing 3500 cells/well. Once the top layer was solidified, it was covered with 2 ml media. After 3 weeks' incubation, 1 mg/ml 4-Nitro blue tetrazolium chloride (NBT) solution (Sigma-Aldrich) was added overnight and incubated at 37 °C to stain the colonies. The clones were assessed using Clono Counter software [253].

CD73 activity assay

The CD73 enzymatic activity of glioma cells was assessed by measuring the conversion of AMP to ADO. Cells were seeded at a density of 1×10^5 cells/ml and incubated with 10 μM AMP for 1 h at 37 °C. The effect of APCP on CD73 activity was investigated by adding 10 μM APCP to the cells 10 min before adding AMP. Subsequently, cells were centrifuged and the amount of AMP and ADO in the supernatants was analysed by high-performance liquid chromatography (HPLC) (Shimadzu, LC-20AT; column: Nucleosil 1000-7 C18 250 mm). The absorbance was measured at 260 nm and 20 μl sample

were injected while the column was kept at room temperature. Methanol and a 0.6 M K_2HPO_4 / 0.4 M KH_2PO_4 aqueous buffer (pH = 6) with a flow rate of 1 ml/min were used to separate the compounds [254]. The column was flushed with buffer for 30 min before each measurement. For the first 2 min, the mobile phase consisted of 100% buffer. Between 2 and 9.5 min, methanol was increasingly added up to a volume of 15.5%, which remained like this until min 17. Between minute 17 and 20, the buffer concentration increased linearly until reaching 100% and finally, the column was flushed with H_2O for 5 min, adding up to a total run time of 25 min per measurement. Quantification of AMP and ADO values was done using a calibration curve of the standards.

In silico analysis of RNA sequencing data

RNA sequencing data was acquired from different anatomic structures of GBM from the Ivy Glioblastoma Atlas Project from the Allen Institute for Brain Science. Five tumour structures including the leading tumour edge, infiltrating zone, tumour parenchyma, hypeplastic blood vasssels and microvascular proliferation were identified by H&E staining and compared to peri-necrotic zone and pseudopalisades. 55 RNA samples were generated and used for sequencing. The data was retrieved in January 2018. Website: © 2015 [Internet]. Available from: glioblastoma.alleninstitute.org.

Statistical Analyses:

All data were obtained from three independent experiments and are the mean ±SD. The statistical significance was calculated using an unpaired student *t* test using the GraphPad Prism software version 8. Differences were considered significant for a p value of $p < 0.05$.

Tables:

Table 2.1. Primer sequences used in RT qPCR

Name	Forward primer (5´-3´)	Reverse primer (3´-5´)
β actin	CCCAGCACAATGAAGATCAA	CGATCCACACGGAGTACTTG
CD73	TCTTCTAAACAGCAGCATTCC	CATTTCATCCGTGTGTCTCAG
MMP2	CCATCGAGACCATGCGGAAG	CCTGTATGTGATCTGGTTCTTG

Acknowledgments: The authors thank Constanze Uhlmann (Department of Neurosurgery, University Medical Center Duesseldorf) and Sandra Nießing (Institute of Inorganic Chemistry and Structural Chemistry, Heinrich Heine University) for technical assistance and Ulf Kahlert (Department of Neurosurgery, University Medical Center Duesseldorf) for his support at the beginning of this project.

Author contributions: Conceptualization, J.M., J.T. and S.N.; methodology, J.T., S.N. and B.G.; validation, J.T.; analysis, J.T., S.N., B.G. and D.M.; investigation, J.T., B.G., K.K. and D.M.; resources, J.M., C.J. and D.H.; data curation, J.T.; writing – original draft preparation, J.M., J.T and S.N.; writing

– review & editing, J.M., J.T., S.N., B.G., K.K., D.M., C.J. and D.H.; visualization, J.T.; supervision, J.M., S.N. and C.J.; project administration, J.M. and S.N.; funding acquisition, J.M., C.J. and D.H.

Conflict of interest: The authors declare no conflict of interest.

2.1.7 Supplement

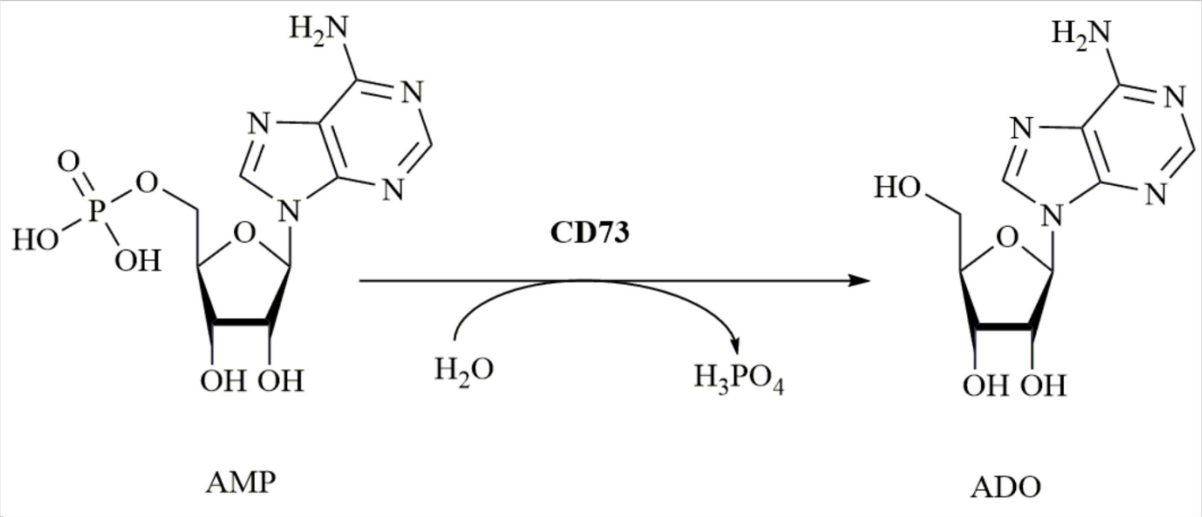

Figure 2.7. Enzymatic conversion of AMP to ADO by CD73.

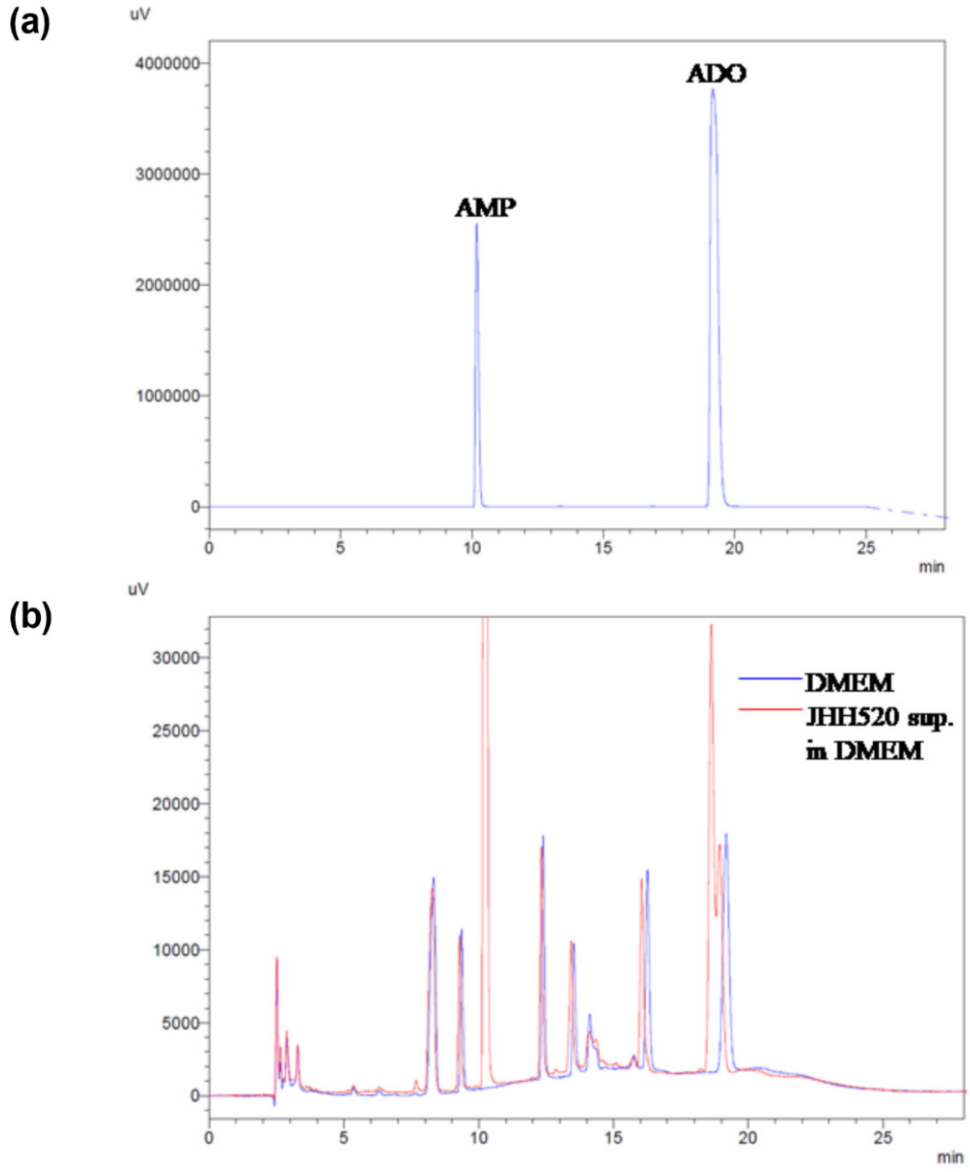

Figure 2.8. HPLC analysis was used to determine AMP and ADO concentrations and thus the enzymatic activity of CD73.

Chromatograms of AMP and ADO standards (a) and of supernatant of JHH520 cells after incubation with AMP (b) are shown. After optimizing the separation conditions of our method, it was possible to identify the peaks corresponding to AMP (retention time: 10 min) and ADO (retention time: 19 min). Even though DMEM medium (b, in blue) presented further signals in the chromatogram, it was possible to locate AMP and ADO in the supernatant solutions (b, in red) and quantify their concentration through standard calibration.

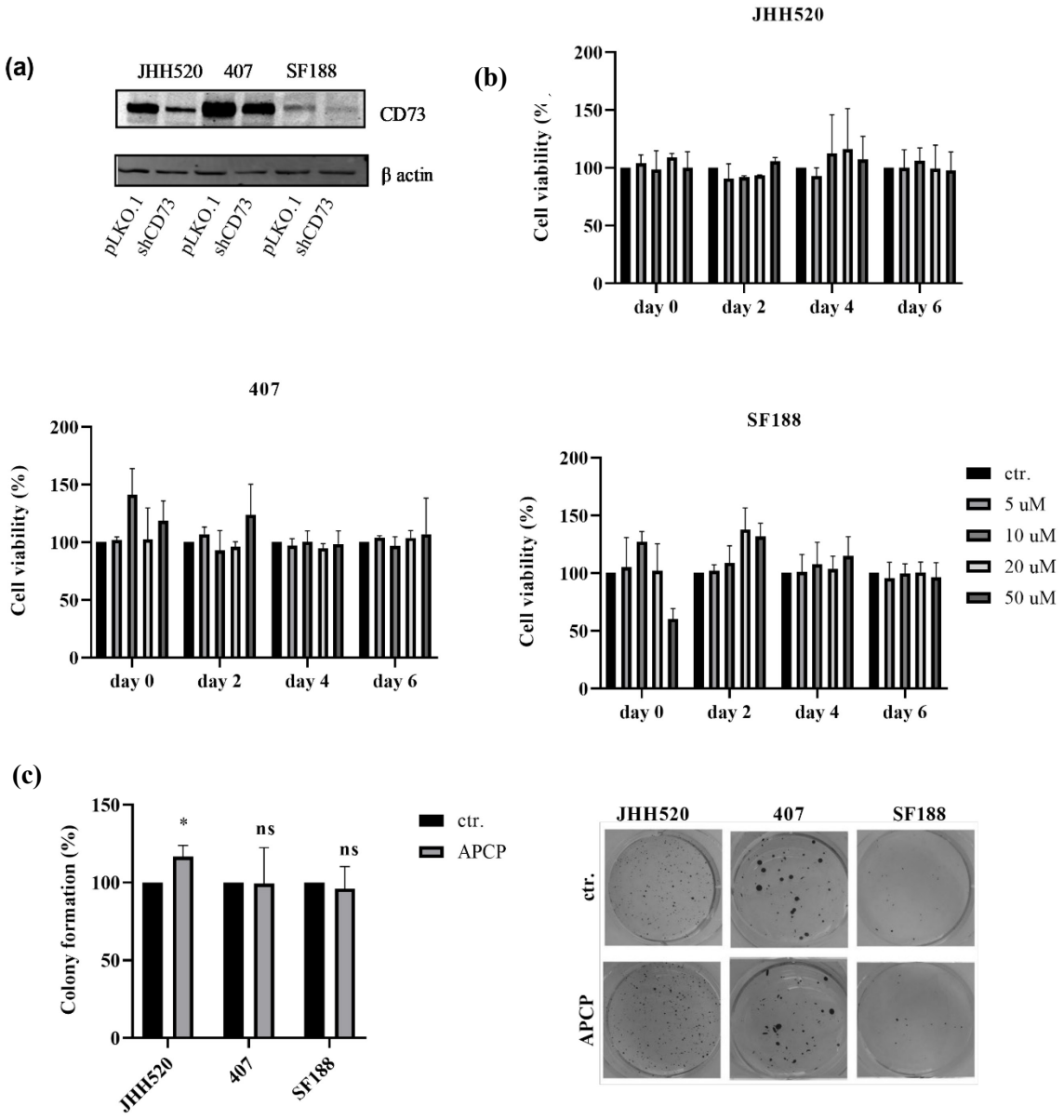

Figure 2.9. **CD73 enzymatic activity does not affect GBMs survival.**

(a) The CD73 knockdown efficiency in GSC lines (JHH520, 407, SF188) was confirmed by western blotting. (b) Cell viability of GBMs upon treatment with APCP (1-50 μM) was not significantly decreased compared with untreated control cells (ctr.). (c) Inhibition of CD73 enzymatic activity with APCP (10 μM) did not affect the clonogenicity of JHH520, 407 and SF188 cells as assessed by soft agar assays. Results are the mean ±SD of three independent experiments performed in triplicate. *$p < 0.05$.

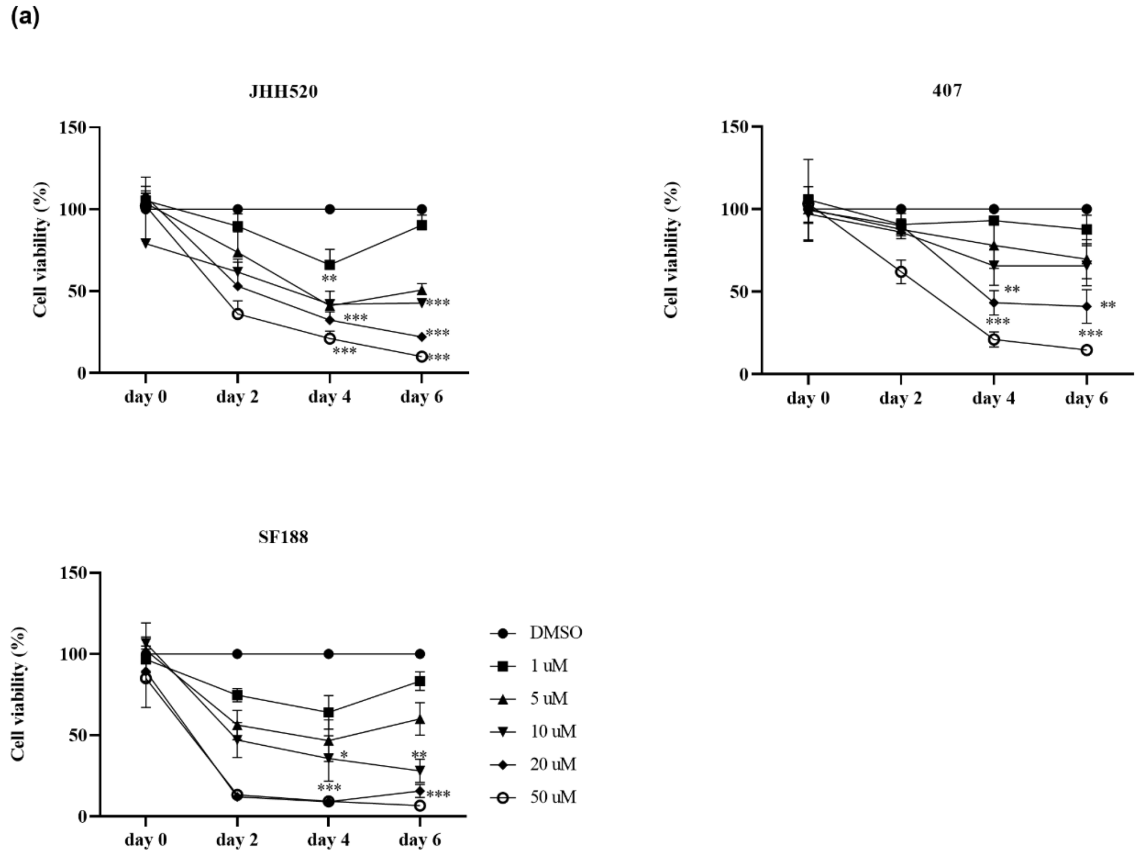

Figure 2.10. Pharmacological inhibition of the A_3A receptor reduces GBM viability.

(a) GBM cell lines (JHH520, 407 and SF188) were treated with increasing concentrations of MRS1220 (1-50 μM) and the cell viability was assessed using an MTT assay. Treatment with MRS1220 reduced cell viability in a dose-dependent manner ($p < 0.0001$). Results are the mean ±SD of three independent experiments performed in triplicate. Results are the mean ±SD of three independent experiments performed in triplicate. *$p < 0.05$, **$p < 0.005$, ***$p < 0.0001$.

2.2 Molecular monitoring of glioblastoma's immunogenicity using a combination of Raman spectroscopy and chemometrics

2.2.1 General Information

Title: **Molecular monitoring of glioblastoma's immunogenicity using a combination of Raman spectroscopy and chemometrics**

Chima Robert[1#], Julia Tsiampali[2#], Sara J. Fraser-Miller[1], Silke Neumann[3], Donata Maciaczyk[3], Sarah L. Young[4], Jaroslaw Maciaczyk[5,6#] and Keith C. Gordon[1#].

[1]*Dodd-Walls Centre for Photonics and Quantum Technologies, Department of Chemistry, University of Otago, Dunedin, New Zealand.*

[2]*Neurosurgery Department, University Hospital Duesseldorf, 40225 Duesseldorf, Germany.*

[3]*Department of Pathology, University of Otago, Dunedin, New Zealand.*

[4]*School of Medical Sciences, Faculty of Medicine and Health, The University of Sydney, Sydney, Australia*

[5]*Department of Neurosurgery, University Hospital Bonn, 53179 Bonn, Germany.*

[6]*Department of Surgical Sciences, University of Otago, Dunedin, New Zealand.*

# equal contribution

Corresponding Authors

Keith C. Gordon (keith.gordon@otago.ac.nz)

Jaroslaw Maciaczyk (Jaroslaw.Maciaczyk@ukbonn.de)

2.2.2 Abstract

Raman spectroscopy (RS) has been used as a powerful diagnostic and non-invasive tool in cancer diagnosis as well as in discrimination of cancer cells and immune cells. In this study RS in combination with chemometrics was applied to cellular Raman spectra to distinguish the phenotype of T-cells and monocytes after incubation with media conditioned by glioblastoma stem-cells (GSCs) showing different molecular background. For this purpose genetic modulations of epithelial-to-mesenchymal transition (EMT) process and expression of immunomodulator CD73 were introduced. Principal component analysis of the Raman spectra showed that T-cells and monocytes incubated with tumour-conditioned media (TCMs) of GSCs with inhibited EMT activator ZEB1 or CD73 formed distinct clusters compared to controls highlighting their differences. Further discriminatory analysis performed using linear discriminant analysis (LDA) and support vector machine classification (SVC) yielded sensitivities and specificities of over 70 and 67% respectively upon validation against an independent test set. Supporting those results, flow cytometric analysis was performed to test the influence of TCMs on cytokine profile of T-cells and monocytes. We found that ZEB1 and CD73 influence T-cell and

monocyte phenotype and promote monocyte differentiation into a population of mixed pro- and anti-tumorigenic macrophages (MΦs) and dendritic cells (DCs) respectively. In conclusion, Raman spectroscopy in combination with chemometrics enabled tracking T-cells and monocyte phenotypes.

Keywords: CD73, EMT, glioblastoma, immunity, cancer, monocytes, T-cells, Raman spectroscopy, chemometrics, cell discrimination

Graphical abstract

Multivariate analysis proffering better insight into the differences in the Raman spectral data of different immune cells with their knockdown treatments.

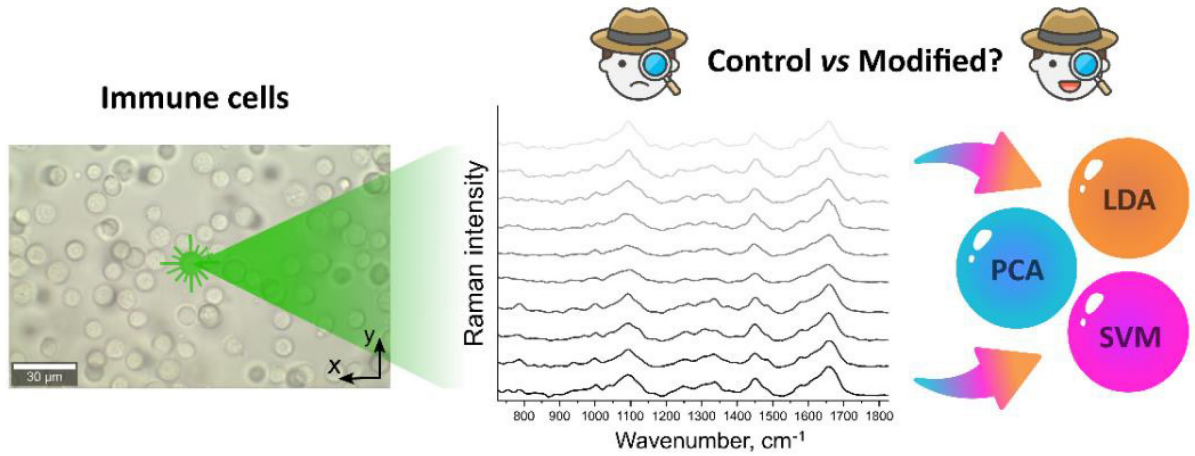

2.2.3 Introduction

Raman spectroscopy (RS) has garnered increased attention as a rapid and non-destructive diagnostic tool for uncovering molecular basis of diseases as well as for evaluating treatment therapies [255]. The contention for this method in biological and clinical spectroscopy is considerably justified owing to its non-invasive and label-free requirement, without interference with water molecules. RS probes vibration of bonds in a sample yielding molecular specific information on the composition/structure of the molecule; which can be utilized for qualitative and quantitative purposes [256, 257]. RS is a two-photon process involving the inelastic scattering of an incident photon from a monochromatic light source (laser) on interaction with a sample. The resulting difference between the energy of the incident and scattered photon is referred to as Raman shift. These Raman shift provide information on the vibration of the chemical bonds present in the sample [258]. A typical Raman spectrum of a biological cell comprises different overlapping peaks relating to the composition of macromolecules like nucleic acids, lipids, protein, carbohydrates and other metabolites [259, 260].

RS has been widely applied in clinical spectroscopy particularly in cancer diagnosis and discrimination, with several studies reporting the sensitivity of RS to changes in molecular conformation and composition in both cells and tissues owing to carcinogenesis [261-265]. The

biochemical changes resulting on transition of normal to malignant tissue (brain cancer) have been investigated using RS, with increased cholesterol (-esters) level reported in the necrotic tissue [266]. RS has also been utilized in the discrimination of normal and malignant cells (tissues) in brain cancer; with some studies reporting an accuracy of over 98% [15, 266-268]. A similar study conducted for oral cancer showed high level of nuclei acid and a corresponding decrease in lipid, glycogen and protein level in the malignant tissue [194, 269].

Despite the apparent applicability of RS in biological cell studies, the inherent weak nature of Raman scattering limits its application in clinical settings. However, recent advancements in optical technologies allowing for integration of RS and confocal microscopy have led to improvements in spectral resolution as well as possibility for live cell imaging [270, 271].

Glioblastomas (GBMs) are the most common and malignant primary brain tumours with an extremely aggressive clinical phenotype and very poor prognosis [1],[4]. One of the biggest challenges in GBM's effective treatment is the presence of highly invasive tumour cells called glioblastoma stem-cells (GSCs) that disseminate into the normal brain parenchyma and lead to tumour recurrence [272]. GSCs are enriched by the molecular pathway called epithelial to mesenchymal-like (EMT-like) transition and its activator, Zinc Finger E-Box Binding Homeobox 1 (ZEB1) , plays a key role in glioma cell invasion [26],[35]. Most recently, an ecto-5'-nucleotidase (NT5E) known as CD73, that catalyses the conversion of adenosine mono phosphate (AMP) to adenosine (ADO), has been shown to regulate EMT in cancers [220]. Both CD73 and the EMT status have been shown to regulate cancer cell immunogenicity [226] [106].

The immune system and its responses can be broadly divided into two parts - innate and adaptive immunity with these two branches interacting closely to efficiently clear the body of invading pathogens and malignant cells. Innate immune cells, such as monocytes, are able to detect and phagocytose cancerous cells [273]. Monocytes can differentiate into MΦs or DCs and play an important role in priming antigen-specific adaptive immune responses [274]. Adaptive immune responses, mediated by B- and T-cells, develop more slowly than innate immune responses but provide antigen-specific responses and are associated with immunological memory [275]. This is an important mechanism to prevent cancer recurrence. In GBM patients, circulating monocytes express higher programmed death-ligand 1 (PD-L1) levels compared to healthy controls, which leads to suppression of T-cell responses [276]. Furthermore, it has been shown that $CD8^+$ and $CD4^+$ T-cells are exhausted in GBMs and are incapable of driving an effector immune response [277]. $CD4^+$ T-cells can secrete cytokines to support other immune cells and $CD8^+$ T-cells, known as cytotoxic T-cells, can destroy infected cells [70, 278].

Given the urgent need of developing techniques for cancer screening, diagnosis and intraoperative surgical guidance, Raman spectroscopy has emerged as a non-invasive therapy guidance and diagnostic tool and has been used to define invasive margin of GBMs [16, 279].

The entire Raman spectra of a single cell referred to as "ramanone" is informative on the composition of all the molecules present in the cell. Modulation of the cell with different treatments lead to changes in physiological and morphological features, as such distinct Raman spectrum [280]. Interpretation of Raman spectra for qualitative purposes have involved both univariate and multivariate approaches. The univariate approach entails visual inspection of one or few Raman peaks belonging to specific chemical components; and making comparison on the intensity changes in such peaks. This technique howbeit informative, results in loss of spectral information in the unselected regions. This challenge can be overcome by utilizing a global spectral (multivariate) approach using a single or combination of chemometric tools such as principal component analysis (PCA) [281], linear discriminant analysis (LDA) [282], K-means clustering [269] and support vector machine classification (SVM) [283]. These tools allow for reduction in dimensionality in large datasets; facilitating interpretability while minimizing loss of information [284].

In the present study, we set out to determine whether confocal Raman micro-spectroscopy in combination with two chemometric tools (PCA-LDA and SVM) would sufficiently detect molecular differences of monocytes and T-cells from a single blood donor after incubation with TCM of GSCs upon ZEB1 inhibition and, therefore, EMT modulation, or CD73 inhibition. Furthermore, since EMT and CD73 are critical in cancer progression and chemoresistance [35, 174], we used confocal Raman micro-spectroscopy in combination with the two chemometric tools to detect differences of the cells upon ZEB1 and CD73 inhibition. Along with T-cells and monocytes discrimination using Raman technology, we assessed differences in the phenotype of the immune cells.

2.2.4 Materials and methods

Cell culture

Three human glioblastoma cell lines were used in this study. JHH520 cells were generously provided by G. Riggins (Baltimore, USA), GBM1 by A. Vescovi (Milan, Italy) and the paediatric GBM cell line SF188 was provided by E. Raabe (Baltimore, USA). The GSCs neurospheres were cultured in DMEM without pyruvate (Gibco, USA), 30% Ham's F12 Nutrient Mix (Gibco, USA), 2% B27 supplement (Gibco, USA), 20 ng/ml human recombinant bFGF (Peprotech, Germany) 20 ng/ml human recombinant EGF (Peprotech, Germany), 5 µg/ml Heparin (Sigma-Aldrich, USA) and 1x Penicillin-Streptomycin (Gibco, USA). HEK293T cells were purchased from American Tissue Culture Collection (Manassas, VA). HEK293T cells were cultured in DMEM with pyruvate (Gibco, USA) plus 10% Fetal Bovine Serum (FBS; Biochrome, Germany) and 1x Penicillin-Streptomycin (Gibco, USA).

Lentivirus production

The third generation lentiviral packaging system was used for the generation of the knockdown cells of the choice. Interference RNA sequences against ZEB1 and CD73 were designed with the software

Primer3 and cloned into the pLKO.1 TRC vector (Addgene plasmid #10878). HEK293T cells were transfected with either the lentiviral vector of shZEB1 or shCD73 and the three different packaging plasmids pRSVREV, pMDLgpRRE and pMD2VSVG using FuGene® Transfection Reagent (Promega, Germany). After 24 h, the media was changed to the one containing antibiotics. The virus supernatants were collected at three consecutive days after 48 h, 72 h and 96 h post transfection and they were concentrated with 50% PEG 8000 and 1.5 M NaCl. The supernatants were finally pooled, passed through a 0.45 micron filter then frozen at -80 °C until needed.

Lentiviral transduction / Generation of EMT knockdown cells

For the generation of GBMs knockdown cells, $1x10^5$ cells were transfected with the shZEB1 or shCD73 and pLKO.1 (empty vector) viruses in a volume of 1 ml culture media (in a T25 cell culture flask). After an overnight incubation at 37 °C, 3 ml of growth media were added. 72 h after transfection, the puromycin resistance gene enabled an antibiotic selection of the transfected cells.

Generation of tumour-conditioned media (TCM)

GBM cell lines GBM1, JHH520 and SF188 (each wildtype (WT), empty vector control (pLKO.1), shCD73 or shZEB1 were cultured in cDMEM [DMEM without pyruvate, 30% Ham's F12 Nutrient Mix, 2% B27 supplement and 1x Penicillin-Streptomycin (all from Gibco, USA)], in T-75 flasks at a concentration of 300.000 cells/mL for 48 h, the supernatants collected and filtered through a 0.45 μm filter to remove cells and debris. Supernatants were aliquoted and stored at -20 °C until needed for experiments.

Isolation of human monocytes and T-cells

Human peripheral blood mononuclear cells (PBMCs) were isolated from the whole blood of healthy donor under approval from the University of Otago Ethics Human Participants Committee (H17/034). Approximately 50 mL blood was collected into several 10 mL collection tubes previously loaded with Heparin. Each 15 mL of heparinised blood sample was diluted with an equal volume of Roswell Park Memorial Institute (RPMI) 1640 media and layered over 15 mL of Ficoll Paque Plus (GE Healthcare, Uppsala, Sweden) and centrifuged for 20 min at 800 x g without brakes. The buffy coat was removed and washed twice with RPMI 1640 media.

$CD3^+$ T-cells were isolated from PBMC using a human Pan T-cell isolation kit (Miltenyi Biotec, Bergisch Gladbach, Germany). Eluted $CD3^+$ T-cells were re-suspended at $1x10^6$ cells/mL in RPMI supplemented with 1% penicillin/streptomycin, 5% human serum, IL-7 (5 ng/mL, BioLegend, USA) and IL-2 (15 ng/mL, BioLegend, USA) and seeded 500 μL to a 48 well plate.

Monocytes were isolated from the remaining $CD3^-$ fraction using a human Pan monocyte isolation kit (Miltenyi Biotec, Germany). Eluted monocytes were re-suspended in a RPMI

supplemented with 20 ng/mL GM-CSF (Biolegend, USA) and were seeded in a 96 well plate at $1x10^5$ cells/well in 200 µL.

Culture of human monocytes and T-cells

Monocytes and T-cells were incubated with 50:50 mixtures of seeding and tumour-conditioned media (TCM) for 5 days. For this, half of the seeding media was replaced with TCM (monocytes 100 µL, T-cells 250 µL). After 2 days, half of the media was replaced with a 50:50 mixture of seeding media and tumour-conditioned media. Adherent monocytes were detached on day five after a 5 min incubation with 0.0002% EDTA solution and washed twice prior to use. Non-adherent T-cells were harvested and washed twice prior to use. Monocytes and T-cells were either measured by Raman spectroscopy or stained with fluorescently-labelled antibodies for flow cytometry.

T-cell activation and phenotyping

After the 5-day culture with TCMs, $CD3^+$ T-cells were activated with a mixture of ionomycin (Sigma Aldrich, 50 ng/mL;phorbol 12-myristate 13-acetate (PMA, Sigma Aldrich, 500 ng/mL):Brefeldin A (BioLegend, 1:1000 dilution) for 6 h to induce cytokine production. After 6 h, T-cells were harvested and stained with fluorescently labelled antibodies against cell surface markers (CD4 and CD8) and intracellular proteins (interleukin (IL)-2, IL-10, IFN-γ and TNF-α) as described below.

Flow cytometry

Cells were harvested, washed with PBS and stained for 10 min with the LIVE/DEAD® Fixable Yellow Dead Cell Stain Kit (Invitrogen, Eugene, USA) to allow identification of dead cells. Next, unspecific antibody binding was blocked using the Human Tru Stain FCX™ (BioLegend, San Diego, USA) before cells were stained with a mixture of antibodies against cell surface markers detailed in (Table 2.2) for 15 min. The True-Nuclear™ Transcription Factor buffer kit (BioLegend, San Diego, USA) was subsequently used according to the manufacturer's instructions to prepare the cells for intracellular staining. After membrane permeabilisation, cells were stained with antibodies against intracellular markers detailed in Table 1 for 15 or 30 min (monocytes and T-cells, respectively). Flow cytometric acquisition was performed on a Beckman Coulter Gallios flow cytometer and samples were analysed using the Kaluza software (version 1.3, Beckman Coulter). Fluorescence minus one controls were used to set gates.

Table 2.2. Antibodies used for flow cytometry

Antibody	Fluorophore	Clone	Company
Surface staining			
CD64	FITC	10.1	BioLegend
PD-L1	PE-CF594	29E.2A3	BioLegend
HLA-DR	Alexa Fluor 700	LN3	BioLegend
CD11c	Pacific Blue	3.9	BioLegend
CD209	APC Fire	9E9A8	BioLegend
CD4	APC Fire	A161A1	BioLegend
CD8	Alexa Fluor 700	HIT8a	BioLegend
Intracellular staining			
IDO	AF647	V50-1886	BD Biosciences
IFN-y	FITC	4S.B3	BioLegend
IL-2	PE-CF594	MQ1-17H12	BioLegend
TNF-α	Brilliant violet 421	MABII	BioLegend

Raman instrument and cell measurements

Raman spectra were collected using an Alpha 300R+ confocal Raman microscope controlled with Project 5.1 software (WITec GmbH, Ulm, Germany). The Raman microscope instrument including laser and CCD camera were turned on for at least 10 minutes for CCD temperature stabilization (-60 ^{o}C). Daily instrument calibration was performed using a silicon wafer sample with Raman peak position at 520.6 cm^{-1}. Spot measurements were carried out using the 532 nm excitation laser (Coherent, California), 20 mW power and 1 second x 60 accumulation integration time per spot. Spectra were collected using the 50x dry objective (Zeiss, Oberkocken, Germany)corresponding to a spot size of ~420 nm over a spectral window of -55 to 3789 cm^{-1}. Spectral acquisition was performed on cells dispersed on a glass slide. A total of 20 cells were measured per sample.

Spectral data analysis

Spectral processing

Raman spectral data were pre-processed using the Project 5.1 software (WiTec, Ulm, Germany). Raman spectral data were first corrected for cosmic spikes using the cosmic ray removal tool (filter size = 4, dynamic factor = 4). The obtained spectra were background subtracted using the dynamic 'shape' background algorithm (shape size = 300) to remove any fluorescence contribution. Standard normal variate (SNV) transformation was performed over the selected spectral region (725 to 1825 cm^{-1}) in The Unscrambler X v10.5 (CAMO, Norway) to account for intensity variations in the collected spectral data.

Multivariate data analysis (chemometrics)

In the present study, principal component analysis (PCA) was utilized as an unsupervised exploratory analysis tool whereas linear discriminant analysis (LDA) and support vector machine (SVM) classification were employed as a supervised multivariate analysis tool for the cells discrimination. All data analysis was performed in The Unscrambler X v10.5 (CAMO, Norway) using the pre-processed spectral data region (725 to 1825 cm^{-1}).

Exploratory analysis - Principal component analysis (PCA)

Principal component analysis (PCA) is an exploratory analysis technique which highlights natural variations in a large dataset without prior knowledge of the data structure [285]. The algorithm reduces the dimensionality of variables within a large dataset by finding new variables (principal components, PC) that are linear functions of the original dataset. The PCs are uncorrelated, with each PC explaining certain percentages of the total variance within the dataset [284]. PCA model was calculated using a K-fold (K=3) random cross validation procedure using the nonlinear iterative partial least squares algorithm to enhance model optimization. PCA was carried on all T-cells and monocytes (after incubation with TCMs) independently.

Linear discriminant analysis (LDA)

Linear discriminant analysis (LDA) technique is a supervised feature extraction tool utilized for qualitative studies. The LDA algorithms provides linear transformation of n-dimensional feature vectors (samples) into an m-dimensional space usually called discriminant variables (where $m < n$), such that the distance between-class variance is maximized relative to the within-class variance [286]. The requirement of samples in the training set being larger than the number of variables poses a challenge to the use of LDA. This constraint however is overcome by utilizing PCA-LDA, where PCA calculations are performed for reduction of data dimensionality prior to LDA calculation. The first four PCs were utilized in performing the LDA calculations in this study. LDA is a supervised method in that sample classes are predefined into groups prior to model creation. The LDA model was created using 67% of the dataset (training set); then validated against 33% of the dataset (test set). LDA was

performed on each of the three cell lines with their respective control and knockdowns (pLKO.1, shCD73 and shZEB1) for both T-cells and monocytes. Model performance was evaluated with respect to the prediction accuracy, sensitivity and specificity.

Support vector machine (SVM) classification

Support vector machine classification first proposed by Vapnik [287], utilizes kernel functions to map data into higher dimensional space; allowing for classification of samples based on set of predefined groups [288]. The algorithm calculates the hyperplane with the maximum margin in the n-dimensional space (where n is the number of variables) and employs this to correctly classify the multivariate data into predefined groups [289]. In this study, we utilized the linear kernel function in creating the model and the model performances were assessed as a function of accuracy, sensitivity and specificity. In all cases, the SVM models were created using 67% of the dataset (training set) and validated against 33% of the dataset (test set). Like LDA, SVM classification was performed on T-cells and monocytes after incubation with the genetically modified (pLKO.1, shCD73 and shZEB1) and WT GSCs.

Model performances were evaluated with respect to the prediction accuracy, sensitivity and specificity. Sensitivity is the ability of the model to detect true positive based on all samples classified as positive whereas specificity is the ability of a model to detect true negative based on all samples classified as negative in a class [290].

2.2.5 Results and discussion

To assess the ability of RS to distinguish between monocytes and T-cells after incubation with TCMs from GSCs with blocked ZEB1 or CD73, twenty cells were measured per sample. The mean Raman spectra were calculated after removal of spectra with low signal to noise ratio for both the T-cells and monocytes (Figure 2.11a). The spectra identified in Figure 1 were dominated by bands at 754, 787, 830, 887, 938, 1003, 1093, 1206, 1258, 1310, 1332, 1450, 1578, 1657 and 1754 cm^{-1}. The Raman signatures are characterized by vibrations associated with proteins including cytochrome C as evident in peaks at ~754 cm^{-1} and 1578 cm^{-1}, with sharp bands at 1003 cm^{-1} corresponding to phenylalanine, tryptophan and tyrosine [281, 291]. Vibrations associated with nucleic acids are observed in the phosphate marker for DNA at 830 cm^{-1}, other nucleic acid signatures can be identified at 787 cm^{-1} (cytosine and uracil residues), 1093 and 1258 cm^{-1} (PO_2^- nucleic acids), 884 cm^{-1} (nucleic acid backbone) [292]. Amide III N-H bending and C-N stretching vibrations in lipids and protein are observed at 1258 cm^{-1} and 1309/1310 cm^{-1}. The peak at 1332/1334 cm^{-1} could also be associated with guanine (DNA/RNA) nucleic acids [293]. The CH_2/CH_3 stretching and amide I vibrations are characterized by peaks at 1450 cm^{-1} and 1657 cm^{-1} respectively [294].

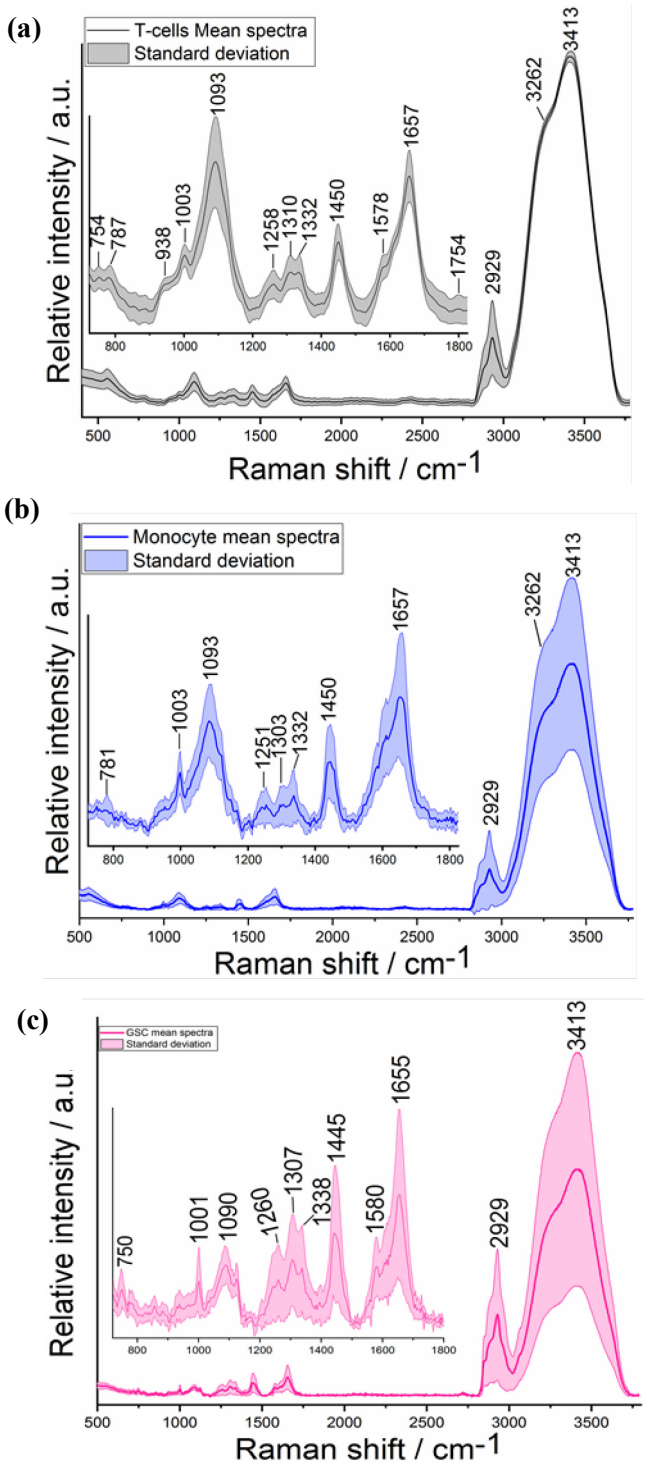

Figure 2.11. Mean pre-processed Raman spectra and standard deviation of the immune cells after incubation with TCMs a) T-cells and b) monocytes and c) GSCs (GBM1, JHH520 and SF188).

Similar spectra signatures were observed for monocytes and GSCs, howbeit recorded spectra were of lower signal to noise ratio on comparison to their T-cells counterpart. A plot of the mean spectra is shown in Figure 2.11b and 2.11c. Despite the slight spectral differences, it is more informative to

employ multivariate analysis technique such as PCA, SVM and LDA, for better spectral visualisation and interpretation.

Exploratory analysis (PCA)

Preliminary spectral analysis was performed using PCA in The Unscrambler X v10.5 (CAMO, Norway). PCA was performed on each of the monocytes and T-cells incubated with TCMs of three GSC lines (GBM1, JHH520 and SF188) with their controls (WT and empty vector pLKO.1) and respective knockdowns (shZEB1 and shCD73), with the data points plotted as a scatter showing clusters of cell groups. Here is a breakdown of the groups used for analysis (GBM1-WT, GBM1-shCD73, GBM1-pLKO.1 and GBM1-shZEB1), (JHH520-WT, JHH520-shCD73, JHH520-pLKO.1 and JHH520-shZEB1) and (SF188-WT, SF188-shCD73, SF188-pLKO.1 and SF188-shZEB1).

Figure 2.12 and 2.13 show the scores and loading plot for the PCA analysis on the T-cells. Despite minor overlaps, distinct separation was observed for the T-cells with TCM pLKO.1 from the rest of the cell groups. The cluster of T-cells with TCM GBM1-pLKO.1 is seen in the positive PC4 space whereas it is observed in the positive PC3 space for T-cells incubated with TCM of JHH520 and SF188. T-cells with TCM GBM1-pLKO.1 clustered in the positive PC4 space whereas T-cell with TCM GBM1-shZEB1 and GBM1-shCD73 clustered in the negative PC4 space. The PC4 loadings plot indicate that delineation of T-cells with TCM pLKO.1 was due to contributions from protein including bands at (1014, 1322, 1464 and 1679 cm^{-1}) and nuclei acids (796, 833, 956, 1108, 1134, 1348 and 1585 cm^{-1}) (Figure 2.13). The negative PC4 loadings show lipid contributions which might be indicative of higher lipid levels in T-cells with TCM GBM1-shZEB1 and GBM-shCD73.

In T-cells with TCM JHH520-pLKO.1 and JHH520-shZEB1 clusters were observed in the negative PC3 space whereas the T-cells with TCM JHH520-WT and JHH520-shCD73 clusters formed in the positive PC3 space. The loadings plot was identical to that observed for the GBM cell line, with separation of pLKO.1 and shZEB1 arising from protein and nuclei acid contributions (Figure 2.12d). Unlike T-cells treated with TCM GBM1 and TCM JHH520, PCA of the T-cells with TCM SF188 show separation along the PC2 line with T-cells with TCM SF188-pLKO.1 cluster formed in the positive PC2 space. Examination of the loadings plot show that major contributions from lipids (band at 1450 and 1657 cm^{-1}) and nuclei acids (1089 cm^{-1}) were responsible for the delineation of the T-cells with TCM SF188-pLKO.1.

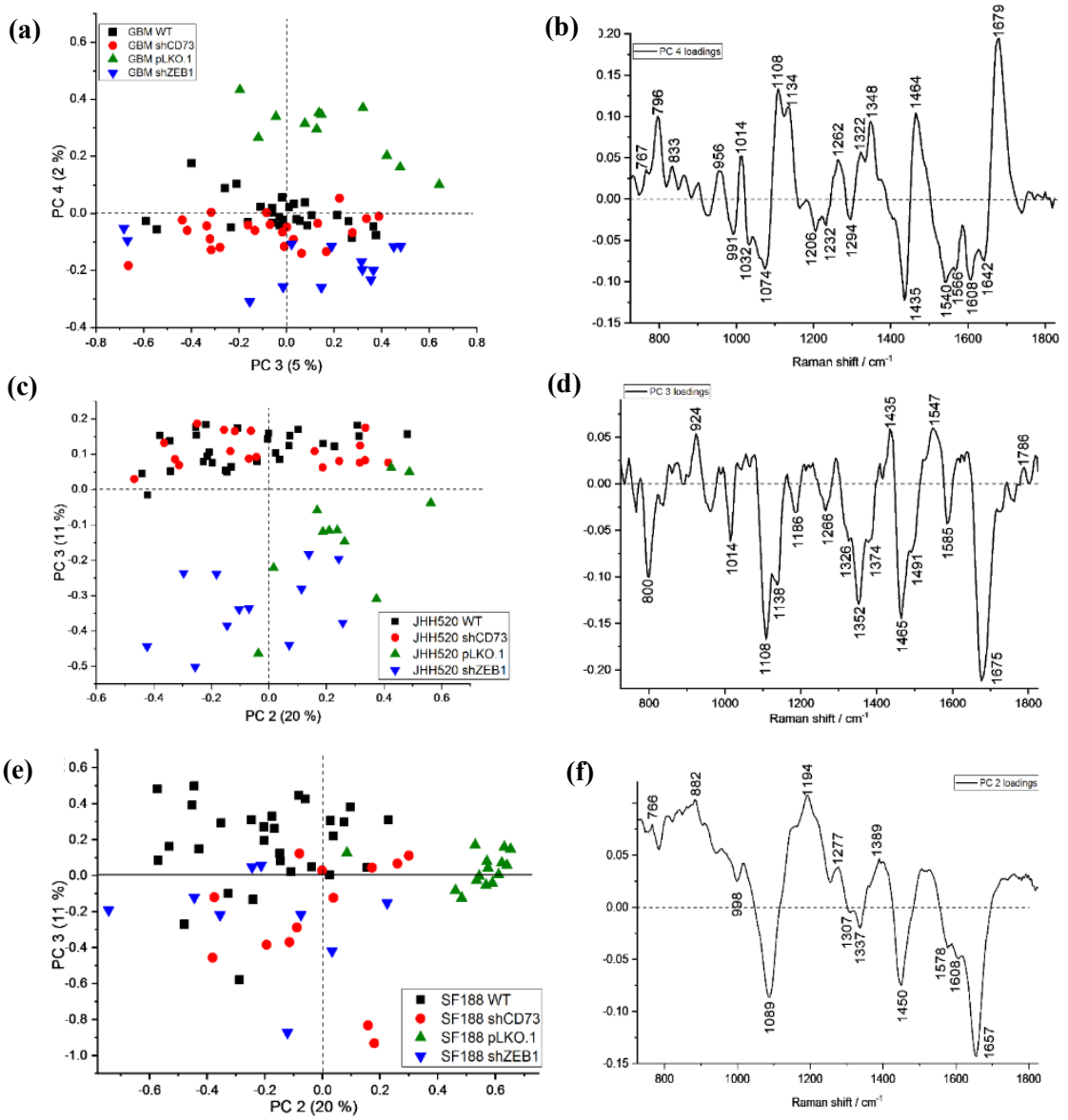

Figure 2.12. PCA scores and loadings plot for T-cells analysis

after incubation with TCMs of three GSC lines with their controls and knockdowns (WT, pLKO.1, shCD73 and shZEB1) a) GBM1 scores plot b) GBM1 loadings plot c) JHH520 scores plot d) JHH520 loadings plot e) SF188 scores plot and f) SF188 loadings plot.

PCA output for the monocyte analysis is shown in Figure 2.13. In the monocytes with TCM of the cell line JHH520, majority of the cells with TCM JHH520-pLKO.1 and TCM JHH520-shZEB1 scores clustered in the positive PC2 space with corresponding loadings showing majority contribution from 1446 and 1656 cm^{-1} which can be associated with both lipid and protein. In monocytes treated with both the TCM of GBM1 and SF188, cell groups had distinct separation indicating the variability across the samples set. The overlap in the scores plot contributes difficulty in identifying the chemical constituents responsible for the separation of the cell groups, hence the use of PCA-LDA and SVM for better interpretation.

However, the observed clusters could be explained by the differences at cytokine profile of the immune cells indicating the presence of the mixed populations including pro-inflammatory and anti-inflammatory MΦs and DCs as well as $CD4^+$ and $CD8^+$ T-cells. Our results indicate that GSCs with ZEB1 and CD73 inhibition can actively influence the phenotype of T-cells and monocytes and these differences in cell state can be visualized by Raman spectrum analysis.

PCA scores plot on the glioma cells, do not show distinct separation for all three GSC lines considered (Figure 2.14). This could be that the largest source of variance that are similar across the various knockdowns. The PCA loadings plots are shown in the supplementary information (Figure 2.20). PCA-LDA and SVM was utilized for classification purposes.

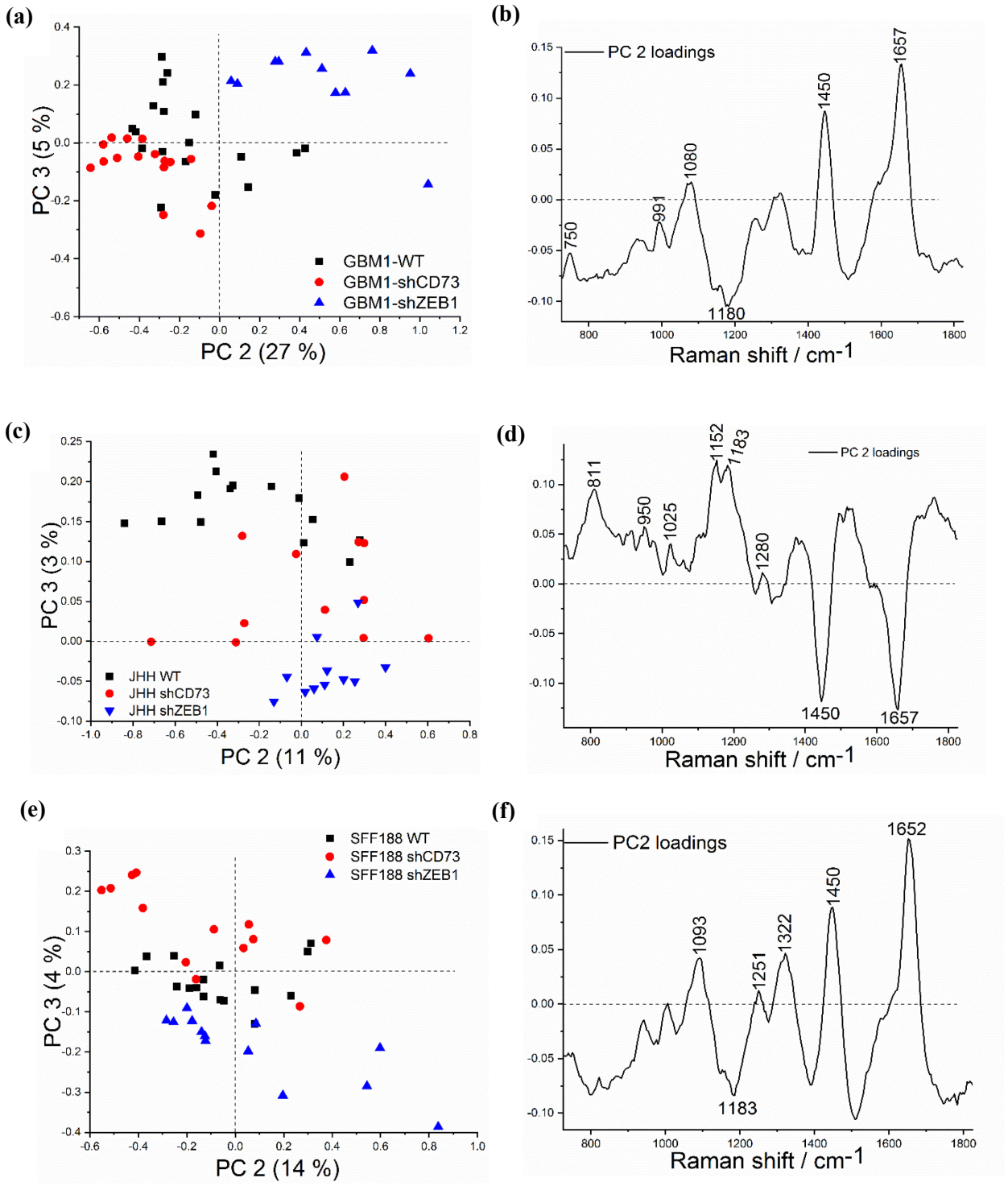

Figure 2.13. PCA scores and loadings plot for monocytes analysis

after incubation with TCMs of three GSC lines with their controls and knockdowns (WT, shCD73 and shZEB1) a) GBM1 scores plot b) GBM1 loadings plot c) JHH520 scores plot d) JHH520 loadings plot e) SF188 scores plot and f) SF188 loadings plot.

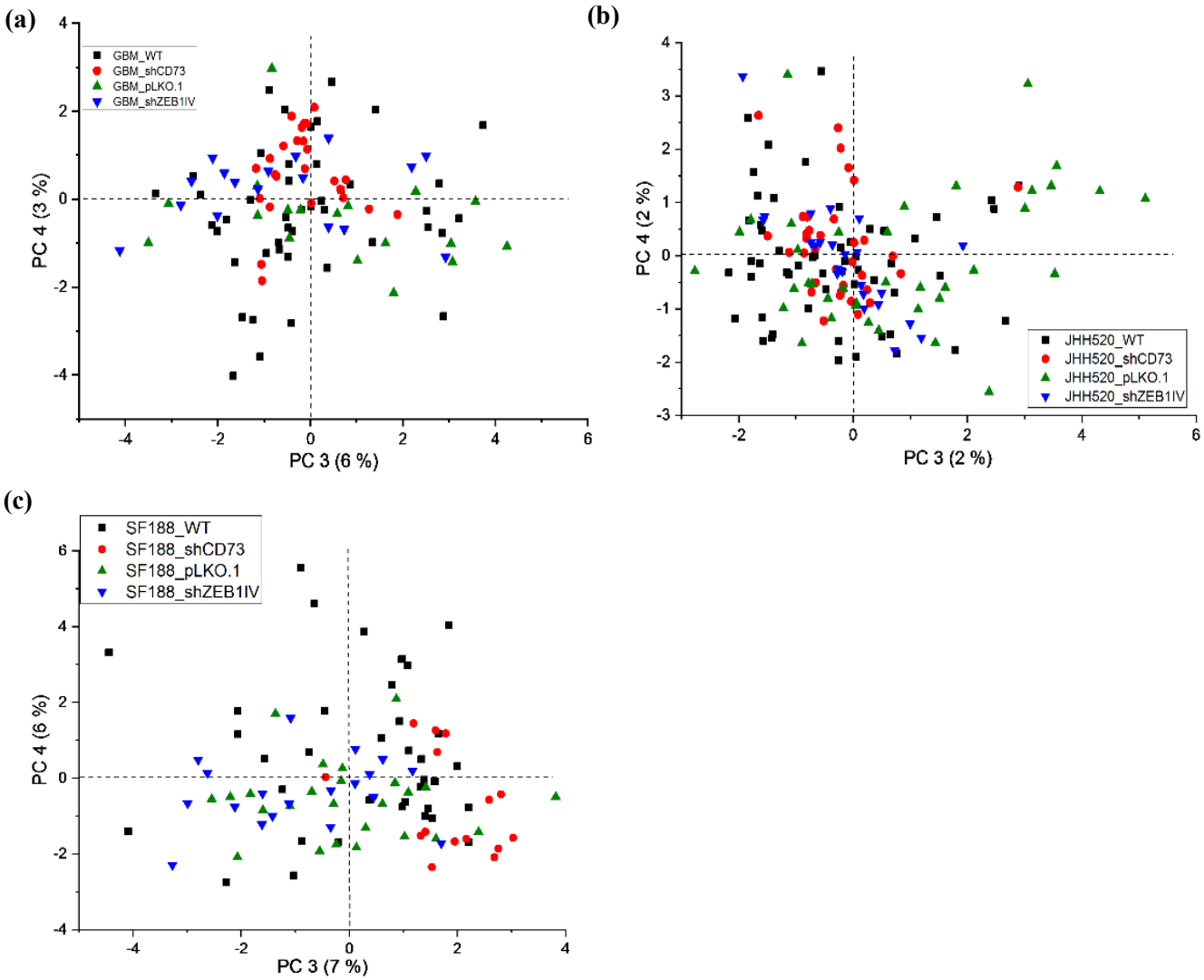

Figure 2.14. PCA scores for GSCs

with their controls and knockdowns (WT, pLKO.1, shCD73 and shZEB1) a) GBM1 b) JHH520 and c) SF188 scores plot.

Discrimination of T-cells/monocytes after incubation with TCMs from GSCs with respective knockdowns

PCA-LDA and SVM have successfully been applied in the classification of cells [293, 295]. Linear c-SVC and PCA-LDA discriminating monocytes and T-cells lines with their respective TCMs treatments. Since PCA-LDA and SVM are supervised techniques, the samples were assigned into predefined group prior to model creation. For TCM of GBM1 cell line: class 1 having GBM1-WT, class 2 having GBM1-shCD73, class 3 having GBM1-pLKO.1 and class 4 having GBM1-shZEB1. This grouping was carried out for the monocytes and T-cells after incubation with TCMs of other GSC lines. In the PCA-LDA,

the pre-processed spectral data were first reduced to PCs prior to performing the LDA whereas SVM utilizes the pre-processed spectral data. The PCA-LDA and SVM classification results are represented as a confusion matrix, which is a square matrix of rows (actual classes) and columns (predicted classes) [296]. These results were used in calculating the accuracy, sensitivity and specificity of RS to discriminate monocytes and T-cells after incubation with TCM of GSCs (WT, pLKO.1 shZEB1, shCD73) (Table 2.2).

The PCA-LDA model yielded a sensitivity and specificity between 83 - 100% and 85 - 100% respectively for the T-cells after incubation with TCM of all the three GSCs lines considered. Validation of this model against an independent test set yielded maximum sensitivity of 100%. The PCA-LDA model worked best for the T-cells treated with TCM of GBM1 with both sensitivity and specificity of 100% for all cell groups considered upon validation against the test set. Improved sensitivity and specificity could be achieved using the SVM model on the training set, with validation on an independent set yielding similar results as the PCA-LDA models. SVM model yielded a 100% accuracy on the training set for all cell lines considered whereas cell group sensitivities ranged between 71 - 100%. Specificity of over 78% was achieved for individual cell groups. The T-cells with TCM SF188-shZEB1 group had the most misclassification with a sensitivity of ~67% for both SVM and PCA-LDA model.

Discriminatory analysis performed using the monocyte samples also highlighted the model's ability to successfully classify cell groups. Both PCA-LDA and SVM models yielded a classification sensitivity over 67% on validating the model against an independent test set, with specificity over 72%. SVM model tend to have better performance for both T-cell and monocytes.

For cancer cell classification, the PCA-LDA model yielded sensitivity and specificity of about 40 - 78% and 57 - 67% respectively on validation against an independent test set (Table 2.3). The PCA-LDA had highest sensitivity and specificity for the JHH520 cell line. Improved sensitivity and specificity was observed on the SVM model using the training set. Validation against the test set yielded sensitivity and specificity of 40 - 88% and 53 - 70% respectively. On comparison to the immune cells, the cancer cell models looks to have a reduced performance. However, discrimination of the cell lines and their knockdown treatments were not random with sensitivities over 25% (4 classes) for all cell groups considered.

The combination of Raman and multivariate analysis techniques yielded good classification result for both the PCA-LDA and SVM models in discriminating differences of monocytes and T-cells after incubation with TCMs. These differences could be present due to the involvement of ZEB1 and CD73 in monocytes and T-cells activation and differentiation. This can offer accurate and fast alternative for non-invasive screening in clinical diagnosis.

Table 2.3. Summary of sensitivities illustrating the efficiency of RS to discriminate monocytes / T-cells for the training and test sets (in red).

T-cells training set (test set)									
PCA-LDA									
Cell line	Accuracy (%)	Sensitivity (%)				Specificity (%)			
		WT	shCD73	pLKO.1	shZEB1	WT	shCD73	pLKO.1	shZEB1
GBM1 WT vs shCD73 vs pLKO.1 vs shZEB1	90.4 (100)	100 (100)	87.5 (100)	100 (100)	77.9 (100)	85.3 (100)	94.3 (100)	88.6 (100)	93.0 (100)
JHH520 WT vs shCD73 vs pLKO.1 vs shZEB1	95.7 (91.7)	100 (100)	83.3 (71.4)	100 (100)	100 (100)	92.9 (85.7)	100 (100)	95.0 (90.0)	94.7 (90.5)
SF188 WT vs shCD73 vs pLKO.1 vs shZEB1	88.6 (79.2)	78.9 (70.0)	88.9 (100)	100 (80.0)	100 (66.7)	96.0 (85.7)	88.6 (72.2)	85.3 (78.9)	86.8 (90.0)
SVM									
GBM1 WT vs shCD73 vs pLKO.1 vs shZEB1	100 (100)	100 (100)	100 (100)	100 (100)	100 (100)	100 (100)	100 (100)	100 (100)	100 (100)
JHH520 WT vs shCD73 vs pLKO.1 vs shZEB1	100 (87.5)	100 (100)	100 (71.4)	100 (75.0)	100 (100)	100 (78.6)	100 (94.1)	100 (90)	100 (85.7)
SF188 WT vs shCD73 vs pLKO.1 vs shZEB1	100 (91.7)	100 (100)	100 (100)	100 (80.0)	100 (66.7)	100 (85.7)	100 (88.9)	100 (94.7)	100 (95.7)
Monocytes									
PCA-LDA									
GBM1 WT vs shCD73 vs pLKO.1 vs shZEB1	84.9 (87.5)	100 (100)	66.7 (71.4)	-	100 (100)	77.3 (81.8)	100 (100)	-	80.8 (87.5)
JHH520 WT vs shCD73 vs pLKO.1 vs shZEB1	73.2 (85.7)	88.9 (100)	72.7 (100)	58.3 (66.7)	77.8 (100)	68.8 (93.8)	73.3 (93.3)	79.3 (100)	71.9 (92.9)
SF188 WT vs shCD73 vs pLKO.1 vs shZEB1	86.7 (80)	76.9 (66.7)	100 (80)	-	88.9 (100)	94.1 (88.9)	81.8 (80)	-	85.7 (72.7)
SVM									
GBM1 WT vs shCD73 vs pLKO.1 vs shZEB1	100 (93.8)	100 (100)	100 (100)	-	100 (75)	100 (100)	100 (100)	-	100 (100)
JHH520 WT vs shCD73 vs pLKO.1 vs shZEB1	100 (95.2)	100 (100)	100 (100)	100 (100)	100 (50)	100 (90.5)	100 (86.7)	100 (100)	100 (86.7)
SF188 WT vs shCD73 vs pLKO.1 vs shZEB1	100 (88.6)	100 (83.3)	100 (80)	-	100 (100)	100 (87.5)	100 (88.9)	-	100 (81.8)

Table 2.4. Summary of sensitivities illustrating the efficiency of RS to discriminate GSCs for the training and test sets (in red).

GSCs Training set (test set)									
PCA-LDA									
Cell line	Accuracy	Sensitivity				Specificity			
		WT	shCD73	pLKO.1	shZEB1	WT	shCD73	pLKO.1	shZEB1
GBM1 WT vs CD73 vs pLKO.1 vs shZEB1	63.4 (61)	40 (56.3)	100 (75)	91.7 (66.7)	41.6 (50)	80.5 (65)	51.9 (57)	57.6 (60)	67.8 (63.3)
JHH520 WT vs CD73 vs pLKO.1 vs shZEB1	59.4 (73.5)	56.8 (77.8)	69.6 (63.6)	56 (53.8)	56.3 (50)	60.9 (56.3)	56.4 (64.1)	60.5 (67.6)	60 (66.7)
SF188 WT vs CD73 vs pLKO.1 vs shZEB1	69.2 (61.8)	61.5 (58.3)	80 (40)	62.5 (66.7)	84.6 (62.5)	74.4 (59)	67.3 (62)	71.4 (56)	65.4 (57.7)
SVM									
GBM1 WT vs CD73 vs pLKO.1 vs shZEB1	100 (64)	100 (62.5)	100 (87.5)	100 (66.7)	100 (33.3)	100 (65)	100 (57)	100 (63)	100 (70)
JHH520 WT vs CD73 vs pLKO.1 vs shZEB1	98 (62)	100 (77.8)	100 (45.5)	96 (46.2)	93.8 (75)	96.9 (53)	97.4 (66.7)	98.7 (67.6)	98.8 (59.5)
SF188 WT vs CD73 vs pLKO.1 vs shZEB1	96.9 (61.8)	96.2 (58.3)	100 (40)	93.8 (77.8)	100 (62.5)	97.4 (68.2)	96.4 (65.5)	98 (56)	96.2 (61.5)

TCMs from GSCs with blocked ZEB1 and CD73 can influence the expression of differentiation markers in monocytes

To investigate whether expression of ZEB1 and CD73 by GSCs affect monocyte phenotypes, monocytes were incubated with TCM of GSCs with blocked ZEB1 (shZEB1) or blocked CD73 (shCD73) as well as with baseline ZEB1 and CD73 expression (pLKO.1 and WT control cells). The flow cytometric analysis revealed that all examined TCMs (WT, pLKO.1, shZEB1 and shCD73) influenced the expression of monocyte surface markers. The gating strategy for monocyte is shown in the supplementary information (Figure 2.21). All TCMs with inhibited ZEB1 increased the percentage of cells expressing CD11c, a marker indicating the presence of monocyte-derived DCs [297], when compared to the media control sample cDMEM (Figure 2.15a). Moreover, TCMs from all WT GSC cell lines induced indoleamine 2,3-dioxygenase (IDO), a key enzyme of the kynurenine pathway that enhances immune escape [298], ($CD11c^+$ IDO^+) (Figure 2.15b). TCMs with inhibited ZEB1 derived from GBM1 and SF188 increased IDO expression in the $CD11c^+$ subset compared to TCM from

pLKO.1 (GBM1 and SF188) (Figure 2.15b). In addition, we found that PD-L1, a transmembrane protein that plays an important role in immunosuppression, was downregulated in monocytes-derived DCs incubated with TCMs from shZEB1 GBM1 and SF188 ($CD11c^+$ $PD\text{-}L1^+$) (Figure 2.15c). Finally, TCMs of GBM1 and SF188 with inhibited ZEB1 decreased the percentage of monocyte-derived DCs ($CD11c^+$) expressing HLA-DR (Figure 2.15d), a common MHC molecule on human cells, necessary for presentation of antigens to T-cells [299]. Our data suggest that ZEB1 expression in GSCs influences the expression of markers involved in immune escape on monocyte-derived DCs.

TCMs with inhibited ZEB1 in GBM1 and SF188 decreased the percentage of $CD64^+$, a marker of monocyte-derived MΦs [300], when compared to pLKO.1 (Figure 2.16a). However, not all TCMs affected the expression of HLA-DR by monocyte-derived MΦs ($CD64^+$) comparing to cDMEM (Figure 2.16b). We found an increase in IDO expression in monocyte-derived MΦs, incubated in TCMs of shZEB1 GBM1 and SF188 as well as shCD73 GBM1 and JHH520 (Figure 2.16c). Furthermore, all TCMs induced CD209 expression ($CD64^+$ $CD209^+$) indicating pro-tumorigenic MΦs [301]. TCMs from GBM1 with inhibited ZEB1 decreased CD209 expression in monocyte-derived MΦs compared to GBM1 controls (pLKO.1 and WT). TCM from SF188 with decreased CD73 reduced the expression of CD209 (Figure 2.16d). Finally, our results showed that all WT TCMs induced IDO ($CD64^+$ IDO^+) expression. TCMs of GBM1 and SF188 with inhibited ZEB1 and GBM1 and JHH520 with inhibited CD73 increased IDO expression comparing to respective pLKO.1 and WT controls (Figure 2.16d). These results match the Raman data, as at the PCA scores of monocytes distinct clusters were formed between GBM1 shZEB1 and WT. In addition, in comparison of the PCA scores in monocytes with TCM of SF188, a clear separation between the WT, shCD73 and shZEB1 groups was obtained. Our data together with the Raman spectra suggest that ZEB1 in GBM1 and SF188 and CD73 in JHH520 affect the phenotype of monocytes, polarizing them towards tumour-promoting populations.

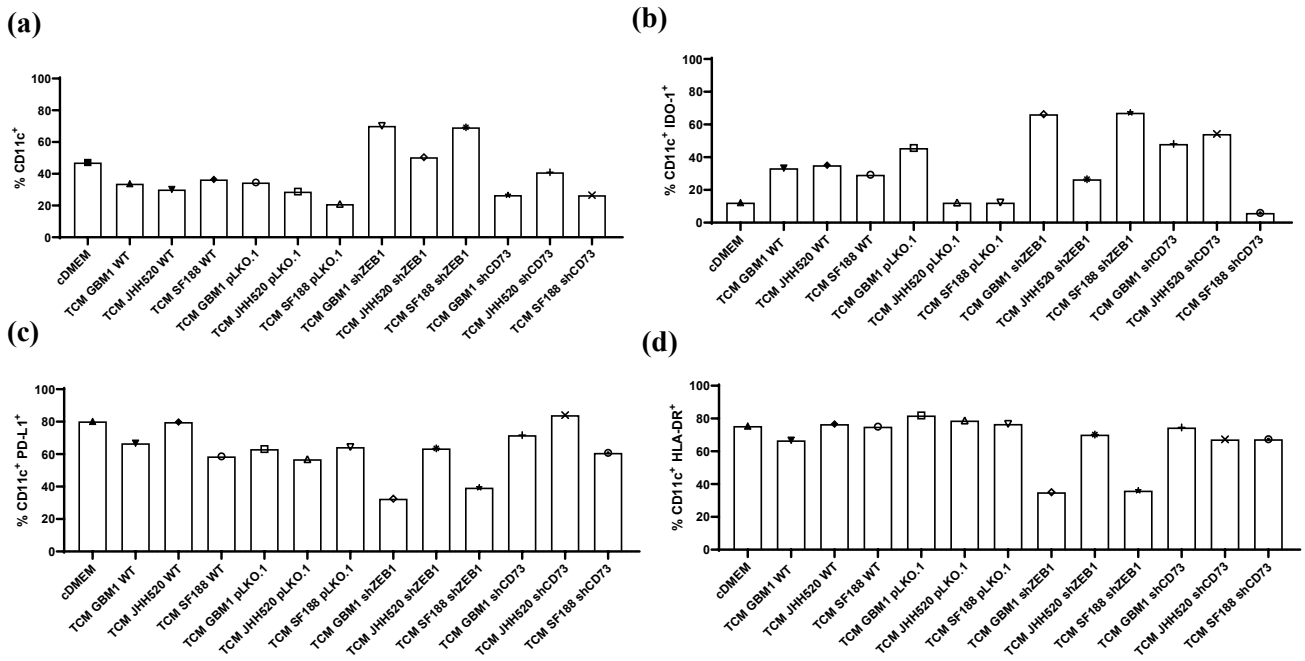

Figure 2.15. TCMs of GSCs influence the viability and the expression of differentiation markers of monocyte-derived DCs ($CD11c^+$).

Influence of TCMs from GSCs (WT, pLKO.1, shZEB1 and shCD73) on a) the viability and the expression of differentiation markers of monocyte-derived DCs ($CD11c^+$) b) IDO-1, c) PD-L1 and HDLA-DR isolated from a single blood donor. The expression of differentiation markers was evaluated flow cytometry.

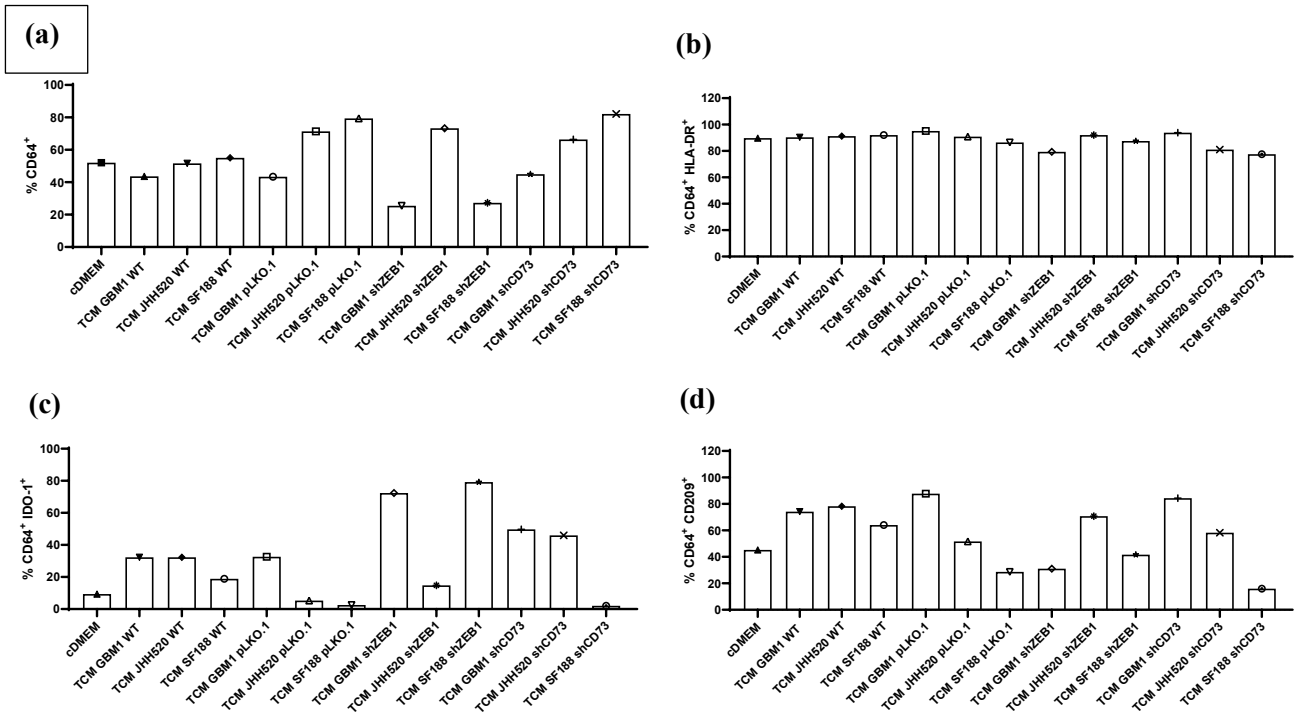

Figure 2.16. TCMs of GSCs influence the viability and the expression of differentiation markers of monocyte-derived MΦs (CD64$^+$).

Influence of TCMs of GSCs (WT, pLKO.1, shZEB1 and shCD73) on a) the viability and the expression of differentiation markers of monocyte-derived MΦs (CD64$^+$) b) HDLA-DR c) IDO-1 and d) CD209 from a single blood donor. The expression of differentiation markers was evaluated by flow cytometry analysis.

Reduced expression of ZEB1 and CD73 in GSCs influences the phenotype of T-cells

To describe the impact of ZEB1 and CD73 on T-cell polarisation into different T-cell subsets, T-cells were cultured with different TCMs (WT, pLKO.1, shZEB1, shCD73) for 5 days and then stimulated to produce cytokines. The expression of cell surface markers CD4, CD8 and intracellular cytokines was determined by flow cytometry. The gating strategy for T-cells is shown in the supplementary information (Figure 2.22). The different cytokines produced can indicate whether they support the tumour cell killing (IFN-γ, TNF-α) [302, 303] or they inhibit tumour cell killing (IL-10) [304]. The percentage of live CD4$^+$ T-cells decreased when incubated with TCM from the two cell lines GBM1 and SF188 upon ZEB1 inhibition (shZEB1) (Figure 2.17a). CD4$^+$ T-cells produced less TNF-α, IFN-γ and IL-2 in the same samples (Figure 2.17b-d). The percentage of CD4$^+$ T-cells secreting IL-2 decreased when incubated with TCM derived from JHH520 and SF188 with a CD73 knockdown when compared to cDMEM. IL-2 is an important factor for the maintenance of CD4$^+$ T-cells [305].

The different TCMs of GSCs (WT, pLKO.1, shZEB1, shCD73) also upregulated the production of several cytokines in $CD8^+$ T-cells (Figure 2.18a). IFN-γ secretion by $CD8^+$ T-cells was decreased after incubation with shZEB1 GBM1 TCM, shZEB1 SF188 TCM and shCD73 JHH20 TCM and shCD73 SF188 TCM (Figure 2.18b). Along with the percentage of live T-cells, TCMs of shZEB1 GBM1 and SF188 reduced the secretion of TNF-α and IFN-γ ($CD8^+$ TNF- α and IFN-γ^+) compared with pLKO.1 (Figure 2.18c). Finally, the percentage of $CD8^+$ T-cells secreting IL-2 ($CD8^+$ $IL2^+$) was reduced when treated with TCM JHH520 and SF188 shCD73 while the percentage of $CD8^+$ T-cells treated with all WT TCMs increased the IL-2 secretion. The reduced expression of ZEB1 in GBM1 and SF188 reduced TNF-α and IFN-γ production in both, $CD4^+$ and $CD8^+$ T-cells, therefore, comparing to PCA scores distinct clusters between T-cells with TCM pLKO.1 and shZEB1 were obtained. However, the reduced expression of ZEB1 in JHH520 led only to a decrease in IL-2 secretion while reduced expression of CD73 in JHH520 had a stronger effect on the cytokine profile of T-cells. These results match the PCA scores of the Raman data, where T-cells formed distinct clusters when exposed to TCMs from pLKO.1 and shCD73 GSCs. No distinct clusters were observed at the PCA scores between pLKO.1 and shZEB1 of JHH520 in T-cells.

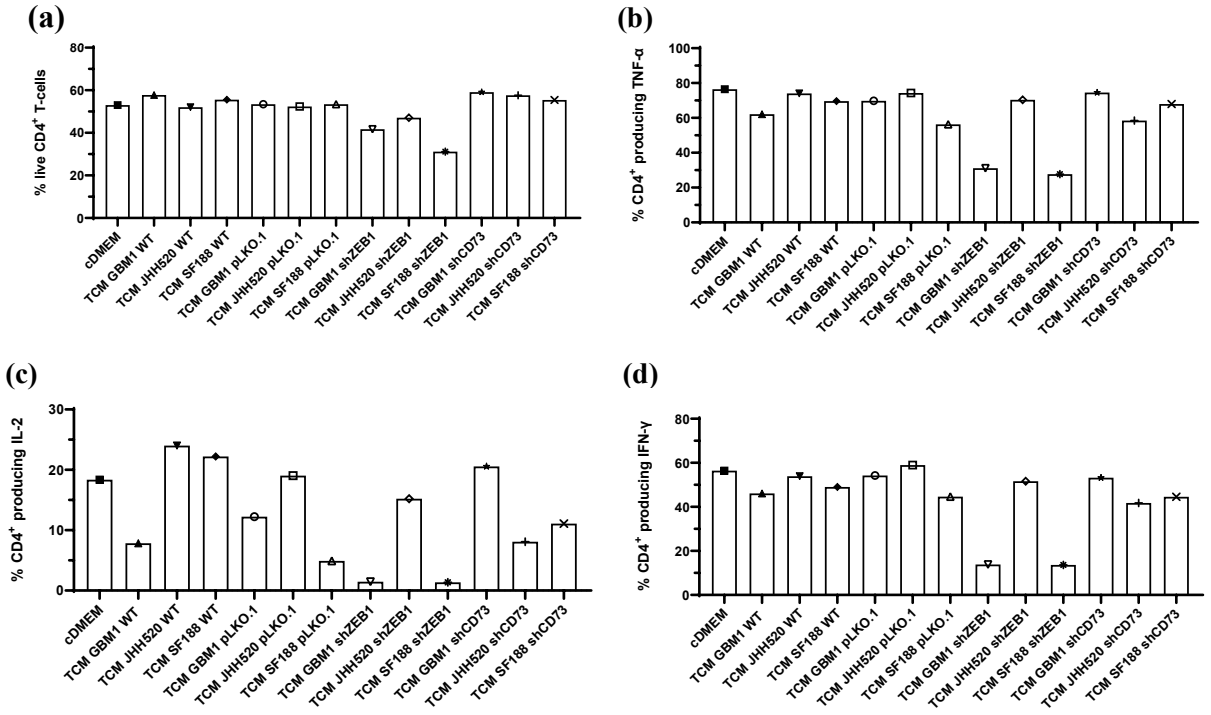

Figure 2.17. TCMs of GSCs influence the viability and the expression of differentiation markers of CD4$^+$ T-cells.

Influence of TCMs of GSCs (WT, pLKO.1, shZEB1 and shCD73) on a) the viability and the expression of differentiation markers of CD4$^+$ T-cells b) TNF-a c) IL-2 and d) IFN-γ from a single blood donor. The expression of differentiation markers was evaluated by means of flow cytometry analysis.

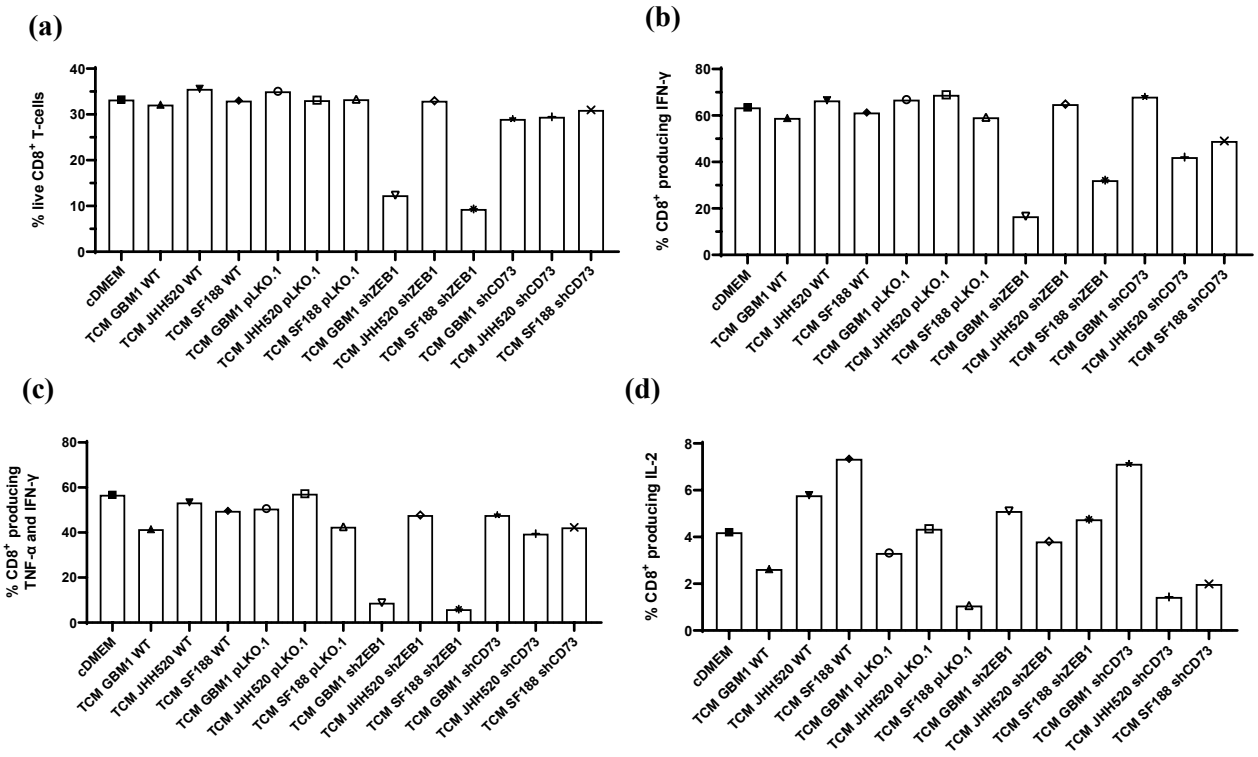

Figure 2.18. TCMs of GSCs influence the viability and the expression of differentiation markers of CD8$^+$ T-cells.

Influence of TCMs of GSCs (WT, pLKO.1, shZEB1 and shCD73) on a) the viability and the expression of differentiation markers of CD8$^+$ T-cells b) IFN-γ c) TNF-a and IFN-γ and d) IL-2 from a single blood donor. The expression of differentiation markers was evaluated by means of flow cytometry analysis.

2.2.6 Conclusion

This study shows the ability of Raman spectroscopy in combination with chemometrics to discriminate T-cells and monocytes upon incubation with TCM of GSCs in different conditions, therefore, to detect glioma associated neuroinflammation caused by molecular differences. Flow cytometry analysis of the same samples used for Raman spectroscopy suggests that GSCs with ZEB1 and CD73 inhibition can actively influence the phenotype of T-cells and monocytes driving their differentiation into a population of mixed pro-inflammatory and anti-inflammatory MΦs and DCs. The changes involved a decrease in the percentage of CD64$^+$ cells and an increase of CD11c$^+$ cells. We observed increased expression of CD209 (CD64$^+$ CD209$^+$) after treatment with TCM of all three WT GSCs, indicating an increase of the tumour-associated MΦs. However, CD73 inhibition only decreased CD209 expression in monocyte-derived MΦs. TCMs of GSCs also influenced the differentiation of CD4$^+$ and CD8$^+$ T-cells. TCMs GBM1 and SF188 with inhibited ZEB1 decreased the expression of IL-2 in CD4$^+$ T-cells, while TCMs

with inhibited CD73 decreased IL-2 production. Our preliminary data suggest that GSCs produce soluble factors that influence monocytes and T-cells differentiation, most probably into suppressive subsets.

PCA-LDA and Linear SVM classification models achieved specificity and sensitivity above 80% for most cell groupings on a training set and 70% on validation on an independent test set. Future studies will involve increasing the sample set to account for interperson variability

Acknowledgment

Chima would like to thank the University of Otago for the PhD scholarship. Julia would like to thank the Duesseldorf School of Oncology for the PhD Scholarship. Sara thanks the Dodd-Walls Centre for Photonics and Quantum for supporting her salary. Many thanks to Karlis Berzins for making the graphical abstract. This work was supported by a University of Otago Research and Lottery Health Research grant.

Declaration of conflict of interest

None

2.2.7 Supplement

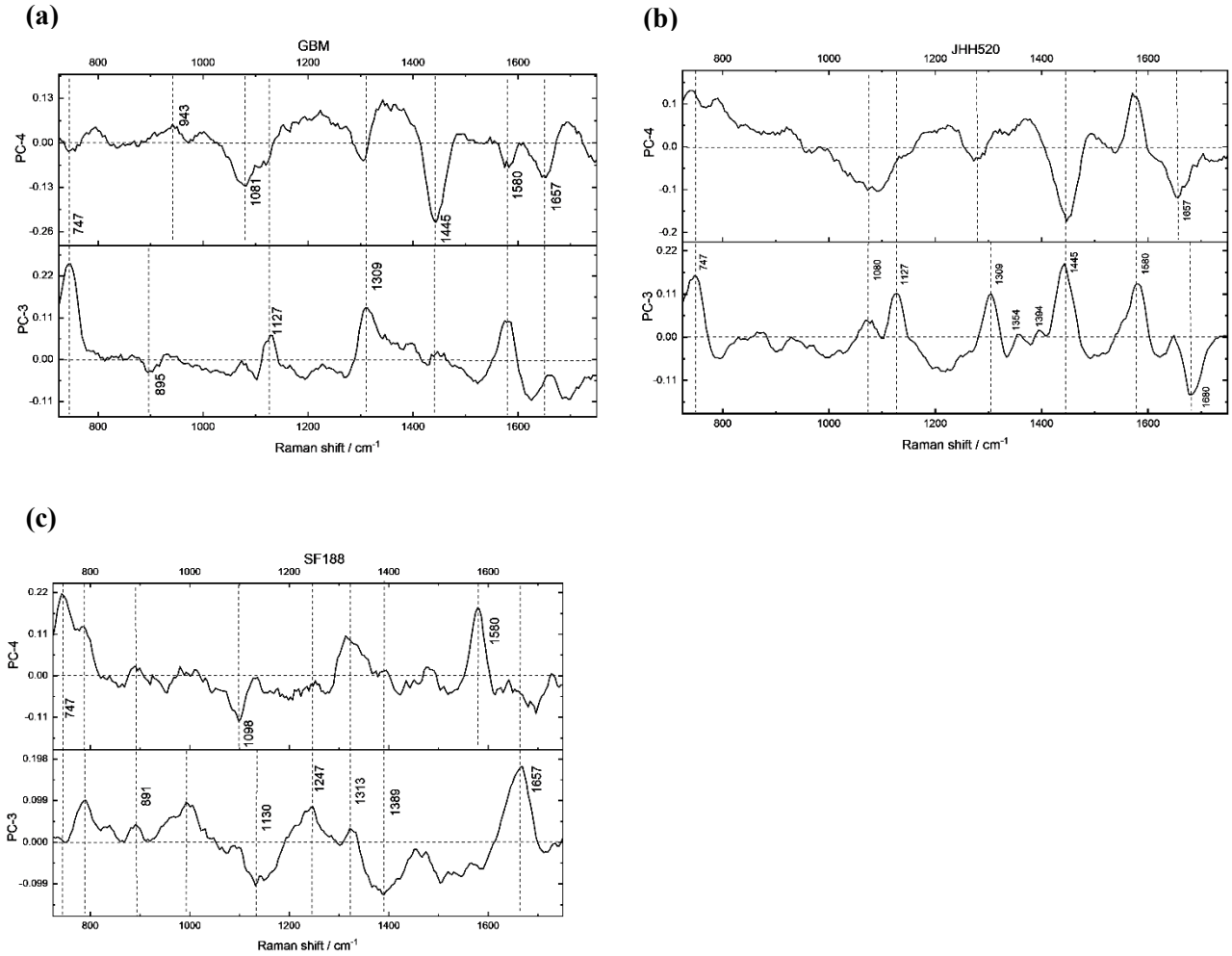

Figure 2.19. PCA loadings for GSCs

with their controls and knockdowns (WT, pLKO.1, shCD73 and shZEB1) a) GBM1 b) JHH520 and c) SF188 scores plot.

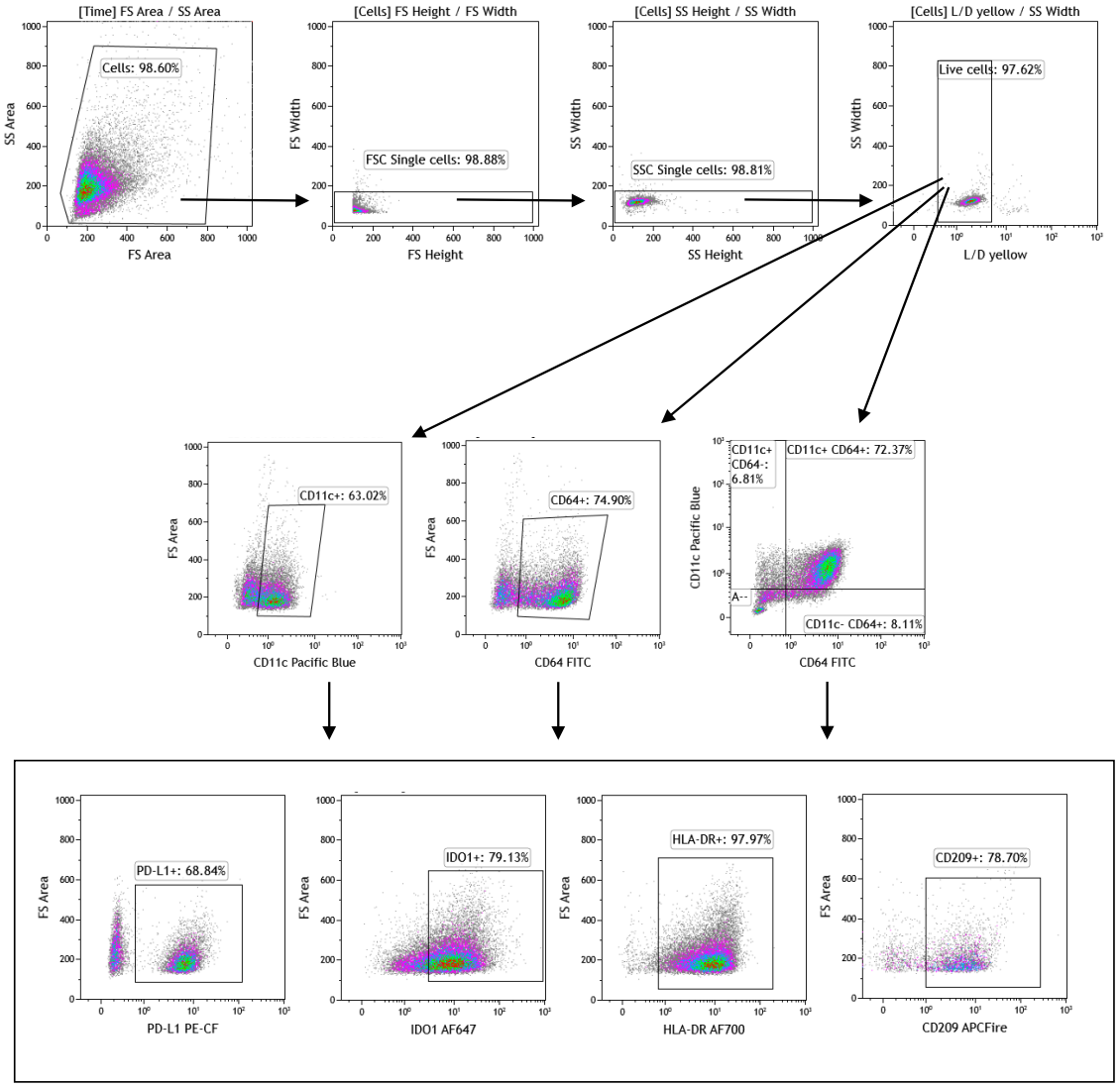

Figure 2.20. Gating strategy for human monocytes.

All data points were analysed and doublets were excluded by using forward scatter height and area (FSC-H/FSC-A) and side scatter height and area (SSC-H/SSC-A). Live cells were detected by gating on Fixable yellow negative cells based on a fluorescence minus one (FMO) control. The gate for CD11c, CD64 or the combination of the two was adjusted by using FMO controls, which did not contain the antibody against either CD11c or CD64. Similarly, the gates for PD-L1, IDO-1, HLA-DR and CD209 were based on FMO controls for the specific marker.

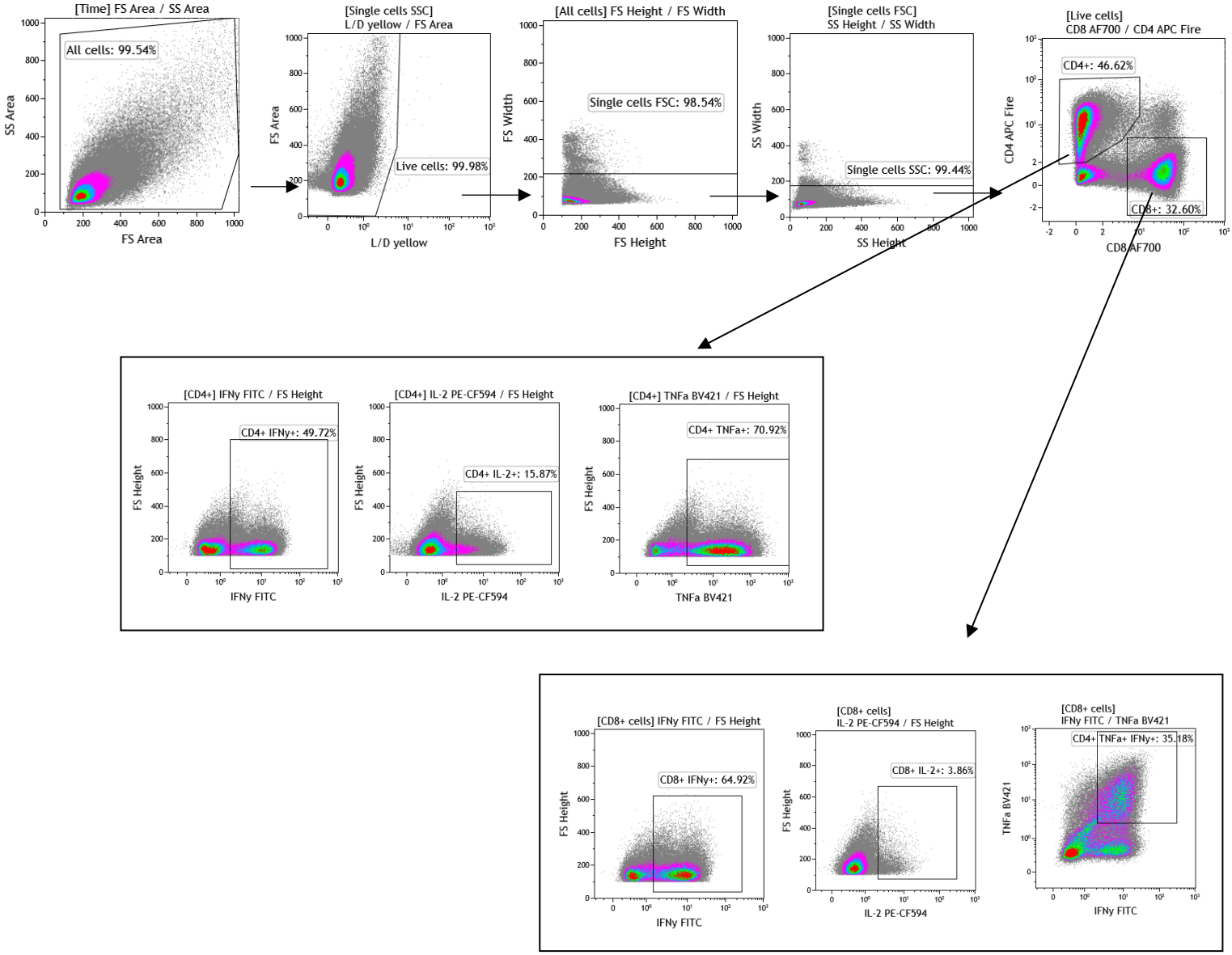

Figure 2.21. Gating strategy for human T-cells.

All data points were analysed and doublets were excluded by using forward scatter height and area (FSC-H/FSC-A) and side scatter height and area (SSC-H/SSC-A). Live cells were detected by gating on Fixable yellow negative cells based on a fluorescence minus one (FMO) control. The gate for CD4, CD8 was adjusted by using FMO controls, which did not contain the antibody against either CD4 or CD8. Similarly, the gates for IFN-γ, IL-2 and TNF-α were based on FMO controls for the specific marker.

3. General Discussion

This PhD thesis describes the role of CD73 in highly aggressive GSCs' growth and the label-free detection of the immunogenic GSCs upon CD73 inhibition and modulation of EMT-like reprogramming. GSCs contribute to the progression and tumour recurrence of GBM and are enriched by the EMT-like genetic preprograming. Current standard therapeutics have limited impact on eradicating this particular subpopulation of cells, therefore, innovative therapies are needed to precisely target GSCs. Most recently, EMT has been shown to be also regulated by CD73, both in ovarian and hepatocellular carcinoma. The aim of this thesis is to present the role of the enzymatic and non-enzymatic function of CD73 in GBM progression and its potential as a novel therapeutic target for GSC-specific therapies. Furthermore, CD73, through its enzymatic activity, promotes the generation of an immunosuppressive microenvironment that further promotes the progression of cancer. CD73 impairs the anti-tumour cell responses including T-cell activation, clonal expansion of tumour-specific T-cells and tumour cell killing by CTL [238]. The EMT status of cancer cells has also been discussed to impact the cancers´ immunogenicity [96]. As such, ZEB1 increases the expression of T-cell activation repressor (PD-L1) on the surface of cancer cells [97]. Hence, the role of CD73 and EMT modulation in immune regulation was investigated and Raman spectroscopy was applied to detect glioma-associated inflammation. Raman imaging has been successfully used to define invasive margin of GBMs, both experimentally and clinically and has therefore been emerging as a precise therapy guidance and diagnostic tool [239, 240].

Considering the correlation between CD73 inhibition and EMT activator ZEB1 reduction in ovarian cancer, we found that ZEB1-dependent reduction of EMT decreased CD73 expression in GBM cultures. To evaluate a possible reciprocal regulation of EMT and CD73 and the enzymatic and non-enzymatic activity of CD73 in GSCs, genetic knockdown of CD73 was generated using RNA interference in GSCs and all GSC cell lines were treated with the enzymatic inhibitor APCP. Both genetic knockdown and pharmacological inhibition of CD73 significantly reduced the expression of the EMT activator SNAIL1 (Section 2.1). SNAIL1 has been shown to promote invasion in human glioblastomas [225]. Coherently, the results showed impaired invasiveness and clonogenicity in GSCs with impaired CD73 expression. Clonogenicity is an important characteristic of GSCs, as they can be responsible for tumour recurrence in GBM patients [241]. The GSC population was effectively reduced by CD73 protein inhibition whereas no similar effect was observed upon enzymatic inhibition. Our results indicate the crucial role of CD73 expression in GSCs' viability, given the significantly reduced cell viability after CD73 inhibition in all tested GSC lines. Although our results highlighted the possible reciprocal regulation between EMT and CD73, the underlying mechanisms are still to be elucidated. Recent data in gastric cancer suggests that CD73 promotes EMT through the activation of GTPase-activating protein RICS, that directly interacts with β-catenin [242]. Considering that the clinically approved compound PTX increases intracellular levels of cAMP, that can affect the EMT mechanism [237, 238], the effect of this

drug on the growth of investigated GSC in vitro cultures was evaluated. Application of PTX effectively inhibited ZEB1 and CD73 expression and significantly decreased viability, clonogenicity and invasion of GSC cultures (Figure 2.5). Our results indicate that PTX inhibits ZEB1 leading to the decrease of its downstream CD73 expression, explaining the phenotype of GSCs after PTX treatment. These results are supported by the evidence that PTX has been reported to possess anticancer properties by increasing the susceptibility of cancer cells to radiation therapy [243].

Interestingly, selective inhibition of CD73 enzymatic activity decreased only the invasive properties of GSCs. Indeed, the addition of ADO could indeed rescue the decreased invasive phenotype caused by APCP. In addition, CD73 inhibition reduced the mRNA expression of the metalloproteinase MMP2. Our findings illustrate that GBM invasion could be partially regulated by CD73 enzymatic activity via this metalloproteinase, giving rise to the question whether the ADO signalling is also involved in GBM invasiveness. This assumption is underlined by recent data revealing the involvement of A_3AR in GBM invasion. Therefore, we investigated the effect of the pharmacological inhibition of A_3AR on GSC maintenance. The results showed that direct A_3AR inhibition effectively impaired the viability through the increase of apoptotic cells, invasiveness and clonogenicity of GSC cultures (Figure 2.6). Similarly, treatment with A_3AR agonist led to inhibition of tumour growth of HCC [244]. Conversely, it has also been reported that A_3AR activation led to a reduced tumour growth and proliferation in several cancers including lymphomas and prostate cancers [245]. In general, both blockage and activation of A_3AR impaired cell proliferation and apoptosis, a fact that can be explained by the different factors such as agonist/antagonist concentration, simultaneous interactions of the receptor, cell type and TME [134]. Furthermore, we could identify the importance of the reciprocal regulation of A_3AR and EMT via ZEB1 (Figure 2.6). Given the involvement of A_3AR and ADO in invasiveness of GSCs, the question to be answered was, whether A_3 could be the main ADO receptor regulating this mechanism. Our results illustrated that inhibition of the A_3AR in the paediatric GSC line SF188 constantly inhibited the invasive properties. However, supplementation with ADO could rescue the effect in the adult-derived cell lines. Our findings indicate the presence and importance of other ADO receptors on the adult-derived cell lines and highlight possible differences between paediatric and adult gliomas. Nevertheless, the overall evidence speaks for the high therapeutic potential of targeting the A_3AR in GSCs while further studies with further mechanistic insight into this phenomenon could support the potential for more therapeutic combinations.

CD73 has also been characterised as novel target for cancer immunotherapy given its involvement in tumour escape via the production of the immunosuppressive ADO [163]. In addition, cancer metastasis and EMT can be promoted by modulation of immune cells towards immunosuppressive regulatory cells [109]. Therefore, since EMT and CD73 are critical in cancer progression and chemoresistance [34, 164], we aimed to evaluate consequences of EMT-like reprogramming and CD73 inhibition on GBM immunogenicity. In addition, we assessed whether confocal Raman spectroscopy in

combination with chemometrics would sufficiently detect molecular differences of monocytes and T-cells in the tumour context (Section 2.2).

TCMs of three GSC lines (GBM1, JHH520 and SF188) with their controls (WT and empty vector pLKO.1) and respective knockdowns (shZEB1 and shCD73) were generated. Monocytes and T-cells were incubated with these TCMs to assess the ability of RS to discriminate between monocytes and T-cells with varied phenotypes (Section 2.2). The spectra of monocytes and T-cells were characterized by bands representing proteins (754, 1578 and 1003 cm^{-1}) as well as nucleic acids (830, 787, 884, 1093 and 1258 cm^{-1}). The peak at 1332/1334 cm^{-1} could also be associated with guanine (DNA/RNA) nucleic acids. The peaks 1258 cm-1 and 1309/1310 cm^{-1} were associated with amide III N-H bending and C-N stretching vibrations in lipids and protein, while the CH_2/CH_3 stretching and amide I vibrations were characterized by peaks at 1450 cm^{-1} and 1657 cm^{-1} respectively. Preliminary spectral analysis was performed using PCA on the monocytes and T-cells after incubation with GSCs with inhibited CD73 (shCD73) as well as ZEB1 (shZEB1) and the data points plotted as a scatter represented clusters of cell groups (Figure 2.11). T-cells with TCM GBM1 pLKO.1 clustered in the positive PC4 space while T-cells with TCM GBM1 shZEB1 and shCD73 clustered in the negative PC4 space. The differences of the clusters can be explained by the PC4 loadings plot due to contributions from protein including bands at 1014, 1322, 1464 and 1679 cm^{-1} and nuclei acids at 796, 833, 956, 1108, 1134, 1348 and 1585 cm^{-1} of T-cells with TCM pLKO.1 (Figure 2.12). The negative PC4 loadings could indicate the presence of higher lipid levels in the T-cells with TCM GBM1 with inhibited ZEB1 and CD73. T-cells with TCM JHH520 pLKO.1 and JHH520 shZEB1 formed clusters in the negative PC3 space while the T-cells with TCM JHH520 WT and shCD73 formed clusters for in the positive PC3 space. The loadings plot showed similarities to the one for the GBM cell line, with separation of pLKO.1 and shZEB1, arising from protein and nuclei acid contributions (Figure 2.12). However, different contribution of the clusters of the T-cells with TCM SF188 were observed (Figure 2.12). According to loading plot, T-cells with TCM SF188 pLKO.1 showed higher contributions from lipids (band at 1450 and 1657 cm^{-1}) and nuclei acids (1089 cm^{-1}). In addition, monocytes with TCM JHH520 pLKO.1 and TCM JHH520 shZEB1 scores formed clusters in the positive PC2 space with corresponding loadings, showing majority contributions associated with both lipid and protein. In monocytes treated with the TCM of GBM1 and SF188 (WT, pLKO.1, shCD73 and shZEB1), cell groups showed clear separations indicating the variability across the samples set.

Supplementary to the usage of Raman technology to discriminate T-cell and monocyte clusters, differences in the phenotype of these immune cells were assessed using flow cytometry. T-cells were cultured with different TCMs from wildtype and modified cell lines (WT, pLKO.1, shZEB1 and shCD73) for 5 days, that were then stimulated to produce cytokines. We observed that inhibition of ZEB1 and CD73 expression in GSCs influenced the phenotype and differentiation of T-cells. The different TCMs of GSCs downregulated the production of several cytokines in $CD4^+$ and $CD8^+$ T-cells,

including IFN-γ and IL-2. IFN-γ, is a cytokine that participates in various immunological functions and in regulation of anti-inflammatory processes [306]. IFN-γ promotes the polarization of the pro-inflammatory profile of M1-type MΦs, that exhibit an increased phagocytic ability [307] leading to an effective immune response. This includes enhanced antigen presentation through upregulation of class II MHC, increased ROS and NOS production as well as increased secretion of pro-inflammatory cytokines [308]. However, due to the complexity of IFN-γ it is difficult to classify it as a pro-inflammatory cytokine or anti-inflammatory [309]. Additionally, we assessed the effect of TCM from GSCs with inhibited ZEB1 and CD73 on monocytes, that were also cultured with different TCMs, showing different molecular background. The changes involved a decrease in the percentage of $CD64^+$ cells and an increase in $CD11c^+$ cells, as well as an increase of tumour-associated MΦs. Furthermore, our results showed that PD-L1 was downregulated in monocytes-derived DCs incubated, with TCMs from shZEB1 GBM1 and SF188. This PD-L1 surface expression on DCs has been demonstrated to suppress $CD4^+$ and $CD8^+$ T-cell activity [310]. Concisely, it has been shown that factors produced by GSCs may be responsible for skewing macrophages towards a M2 phenotype in the GBM's TME [311].

In conclusion, our preliminary data indicate that GSCs produce soluble factors that influence monocytes and T-cells differentiation, most probably towards suppressive subsets due to the presence of the EMT activator ZEB1 and CD73. Recent data indicate a role for CD73 in regulating the inflammatory TME. However, this was mediated via the reduction of Treg, microglia and MΦ populations through the secretion of IL-6, CCL17 and CCL22 [312]. Despite that, it has been recently shown that the loss of ZEB1 in stromal fibroblasts reduced the recruitment of cancer-associated immune cells [313]. According to our data, inhibition of ZEB1 decreased IFN-γ which could explain the reduced recruitment of these immune cells.

The observed clusters of T-cells and monocytes in the control and knockdown conditions could be explained by the different cytokine profiles of the immune cells, which indicated the presence of mixed populations of pro- and anti-inflammatory MΦs, DCs and $CD4^+$ and $CD8^+$ T-cells. Therefore, results obtained from traditional immunology correspond to the RS results. As our results indicate that GSCs with ZEB1 and CD73 inhibition can actively influence the phenotype of T-cells and monocytes, further investigation would be required to elucidate whether immunogenic GBMs, with active EMT-like status and CD73, would be more suitable for treatment with immune checkpoint blockers.

In conclusion, this PhD thesis highlights the role of the enzymatic and non-enzymatic activity of CD73 on GBM growth and the ability of RS to detect glioma-associated inflammation upon CD73 and ZEB1 inhibition. In this work, two exciting targets for novel anti-GSC-therapies are identified, CD73 and A_3AR, whose inhibition robustly decreased the growth of GBM cultures. Our data highlighted the importance of CD73 and ZEB1 expression in modulating cytokine secretion in monocytes and T-cells and hence their role in glioma-associated immunosuppression. Finally, our data displayed the ability of

RS to discriminate monocytes and T-cells with different phenotypes based on their molecular composition with main differences arising from DNA profile and protein/lipid content.

4. Bibliography

1. Ostrom, Q.T., et al., *CBTRUS Statistical Report: Primary brain and other central nervous system tumors diagnosed in the United States in 2010-2014.* Neuro Oncol, 2017. **19**(suppl_5): p. v1-v88.
2. Thakkar, J.P., et al., *Epidemiologic and molecular prognostic review of glioblastoma.* Cancer Epidemiol Biomarkers Prev, 2014. **23**(10): p. 1985-96.
3. Louis, D.N., et al., *The 2016 World Health Organization Classification of Tumors of the Central Nervous System: a summary.* Acta Neuropathol, 2016. **131**(6): p. 803-20.
4. Stupp, R., et al., *Effects of radiotherapy with concomitant and adjuvant temozolomide versus radiotherapy alone on survival in glioblastoma in a randomised phase III study: 5-year analysis of the EORTC-NCIC trial.* Lancet Oncol, 2009. **10**(5): p. 459-66.
5. Hegi, M.E., et al., *MGMT gene silencing and benefit from temozolomide in glioblastoma.* N Engl J Med, 2005. **352**(10): p. 997-1003.
6. Weller, M., et al., *EANO guideline for the diagnosis and treatment of anaplastic gliomas and glioblastoma.* Lancet Oncol, 2014. **15**(9): p. e395-403.
7. Ohgaki, H. and P. Kleihues, *The definition of primary and secondary glioblastoma.* Clin Cancer Res, 2013. **19**(4): p. 764-72.
8. Guan, X., et al., *Molecular subtypes of glioblastoma are relevant to lower grade glioma.* PLoS One, 2014. **9**(3): p. e91216.
9. Verhaak, R.G., et al., *Integrated genomic analysis identifies clinically relevant subtypes of glioblastoma characterized by abnormalities in PDGFRA, IDH1, EGFR, and NF1.* Cancer Cell, 2010. **17**(1): p. 98-110.
10. Wick, A., et al., *Glioblastoma in elderly patients: solid conclusions built on shifting sand?* Neuro Oncol, 2018. **20**(2): p. 174-183.
11. Kaffes, I., et al., *Human Mesenchymal glioblastomas are characterized by an increased immune cell presence compared to Proneural and Classical tumors.* Oncoimmunology, 2019. **8**(11): p. e1655360.
12. Ravikanth, R., *Advanced Magnetic Resonance Imaging of Glioblastoma Multiforme.* J Neurosci Rural Pract, 2017. **8**(3): p. 439-440.
13. Verger A, L.K., *PET Imaging in Glioblastoma: Use in Clinical Practice.* De Vleeschouwer S, editor. Glioblastoma [Internet]. Brisbane (AU): Codon Publications, 2017.
14. Riva, M., et al., *3D intra-operative ultrasound and MR image guidance: pursuing an ultrasound-based management of brainshift to enhance neuronavigation.* Int J Comput Assist Radiol Surg, 2017. **12**(10): p. 1711-1725.
15. Zhang, J., et al., *Accuracy of Raman spectroscopy in differentiating brain tumor from normal brain tissue.* Oncotarget, 2017. **8**(22): p. 36824-36831.
16. Auner, G.W., et al., *Applications of Raman spectroscopy in cancer diagnosis.* Cancer Metastasis Rev, 2018. **37**(4): p. 691-717.
17. Noch, E.K., R. Ramakrishna, and R. Magge, *Challenges in the Treatment of Glioblastoma: Multisystem Mechanisms of Therapeutic Resistance.* World Neurosurg, 2018. **116**: p. 505-517.
18. Kesari, S., *Understanding glioblastoma tumor biology: the potential to improve current diagnosis and treatments.* Semin Oncol, 2011. **38 Suppl 4**: p. S2-10.
19. Diksin, M., S.J. Smith, and R. Rahman, *The Molecular and Phenotypic Basis of the Glioma Invasive Perivascular Niche.* Int J Mol Sci, 2017. **18**(11).

20. Persano, L., et al., *Glioblastoma cancer stem cells: role of the microenvironment and therapeutic targeting.* Biochem Pharmacol, 2013. **85**(5): p. 612-622.
21. Zou, J.P., et al., *Human glioma-induced immunosuppression involves soluble factor(s) that alters monocyte cytokine profile and surface markers.* J Immunol, 1999. **162**(8): p. 4882-92.
22. Chen, J., et al., *A restricted cell population propagates glioblastoma growth after chemotherapy.* Nature, 2012. **488**(7412): p. 522-6.
23. Lau, E.Y., N.P. Ho, and T.K. Lee, *Cancer Stem Cells and Their Microenvironment: Biology and Therapeutic Implications.* Stem Cells Int, 2017. **2017**: p. 3714190.
24. Calabrese, C., et al., *A perivascular niche for brain tumor stem cells.* Cancer Cell, 2007. **11**(1): p. 69-82.
25. Dirkse, A., et al., *Stem cell-associated heterogeneity in Glioblastoma results from intrinsic tumor plasticity shaped by the microenvironment.* Nat Commun, 2019. **10**(1): p. 1787.
26. Kahlert, U.D., G. Nikkhah, and J. Maciaczyk, *Epithelial-to-mesenchymal(-like) transition as a relevant molecular event in malignant gliomas.* Cancer Lett, 2013. **331**(2): p. 131-8.
27. Thiery, J.P., *Epithelial-mesenchymal transitions in development and pathologies.* Curr Opin Cell Biol, 2003. **15**(6): p. 740-6.
28. Thiery, J.P., *[Epithelial-mesenchymal transitions in cancer onset and progression].* Bull Acad Natl Med, 2009. **193**(9): p. 1969-78; discussion 1978-9.
29. Kalluri, R. and R.A. Weinberg, *The basics of epithelial-mesenchymal transition.* J Clin Invest, 2009. **119**(6): p. 1420-8.
30. Mani, S.A., et al., *The epithelial-mesenchymal transition generates cells with properties of stem cells.* Cell, 2008. **133**(4): p. 704-15.
31. Mikheeva, S.A., et al., *TWIST1 promotes invasion through mesenchymal change in human glioblastoma.* Mol Cancer, 2010. **9**: p. 194.
32. Sui, H., et al., *Epithelial-mesenchymal transition and drug resistance: role, molecular mechanisms, and therapeutic strategies.* Oncol Res Treat, 2014. **37**(10): p. 584-9.
33. Kahlert, U.D., et al., *Activation of canonical WNT/beta-catenin signaling enhances in vitro motility of glioblastoma cells by activation of ZEB1 and other activators of epithelial-to-mesenchymal transition.* Cancer Lett, 2012. **325**(1): p. 42-53.
34. Kahlert, U.D., et al., *ZEB1 Promotes Invasion in Human Fetal Neural Stem Cells and Hypoxic Glioma Neurospheres.* Brain Pathol, 2015. **25**(6): p. 724-32.
35. Siebzehnrubl, F.A., et al., *The ZEB1 pathway links glioblastoma initiation, invasion and chemoresistance.* EMBO Mol Med, 2013. **5**(8): p. 1196-212.
36. Wellner, U., et al., *The EMT-activator ZEB1 promotes tumorigenicity by repressing stemness-inhibiting microRNAs.* Nat Cell Biol, 2009. **11**(12): p. 1487-95.
37. Feldman, N., A. Rotter-Maskowitz, and E. Okun, *DAMPs as mediators of sterile inflammation in aging-related pathologies.* Ageing Res Rev, 2015. **24**(Pt A): p. 29-39.
38. Lee, M.S. and Y.J. Kim, *Pattern-recognition receptor signaling initiated from extracellular, membrane, and cytoplasmic space.* Mol Cells, 2007. **23**(1): p. 1-10.
39. Akira, S., S. Uematsu, and O. Takeuchi, *Pathogen recognition and innate immunity.* Cell, 2006. **124**(4): p. 783-801.
40. Kawai, T. and S. Akira, *The role of pattern-recognition receptors in innate immunity: update on Toll-like receptors.* Nat Immunol, 2010. **11**(5): p. 373-84.
41. Jiménez-Dalmaroni, M.J., M.E. Gerswhin, and I.E. Adamopoulos, *The critical role of toll-like receptors--From microbial recognition to autoimmunity: A comprehensive review.* Autoimmun Rev, 2016. **15**(1): p. 1-8.

42. Takeuchi, O. and S. Akira, *Pattern recognition receptors and inflammation.* Cell, 2010. **140**(6): p. 805-20.
43. Karasawa, T. and M. Takahashi, *Saturated fatty acid-crystals activate NLRP3 inflammasome.* Aging (Albany NY), 2019. **11**(6): p. 1613-1614.
44. Wilmanski, J.M., T. Petnicki-Ocwieja, and K.S. Kobayashi, *NLR proteins: integral members of innate immunity and mediators of inflammatory diseases.* J Leukoc Biol, 2008. **83**(1): p. 13-30.
45. de Zoete, M.R., et al., *Inflammasomes.* Cold Spring Harb Perspect Biol, 2014. **6**(12): p. a016287.
46. Martinon, F., K. Burns, and J. Tschopp, *The inflammasome: a molecular platform triggering activation of inflammatory caspases and processing of proIL-beta.* Mol Cell, 2002. **10**(2): p. 417-26.
47. Latz, E., T.S. Xiao, and A. Stutz, *Activation and regulation of the inflammasomes.* Nat Rev Immunol, 2013. **13**(6): p. 397-411.
48. Akira, S., K. Takeda, and T. Kaisho, *Toll-like receptors: critical proteins linking innate and acquired immunity.* Nat Immunol, 2001. **2**(8): p. 675-80.
49. Kumar, H., T. Kawai, and S. Akira, *Pathogen recognition by the innate immune system.* Int Rev Immunol, 2011. **30**(1): p. 16-34.
50. Vénéreau, E., C. Ceriotti, and M.E. Bianchi, *DAMPs from Cell Death to New Life.* Front Immunol, 2015. **6**: p. 422.
51. Arango Duque, G. and A. Descoteaux, *Macrophage cytokines: involvement in immunity and infectious diseases.* Front Immunol, 2014. **5**: p. 491.
52. Mosser, D.M. and J.P. Edwards, *Exploring the full spectrum of macrophage activation.* Nat Rev Immunol, 2008. **8**(12): p. 958-69.
53. Ley, K., *M1 Means Kill; M2 Means Heal.* The Journal of Immunology, 2017. **199**(7): p. 2191-2193.
54. Martinez, F.O. and S. Gordon, *The M1 and M2 paradigm of macrophage activation: time for reassessment.* F1000Prime Rep, 2014. **6**: p. 13.
55. Lee, C., et al., *Targeting of M2-like tumor-associated macrophages with a melittin-based pro-apoptotic peptide.* J Immunother Cancer, 2019. **7**(1): p. 147.
56. Satpathy, A.T., et al., *Re(de)fining the dendritic cell lineage.* Nat Immunol, 2012. **13**(12): p. 1145-54.
57. Steinman, R.M. and Z.A. Cohn, *Identification of a novel cell type in peripheral lymphoid organs of mice. I. Morphology, quantitation, tissue distribution.* J Exp Med, 1973. **137**(5): p. 1142-62.
58. Gardner, A. and B. Ruffell, *Dendritic Cells and Cancer Immunity.* Trends Immunol, 2016. **37**(12): p. 855-865.
59. Delamarre, L., et al., *Differential lysosomal proteolysis in antigen-presenting cells determines antigen fate.* Science, 2005. **307**(5715): p. 1630-4.
60. Fu, C. and A. Jiang, *Dendritic Cells and CD8 T Cell Immunity in Tumor Microenvironment.* Front Immunol, 2018. **9**: p. 3059.
61. Kushwah, R. and J. Hu, *Complexity of dendritic cell subsets and their function in the host immune system.* Immunology, 2011. **133**(4): p. 409-19.
62. Chaplin, D.D., *Overview of the immune response.* The Journal of allergy and clinical immunology, 2010. **125**(2 Suppl 2): p. S3-S23.
63. Wieczorek, M., et al., *Major Histocompatibility Complex (MHC) Class I and MHC Class II Proteins: Conformational Plasticity in Antigen Presentation.* Front Immunol, 2017. **8**: p. 292.

64. Germain, R.N. and D.H. Margulies, *The biochemistry and cell biology of antigen processing and presentation.* Annu Rev Immunol, 1993. **11**: p. 403-50.
65. Zhu, J., H. Yamane, and W.E. Paul, *Differentiation of effector CD4 T cell populations (*).* Annu Rev Immunol, 2010. **28**: p. 445-89.
66. Sallusto, F. and A. Lanzavecchia, *The instructive role of dendritic cells on T-cell responses.* Arthritis Res, 2002. **4 Suppl 3**(Suppl 3): p. S127-32.
67. Liechtenstein, T., et al., *PD-L1/PD-1 Co-Stimulation, a Brake for T cell Activation and a T cell Differentiation Signal.* J Clin Cell Immunol, 2012. **S12**.
68. Curtsinger, J.M. and M.F. Mescher, *Inflammatory cytokines as a third signal for T cell activation.* Curr Opin Immunol, 2010. **22**(3): p. 333-40.
69. Wang, C., et al., *Bioengineering of Artificial Antigen Presenting Cells and Lymphoid Organs.* Theranostics, 2017. **7**(14): p. 3504-3516.
70. Luckheeram, R.V., et al., *CD4(+)T cells: differentiation and functions.* Clin Dev Immunol, 2012. **2012**: p. 925135.
71. Jenkins, M.K., et al., *In vivo activation of antigen-specific CD4 T cells.* Annu Rev Immunol, 2001. **19**: p. 23-45.
72. Lund, F.E. and T.D. Randall, *Effector and regulatory B cells: modulators of CD4+ T cell immunity.* Nat Rev Immunol, 2010. **10**(4): p. 236-47.
73. Feau, S., et al., *The CD4(+) T-cell help signal is transmitted from APC to CD8(+) T-cells via CD27-CD70 interactions.* Nat Commun, 2012. **3**: p. 948.
74. Golubovskaya, V. and L. Wu, *Different Subsets of T Cells, Memory, Effector Functions, and CAR-T Immunotherapy.* Cancers (Basel), 2016. **8**(3).
75. Korn, T., et al., *IL-17 and Th17 Cells.* Annu Rev Immunol, 2009. **27**: p. 485-517.
76. Gong, F., T. Zheng, and P. Zhou, *T Follicular Helper Cell Subsets and the Associated Cytokine IL-21 in the Pathogenesis and Therapy of Asthma.* Frontiers in Immunology, 2019. **10**(2918).
77. Rock, K.L., E. Reits, and J. Neefjes, *Present Yourself! By MHC Class I and MHC Class II Molecules.* Trends Immunol, 2016. **37**(11): p. 724-737.
78. Obar, J.J. and L. Lefrançois, *Memory CD8+ T cell differentiation.* Ann N Y Acad Sci, 2010. **1183**: p. 251-66.
79. Stinchcombe, J.C., et al., *The immunological synapse of CTL contains a secretory domain and membrane bridges.* Immunity, 2001. **15**(5): p. 751-61.
80. Gattinoni, L., et al., *Acquisition of full effector function in vitro paradoxically impairs the in vivo antitumor efficacy of adoptively transferred CD8+ T cells.* J Clin Invest, 2005. **115**(6): p. 1616-26.
81. Volpe, E., et al., *Fas–Fas Ligand: Checkpoint of T Cell Functions in Multiple Sclerosis.* Frontiers in Immunology, 2016. **7**(382).
82. Schiffer, D., et al., *Glioblastoma: Microenvironment and Niche Concept.* Cancers (Basel), 2018. **11**(1).
83. Velásquez, C., et al., *Hypoxia Can Induce Migration of Glioblastoma Cells Through a Methylation-Dependent Control of ODZ1 Gene Expression.* Frontiers in Oncology, 2019. **9**(1036).
84. Monteiro, A.R., et al., *The Role of Hypoxia in Glioblastoma Invasion.* Cells, 2017. **6**(4).
85. Yang, L., et al., *Hypoxia and hypoxia-inducible factors in glioblastoma multiforme progression and therapeutic implications.* Exp Cell Res, 2012. **318**(19): p. 2417-26.
86. Vaupel, P., *Hypoxia and aggressive tumor phenotype: implications for therapy and prognosis.* Oncologist, 2008. **13 Suppl 3**: p. 21-6.

87. Graeber, M.B., B.W. Scheithauer, and G.W. Kreutzberg, *Microglia in brain tumors.* Glia, 2002. **40**(2): p. 252-9.
88. Watters, J.J., J.M. Schartner, and B. Badie, *Microglia function in brain tumors.* J Neurosci Res, 2005. **81**(3): p. 447-55.
89. Kvisten, M., et al., *Microglia and macrophages in human glioblastomas: A morphological and immunohistochemical study.* Mol Clin Oncol, 2019. **11**(1): p. 31-36.
90. Chen, Z. and D. Hambardzumyan, *Immune Microenvironment in Glioblastoma Subtypes.* Front Immunol, 2018. **9**: p. 1004.
91. Kitamura, T., B.Z. Qian, and J.W. Pollard, *Immune cell promotion of metastasis.* Nat Rev Immunol, 2015. **15**(2): p. 73-86.
92. Razavi, S.M., et al., *Immune Evasion Strategies of Glioblastoma.* Front Surg, 2016. **3**: p. 11.
93. Engelhardt, B. and S. Liebner, *Novel insights into the development and maintenance of the blood-brain barrier.* Cell Tissue Res, 2014. **355**(3): p. 687-99.
94. Patel, A.P., et al., *Single-cell RNA-seq highlights intratumoral heterogeneity in primary glioblastoma.* Science, 2014. **344**(6190): p. 1396-401.
95. Dirkse, A., et al., *Stem cell-associated heterogeneity in Glioblastoma results from intrinsic tumor plasticity shaped by the microenvironment.* Nature Communications, 2019. **10**(1): p. 1787.
96. Vinay, D.S., et al., *Immune evasion in cancer: Mechanistic basis and therapeutic strategies.* Seminars in Cancer Biology, 2015. **35**: p. S185-S198.
97. Schartner, J.M., et al., *Impaired capacity for upregulation of MHC class II in tumor-associated microglia.* Glia, 2005. **51**(4): p. 279-85.
98. Romani, M., et al., *Immune Checkpoints and Innovative Therapies in Glioblastoma.* Front Oncol, 2018. **8**: p. 464.
99. Francisco, L.M., et al., *PD-L1 regulates the development, maintenance, and function of induced regulatory T cells.* J Exp Med, 2009. **206**(13): p. 3015-29.
100. Wilmotte, R., et al., *B7-homolog 1 expression by human glioma: a new mechanism of immune evasion.* Neuroreport, 2005. **16**(10): p. 1081-5.
101. Nduom, E.K., et al., *PD-L1 expression and prognostic impact in glioblastoma.* Neuro Oncol, 2016. **18**(2): p. 195-205.
102. Huang, J., et al., *Immune Checkpoint in Glioblastoma: Promising and Challenging.* Front Pharmacol, 2017. **8**: p. 242.
103. Liu, F., et al., *CTLA-4 correlates with immune and clinical characteristics of glioma.* Cancer Cell Int, 2020. **20**: p. 7.
104. Romeo, E., et al., *The Vicious Cross-Talk between Tumor Cells with an EMT Phenotype and Cells of the Immune System.* Cells, 2019. **8**(5).
105. Gao, D., et al., *Microenvironmental regulation of epithelial-mesenchymal transitions in cancer.* Cancer Res, 2012. **72**(19): p. 4883-9.
106. Chockley, P.J. and V.G. Keshamouni, *Immunological Consequences of Epithelial-Mesenchymal Transition in Tumor Progression.* J Immunol, 2016. **197**(3): p. 691-8.
107. Chen, L., et al., *Metastasis is regulated via microRNA-200/ZEB1 axis control of tumour cell PD-L1 expression and intratumoral immunosuppression.* Nat Commun, 2014. **5**: p. 5241.
108. Dongre, A., et al., *Epithelial-to-Mesenchymal Transition Contributes to Immunosuppression in Breast Carcinomas.* Cancer Res, 2017. **77**(15): p. 3982-3989.
109. Kudo-Saito, C., et al., *Cancer metastasis is accelerated through immunosuppression during Snail-induced EMT of cancer cells.* Cancer Cell, 2009. **15**(3): p. 195-206.

110. Bahadur, S., et al., *Current promising treatment strategy for glioblastoma multiform: A review.* Oncol Rev, 2019. **13**(2): p. 417.
111. Kirson, E.D., et al., *Alternating electric fields arrest cell proliferation in animal tumor models and human brain tumors.* Proc Natl Acad Sci U S A, 2007. **104**(24): p. 10152-7.
112. Lieberman, F., *Glioblastoma update: molecular biology, diagnosis, treatment, response assessment, and translational clinical trials.* F1000Res, 2017. **6**: p. 1892.
113. Olar, A. and K.D. Aldape, *Using the molecular classification of glioblastoma to inform personalized treatment.* J Pathol, 2014. **232**(2): p. 165-77.
114. Lim, M., et al., *Current state of immunotherapy for glioblastoma.* Nat Rev Clin Oncol, 2018. **15**(7): p. 422-442.
115. Stupp, R., et al., *Radiotherapy plus concomitant and adjuvant temozolomide for glioblastoma.* N Engl J Med, 2005. **352**(10): p. 987-96.
116. Ballesta, A., et al., *Multiscale design of cell-type-specific pharmacokinetic/pharmacodynamic models for personalized medicine: application to temozolomide in brain tumors.* CPT Pharmacometrics Syst Pharmacol, 2014. **3**: p. e112.
117. Newlands, E.S., et al., *Temozolomide: a review of its discovery, chemical properties, pre-clinical development and clinical trials.* Cancer Treat Rev, 1997. **23**(1): p. 35-61.
118. Klapacz, J., et al., *O6-methylguanine-induced cell death involves exonuclease 1 as well as DNA mismatch recognition in vivo.* Proc Natl Acad Sci U S A, 2009. **106**(2): p. 576-81.
119. Esteller, M., et al., *Inactivation of the DNA-repair gene MGMT and the clinical response of gliomas to alkylating agents.* N Engl J Med, 2000. **343**(19): p. 1350-4.
120. Wick, W., et al., *MGMT testing--the challenges for biomarker-based glioma treatment.* Nat Rev Neurol, 2014. **10**(7): p. 372-85.
121. Wang, T., A.J. Pickard, and J.M. Gallo, *Histone Methylation by Temozolomide; A Classic DNA Methylating Anticancer Drug.* Anticancer Res, 2016. **36**(7): p. 3289-99.
122. Weller, M., et al., *Glioma.* Nat Rev Dis Primers, 2015. **1**: p. 15017.
123. Brown, N.F., et al., *Harnessing the immune system in glioblastoma.* Br J Cancer, 2018. **119**(10): p. 1171-1181.
124. Iorgulescu, J.B., et al., *Immunotherapy for glioblastoma: going viral.* Nat Med, 2018. **24**(8): p. 1094-1096.
125. McGranahan, T., et al., *Current State of Immunotherapy for Treatment of Glioblastoma.* Curr Treat Options Oncol, 2019. **20**(3): p. 24.
126. Westphal, M., et al., *Adenovirus-mediated gene therapy with sitimagene ceradenovec followed by intravenous ganciclovir for patients with operable high-grade glioma (ASPECT): a randomised, open-label, phase 3 trial.* Lancet Oncol, 2013. **14**(9): p. 823-33.
127. Pehlivan, K.C., B.B. Duncan, and D.W. Lee, *CAR-T Cell Therapy for Acute Lymphoblastic Leukemia: Transforming the Treatment of Relapsed and Refractory Disease.* Curr Hematol Malig Rep, 2018. **13**(5): p. 396-406.
128. Chavez, J.C., C. Bachmeier, and M.A. Kharfan-Dabaja, *CAR T-cell therapy for B-cell lymphomas: clinical trial results of available products.* Ther Adv Hematol, 2019. **10**: p. 2040620719841581.
129. Brown, M.P., L.M. Ebert, and T. Gargett, *Clinical chimeric antigen receptor-T cell therapy: a new and promising treatment modality for glioblastoma.* Clin Transl Immunology, 2019. **8**(5): p. e1050.
130. Miliotou, A.N. and L.C. Papadopoulou, *CAR T-cell Therapy: A New Era in Cancer Immunotherapy.* Curr Pharm Biotechnol, 2018. **19**(1): p. 5-18.

131. Akhavan, D., et al., *CAR T cells for brain tumors: Lessons learned and road ahead.* Immunol Rev, 2019. **290**(1): p. 60-84.
132. Platten, M., *EGFRvIII vaccine in glioblastoma-InACT-IVe or not ReACTive enough?* Neuro Oncol, 2017. **19**(11): p. 1425-1426.
133. Coxon, A.T., T.M. Johanns, and G.P. Dunn, *An Innovative Immunotherapy Vaccine with Combination Checkpoint Blockade as a First Line Treatment for Glioblastoma in the Context of Current Treatments.* Mo Med, 2020. **117**(1): p. 45-49.
134. Weenink, B., et al., *Immunotherapy in Glioblastoma: Current Shortcomings and Future Perspectives.* Cancers (Basel), 2020. **12**(3).
135. Preusser, M., et al., *Prospects of immune checkpoint modulators in the treatment of glioblastoma.* Nat Rev Neurol, 2015. **11**(9): p. 504-14.
136. Reardon, D.A., et al., *OS10.3 Randomized Phase 3 Study Evaluating the Efficacy and Safety of Nivolumab vs Bevacizumab in Patients With Recurrent Glioblastoma: CheckMate 143.* Neuro-Oncology, 2017. **19**(suppl_3): p. iii21-iii21.
137. Yan, S., et al., *Current applications and future prospects of nanotechnology in cancer immunotherapy.* Cancer Biol Med, 2019. **16**(3): p. 486-497.
138. Ung, N. and I. Yang, *Nanotechnology to augment immunotherapy for the treatment of glioblastoma multiforme.* J Neurooncol, 2015. **123**(3): p. 473-81.
139. Leone, R.D. and L.A. Emens, *Targeting adenosine for cancer immunotherapy.* J Immunother Cancer, 2018. **6**(1): p. 57.
140. Eltzschig, H.K., *Extracellular adenosine signaling in molecular medicine.* J Mol Med (Berl), 2013. **91**(2): p. 141-6.
141. Junger, W.G., *Immune cell regulation by autocrine purinergic signalling.* Nat Rev Immunol, 2011. **11**(3): p. 201-12.
142. Abbracchio, M.P., et al., *Purinergic signalling in the nervous system: an overview.* Trends in Neurosciences, 2009. **32**(1): p. 19-29.
143. Borea, P.A., et al., *The A3 adenosine receptor: history and perspectives.* Pharmacol Rev, 2015. **67**(1): p. 74-102.
144. Morelli, M., et al., *Chapter 11 - Role of Adenosine in the Basal Ganglia*, in *Handbook of Behavioral Neuroscience*, H. Steiner and K.Y. Tseng, Editors. 2010, Elsevier. p. 201-217.
145. Burnstock, G. and F. Di Virgilio, *Purinergic signalling and cancer.* Purinergic Signal, 2013. **9**(4): p. 491-540.
146. Del Puerto, A., F. Wandosell, and J.J. Garrido, *Neuronal and glial purinergic receptors functions in neuron development and brain disease.* Front Cell Neurosci, 2013. **7**: p. 197.
147. Johnston-Cox, H.A., M. Koupenova, and K. Ravid, *A2 adenosine receptors and vascular pathologies.* Arterioscler Thromb Vasc Biol, 2012. **32**(4): p. 870-8.
148. Sachdeva, S. and M. Gupta, *Adenosine and its receptors as therapeutic targets: An overview.* Saudi Pharm J, 2013. **21**(3): p. 245-53.
149. Torres, A., et al., *Extracellular adenosine promotes cell migration/invasion of Glioblastoma Stem-like Cells through A3 Adenosine Receptor activation under hypoxia.* Cancer Lett, 2019. **446**: p. 112-122.
150. Gorain, B., et al., *Adenosine Receptors as Novel Targets for the Treatment of Various Cancers.* Curr Pharm Des, 2019. **25**(26): p. 2828-2841.
151. Synowitz, M., et al., *A1 adenosine receptors in microglia control glioblastoma-host interaction.* Cancer Res, 2006. **66**(17): p. 8550-7.
152. Borroto-Escuela, D.O., et al., *Understanding the Role of Adenosine A2AR Heteroreceptor Complexes in Neurodegeneration and Neuroinflammation.* Front Neurosci, 2018. **12**: p. 43.

153. Leone, R.D., Y.-C. Lo, and J.D. Powell, *A2aR antagonists: Next generation checkpoint blockade for cancer immunotherapy.* Computational and Structural Biotechnology Journal, 2015. **13**: p. 265-272.
154. Young, A., et al., *Co-inhibition of CD73 and A2AR Adenosine Signaling Improves Anti-tumor Immune Responses.* Cancer Cell, 2016. **30**(3): p. 391-403.
155. Sepúlveda, C., I. Palomo, and E. Fuentes, *Role of adenosine A2b receptor overexpression in tumor progression.* Life Sciences, 2016. **166**: p. 92-99.
156. Giacomelli, C., et al., *The A2B Adenosine Receptor Modulates the Epithelial- Mesenchymal Transition through the Balance of cAMP/PKA and MAPK/ERK Pathway Activation in Human Epithelial Lung Cells.* Front Pharmacol, 2018. **9**: p. 54.
157. Desmet, C.J., et al., *Identification of a pharmacologically tractable Fra-1/ADORA2B axis promoting breast cancer metastasis.* Proc Natl Acad Sci U S A, 2013. **110**(13): p. 5139-44.
158. Fishman, P., et al., *Pharmacological and therapeutic effects of A3 adenosine receptor agonists.* Drug Discov Today, 2012. **17**(7-8): p. 359-66.
159. Wang, J. and S. Matosevic, *NT5E/CD73 as Correlative Factor of Patient Survival and Natural Killer Cell Infiltration in Glioblastoma.* J Clin Med, 2019. **8**(10).
160. Torres, A., et al., *Adenosine A3 receptor elicits chemoresistance mediated by multiple resistance-associated protein-1 in human glioblastoma stem-like cells.* Oncotarget, 2016. **7**(41): p. 67373-67386.
161. Blay, J., T.D. White, and D.W. Hoskin, *The extracellular fluid of solid carcinomas contains immunosuppressive concentrations of adenosine.* Cancer Res, 1997. **57**(13): p. 2602-5.
162. Kim, S.Y., *Cancer Energy Metabolism: Shutting Power off Cancer Factory.* Biomol Ther (Seoul), 2018. **26**(1): p. 39-44.
163. Dosch, M., et al., *Mechanisms of ATP Release by Inflammatory Cells.* Int J Mol Sci, 2018. **19**(4).
164. Tanaka, K., et al., *Extracellular ATP acts as a damage-associated molecular pattern (DAMP) signal in plants.* Front Plant Sci, 2014. **5**: p. 446.
165. Antonioli, L., et al., *Adenosine signaling and the immune system: When a lot could be too much.* Immunol Lett, 2019. **205**: p. 9-15.
166. Di Virgilio, F. and E. Adinolfi, *Extracellular purines, purinergic receptors and tumor growth.* Oncogene, 2017. **36**(3): p. 293-303.
167. Beavis, P.A., et al., *CD73: a potent suppressor of antitumor immune responses.* Trends Immunol, 2012. **33**(5): p. 231-7.
168. Colgan, S.P., et al., *Physiological roles for ecto-5'-nucleotidase (CD73).* Purinergic Signal, 2006. **2**(2): p. 351-60.
169. Knapp, K., et al., *Crystal structure of the human ecto-5'-nucleotidase (CD73): insights into the regulation of purinergic signaling.* Structure, 2012. **20**(12): p. 2161-73.
170. Heuts, D.P., et al., *Crystal structure of a soluble form of human CD73 with ecto-5'-nucleotidase activity.* Chembiochem, 2012. **13**(16): p. 2384-91.
171. Klemens, M.R., et al., *Characterization of soluble vs membrane-bound human placental 5'-nucleotidase.* Biochemical and Biophysical Research Communications, 1990. **172**(3): p. 1371-1377.
172. Synnestvedt, K., et al., *Ecto-5'-nucleotidase (CD73) regulation by hypoxia-inducible factor-1 mediates permeability changes in intestinal epithelia.* J Clin Invest, 2002. **110**(7): p. 993-1002.
173. Ghalamfarsa, G., et al., *CD73 as a potential opportunity for cancer immunotherapy.* Expert Opin Ther Targets, 2019. **23**(2): p. 127-142.

174. Azambuja, J.H., et al., *CD73 Downregulation Decreases In Vitro and In Vivo Glioblastoma Growth.* Mol Neurobiol, 2019. **56**(5): p. 3260-3279.
175. Zhu, J., et al., *CD73/NT5E is a target of miR-30a-5p and plays an important role in the pathogenesis of non-small cell lung cancer.* Mol Cancer, 2017. **16**(1): p. 34.
176. Yan, A., et al., *CD73 Promotes Glioblastoma Pathogenesis and Enhances Its Chemoresistance via A2B Adenosine Receptor Signaling.* J Neurosci, 2019. **39**(22): p. 4387-4402.
177. Ren, Z.H., et al., *CD73 is associated with poor prognosis in HNSCC.* Oncotarget, 2016. **7**(38): p. 61690-61702.
178. Ludwig, H.C., et al., *Expression of CD 73 (ecto-5'-nucleotidase) in 165 glioblastomas by immunohistochemistry and electronmicroscopic histochemistry.* Anticancer Res, 1999. **19**(3a): p. 1747-52.
179. Gao, Z.W., et al., *CD73 promotes proliferation and migration of human cervical cancer cells independent of its enzyme activity.* BMC Cancer, 2017. **17**(1): p. 135.
180. Zhi, X., et al., *RNA interference of ecto-5'-nucleotidase (CD73) inhibits human breast cancer cell growth and invasion.* Clin Exp Metastasis, 2007. **24**(6): p. 439-48.
181. Zhou, L., et al., *The distinct role of CD73 in the progression of pancreatic cancer.* J Mol Med (Berl), 2019. **97**(6): p. 803-815.
182. Resta, R., Y. Yamashita, and L.F. Thompson, *Ecto-enzyme and signaling functions of lymphocyte CD73.* Immunol Rev, 1998. **161**: p. 95-109.
183. Kong, Y., et al., *Downregulation of CD73 associates with T cell exhaustion in AML patients.* J Hematol Oncol, 2019. **12**(1): p. 40.
184. Antonioli, L., et al., *Anti-CD73 in Cancer Immunotherapy: Awakening New Opportunities.* Trends in Cancer, 2016. **2**(2): p. 95-109.
185. Perrot, I., et al., *Blocking Antibodies Targeting the CD39/CD73 Immunosuppressive Pathway Unleash Immune Responses in Combination Cancer Therapies.* Cell Rep, 2019. **27**(8): p. 2411-2425.e9.
186. Cui, S., S. Zhang, and S. Yue, *Raman Spectroscopy and Imaging for Cancer Diagnosis.* Journal of Healthcare Engineering, 2018. **2018**: p. 8619342.
187. Fenn, M.B., et al., *Raman Spectroscopy for Clinical Oncology.* Advances in Optical Technologies, 2011. **2011**: p. 213783.
188. Gordon, K.C. and S.J. Fraser-Miller, *Raman Spectroscopy*, in *Analytical Techniques in the Pharmaceutical Sciences*, A. Müllertz, Y. Perrie, and T. Rades, Editors. 2016, Springer New York: New York, NY. p. 139-169.
189. Bumbrah, G.S. and R.M. Sharma, *Raman spectroscopy – Basic principle, instrumentation and selected applications for the characterization of drugs of abuse.* Egyptian Journal of Forensic Sciences, 2016. **6**(3): p. 209-215.
190. Paudel, A., D. Raijada, and J. Rantanen, *Raman spectroscopy in pharmaceutical product design.* Advanced Drug Delivery Reviews, 2015. **89**: p. 3-20.
191. Bergholt, M.S., et al., *Raman endoscopy for in vivo differentiation between benign and malignant ulcers in the stomach.* Analyst, 2010. **135**(12): p. 3162-8.
192. Bergholt, M.S., et al., *In Vivo Diagnosis of Esophageal Cancer Using Image-Guided Raman Endoscopy and Biomolecular Modeling.* Technology in Cancer Research & Treatment, 2011. **10**(2): p. 103-112.
193. Tashibu, K., *[Analysis of water content in rat brain using Raman spectroscopy].* No To Shinkei, 1990. **42**(10): p. 999-1004.
194. Mizuno, A., et al., *Near-infrared Fourier transform Raman spectroscopic study of human brain tissues and tumours.* Journal of Raman Spectroscopy, 1994. **25**(1): p. 25-29.

195. Hollon, T., et al., *Improving the accuracy of brain tumor surgery via Raman-based technology.* Neurosurg Focus, 2016. **40**(3): p. E9.
196. Koljenovic, S., et al., *Discriminating vital tumor from necrotic tissue in human glioblastoma tissue samples by Raman spectroscopy.* Lab Invest, 2002. **82**(10): p. 1265-77.
197. Kalkanis, S.N., et al., *Raman spectroscopy to distinguish grey matter, necrosis, and glioblastoma multiforme in frozen tissue sections.* J Neurooncol, 2014. **116**(3): p. 477-85.
198. Petrecca, K., et al., *Failure pattern following complete resection plus radiotherapy and temozolomide is at the resection margin in patients with glioblastoma.* J Neurooncol, 2013. **111**(1): p. 19-23.
199. Desroches, J., et al., *A new method using Raman spectroscopy for in vivo targeted brain cancer tissue biopsy.* Scientific Reports, 2018. **8**(1): p. 1792.
200. Livermore, L.J., et al., *Rapid intraoperative molecular genetic classification of gliomas using Raman spectroscopy.* Neuro-Oncology Advances, 2019. **1**(1).
201. Short, K.W., et al., *Raman Spectroscopy Detects Biochemical Changes Due to Proliferation in Mammalian Cell Cultures.* Biophysical Journal, 2005. **88**(6): p. 4274-4288.
202. Camp, C.H., Jr., et al., *High-Speed Coherent Raman Fingerprint Imaging of Biological Tissues.* Nat Photonics, 2014. **8**: p. 627-634.
203. Santos, I.P., et al., *Raman Spectroscopic Characterization of Melanoma and Benign Melanocytic Lesions Suspected of Melanoma Using High-Wavenumber Raman Spectroscopy.* Anal Chem, 2016. **88**(15): p. 7683-8.
204. Mo, J., et al., *High wavenumber Raman spectroscopy for in vivo detection of cervical dysplasia.* Anal Chem, 2009. **81**(21): p. 8908-15.
205. Verrier, S., et al., *In situ monitoring of cell death using Raman microspectroscopy.* Biopolymers, 2004. **74**(1-2): p. 157-62.
206. Notingher, I., et al., *In situ spectral monitoring of mRNA translation in embryonic stem cells during differentiation in vitro.* Anal Chem, 2004. **76**(11): p. 3185-93.
207. Owen, C.A., et al., *In vitro toxicology evaluation of pharmaceuticals using Raman micro-spectroscopy.* J Cell Biochem, 2006. **99**(1): p. 178-86.
208. Klein, K., et al., *Label-free live-cell imaging with confocal Raman microscopy.* Biophys J, 2012. **102**(2): p. 360-8.
209. Devpura, S., et al., *Detection of benign epithelia, prostatic intraepithelial neoplasia, and cancer regions in radical prostatectomy tissues using Raman spectroscopy.* Vibrational Spectroscopy, 2010. **53**(2): p. 227-232.
210. Dai, W.-Y., S. Lee, and Y.-C. Hsu, *Discrimination between oral cancer and healthy cells based on the adenine signature detected by using Raman spectroscopy.* Journal of Raman Spectroscopy, 2018. **49**(2): p. 336-342.
211. González-Solís, J., G. Luévano-Colmenero, and J. Vargas-Mancilla, *Surface enhanced Raman spectroscopy in breast cancer cells.* Laser Ther, 2013. **22**(1): p. 37-42.
212. Chen, M., et al., *The use of wavelength modulated Raman spectroscopy in label-free identification of T lymphocyte subsets, natural killer cells and dendritic cells.* PLoS One, 2015. **10**(5): p. e0125158.
213. Ichimura, T., et al., *Non-label immune cell state prediction using Raman spectroscopy.* Scientific Reports, 2016. **6**(1): p. 37562.
214. McReynolds, N., et al., *Multimodal discrimination of immune cells using a combination of Raman spectroscopy and digital holographic microscopy.* Sci Rep, 2017. **7**: p. 43631.

215. Bertani, F.R., et al., *Classification of M1/M2-polarized human macrophages by label-free hyperspectral reflectance confocal microscopy and multivariate analysis.* Sci Rep, 2017. **7**(1): p. 8965.
216. Carlsson, S.K., S.P. Brothers, and C. Wahlestedt, *Emerging treatment strategies for glioblastoma multiforme.* EMBO Mol Med, 2014. **6**(11): p. 1359-70.
217. Bao, S., et al., *Glioma stem cells promote radioresistance by preferential activation of the DNA damage response.* Nature, 2006. **444**(7120): p. 756-60.
218. Singh, S.K., et al., *Identification of a cancer stem cell in human brain tumors.* Cancer Res, 2003. **63**(18): p. 5821-8.
219. Han, S.P., et al., *SNAI1 is involved in the proliferation and migration of glioblastoma cells.* Cell Mol Neurobiol, 2011. **31**(3): p. 489-96.
220. Lupia, M., et al., *CD73 Regulates Stemness and Epithelial-Mesenchymal Transition in Ovarian Cancer-Initiating Cells.* Stem Cell Reports, 2018. **10**(4): p. 1412-1425.
221. Ma, X.L., et al., *CD73 promotes hepatocellular carcinoma progression and metastasis via activating PI3K/AKT signaling by inducing Rap1-mediated membrane localization of P110beta and predicts poor prognosis.* J Hematol Oncol, 2019. **12**(1): p. 37.
222. Burnstock, G., *Purinergic Signalling: Therapeutic Developments.* Front Pharmacol, 2017. **8**: p. 661.
223. Zimmermann, H., M. Zebisch, and N. Sträter, *Cellular function and molecular structure of ecto-nucleotidases.* Purinergic Signal, 2012. **8**(3): p. 437-502.
224. Bavaresco, L., et al., *The role of ecto-5'-nucleotidase/CD73 in glioma cell line proliferation.* Mol Cell Biochem, 2008. **319**(1-2): p. 61-8.
225. Cappellari, A.R., et al., *Involvement of ecto-5'-nucleotidase/CD73 in U138MG glioma cell adhesion.* Mol Cell Biochem, 2012. **359**(1-2): p. 315-22.
226. Antonioli, L., et al., *CD39 and CD73 in immunity and inflammation.* Trends Mol Med, 2013. **19**(6): p. 355-67.
227. Sadej, R. and A.C. Skladanowski, *Dual, enzymatic and non-enzymatic, function of ecto-5'-nucleotidase (eN, CD73) in migration and invasion of A375 melanoma cells.* Acta Biochim Pol, 2012. **59**(4): p. 647-52.
228. Boison, D., *Adenosine as a modulator of brain activity.* Drug News Perspect, 2007. **20**(10): p. 607-11.
229. Fredholm, B.B., et al., *International Union of Basic and Clinical Pharmacology. LXXXI. Nomenclature and classification of adenosine receptors--an update.* Pharmacol Rev, 2011. **63**(1): p. 1-34.
230. Gessi, S., et al., *Adenosine receptors and cancer.* Biochim Biophys Acta, 2011. **1808**(5): p. 1400-12.
231. Giacomelli, C., et al., *The A(2B) Adenosine Receptor Modulates the Epithelial- Mesenchymal Transition through the Balance of cAMP/PKA and MAPK/ERK Pathway Activation in Human Epithelial Lung Cells.* Front Pharmacol, 2018. **9**: p. 54.
232. Brat, D.J., et al., *Pseudopalisades in glioblastoma are hypoxic, express extracellular matrix proteases, and are formed by an actively migrating cell population.* Cancer Res, 2004. **64**(3): p. 920-7.
233. Zhang, W., et al., *HIF-1alpha Promotes Epithelial-Mesenchymal Transition and Metastasis through Direct Regulation of ZEB1 in Colorectal Cancer.* PLoS One, 2015. **10**(6): p. e0129603.
234. Gerdes, J., et al., *Production of a mouse monoclonal antibody reactive with a human nuclear antigen associated with cell proliferation.* Int J Cancer, 1983. **31**(1): p. 13-20.

235. Talar, B., et al., *Pentoxifylline Inhibits WNT Signalling in beta-Cateninhigh Patient-Derived Melanoma Cell Populations.* PLoS One, 2016. **11**(6): p. e0158275.
236. Pridjian, A.K., et al., *Developmental differences in myocardial protection in response to 5'-nucleotidase inhibition.* J Thorac Cardiovasc Surg, 1994. **107**(2): p. 520-6.
237. Kreth, S., et al., *Immunomodulatory properties of pentoxifylline are mediated via adenosine-dependent pathways.* Shock, 2010. **34**(1): p. 10-6.
238. Zuccarini, M., et al., *Modulation of the TGF-β1-induced epithelial to mesenchymal transition (EMT) mediated by P1 and P2 purine receptors in MDCK cells.* Purinergic Signal, 2017. **13**(4): p. 429-442.
239. Koch, K., et al., *A comparative pharmaco-metabolomic study of glutaminase inhibitors in glioma stem-like cells confirms biological effectiveness but reveals differences in target-specificity.* Cell Death Discovery, 2020. **6**(1): p. 20.
240. Lu, Z.Y., et al., *SNAI1 overexpression induces stemness and promotes ovarian cancer cell invasion and metastasis.* Oncol Rep, 2012. **27**(5): p. 1587-91.
241. Koch, K., et al., *Reciprocal regulation of the cholinic phenotype and epithelial-mesenchymal transition in glioblastoma cells.* Oncotarget, 2016. **7**(45): p. 73414-73431.
242. Eley, K.W., et al., *The effects of pentoxifylline on the survival of human glioma cells with continuous and intermittent stereotactic radiosurgery irradiation.* Int J Radiat Oncol Biol Phys, 2002. **54**(2): p. 542-50.
243. Hill, S.J., et al., *Allosteric interactions at adenosine A(1) and A(3) receptors: new insights into the role of small molecules and receptor dimerization.* Br J Pharmacol, 2014. **171**(5): p. 1102-13.
244. Jajoo, S., et al., *Adenosine A(3) receptor suppresses prostate cancer metastasis by inhibiting NADPH oxidase activity.* Neoplasia, 2009. **11**(11): p. 1132-45.
245. Zhao, Z., et al., *A role for the A3 adenosine receptor in determining tissue levels of cAMP and blood pressure: studies in knock-out mice.* Biochim Biophys Acta, 2000. **1500**(3): p. 280-90.
246. Gessi, S., et al., *The A3 adenosine receptor: an enigmatic player in cell biology.* Pharmacol Ther, 2008. **117**(1): p. 123-40.
247. Zhi, X., et al., *Potential prognostic biomarker CD73 regulates epidermal growth factor receptor expression in human breast cancer.* IUBMB Life, 2012. **64**(11): p. 911-20.
248. Yu, J., et al., *A preliminary study of the role of extracellular -5'- nucleotidase in breast cancer stem cells and epithelial-mesenchymal transition.* In Vitro Cell Dev Biol Anim, 2017. **53**(2): p. 132-140.
249. Derynck, R., B.P. Muthusamy, and K.Y. Saeteurn, *Signaling pathway cooperation in TGF-beta-induced epithelial-mesenchymal transition.* Curr Opin Cell Biol, 2014. **31**: p. 56-66.
250. Joseph, J.V., et al., *TGF-β is an inducer of ZEB1-dependent mesenchymal transdifferentiation in glioblastoma that is associated with tumor invasion.* Cell Death Dis, 2014. **5**(10): p. e1443.
251. Wu, R., et al., *Effects of CD73 on human colorectal cancer cell growth in vivo and in vitro.* Oncol Rep, 2016. **35**(3): p. 1750-6.
252. Moffat, J., et al., *A lentiviral RNAi library for human and mouse genes applied to an arrayed viral high-content screen.* Cell, 2006. **124**(6): p. 1283-98.
253. Niyazi, M., I. Niyazi, and C. Belka, *Counting colonies of clonogenic assays by using densitometric software.* Radiat Oncol, 2007. **2**: p. 4.
254. Coolen, E.J.C.M., et al., *Simultaneous determination of adenosine triphosphate and its metabolites in human whole blood by RP-HPLC and UV-detection.* Journal of chromatography. B, Analytical technologies in the biomedical and life sciences, 2008. **864**(1-2): p. 43-51.

255. Auner, G.W., et al., *Applications of Raman spectroscopy in cancer diagnosis.* Cancer metastasis reviews, 2018. **37**(4): p. 691-717.
256. McReynolds, N., et al., *Multimodal discrimination of immune cells using a combination of Raman spectroscopy and digital holographic microscopy.* Scientific Reports, 2017. **7**(1): p. 43631.
257. Raman, C.V. and K.S. Krishnan, *A New Type of Secondary Radiation.* Nature, 1928. **121**(3048): p. 501-502.
258. Smith, G.P.S., et al., *Raman imaging of drug delivery systems.* Advanced Drug Delivery Reviews, 2015. **89**: p. 21-41.
259. De Gelder, J., et al., *Reference database of Raman spectra of biological molecules.* Journal of Raman Spectroscopy, 2007. **38**(9): p. 1133-1147.
260. Ong, Y.H., M. Lim, and Q. Liu, *Comparison of principal component analysis and biochemical component analysis in Raman spectroscopy for the discrimination of apoptosis and necrosis in K562 leukemia cells.* Optics express, 2012. **20**: p. 22158-71.
261. Pence, I. and A. Mahadevan-Jansen, *Clinical instrumentation and applications of Raman spectroscopy.* Chemical Society Reviews, 2016. **45**(7): p. 1958-1979.
262. Kong, K., et al., *Raman spectroscopy for medical diagnostics — From in-vitro biofluid assays to in-vivo cancer detection.* Advanced Drug Delivery Reviews, 2015. **89**: p. 121-134.
263. Haka, A.S., et al., *Diagnosing breast cancer using Raman spectroscopy: prospective analysis.* Journal of biomedical optics, 2009. **14**(5): p. 054023-054023.
264. Beljebbar, A., et al., *Ex vivo and in vivo diagnosis of C6 glioblastoma development by Raman spectroscopy coupled to a microprobe.* Anal Bioanal Chem, 2010. **398**(1): p. 477-87.
265. D'Acunto, M., et al., *Contribution of Raman Spectroscopy to Diagnosis and Grading of Chondrogenic Tumors.* Scientific Reports, 2020. **10**(1): p. 2155.
266. Koljenović, S., et al., *Discriminating Vital Tumor from Necrotic Tissue in Human Glioblastoma Tissue Samples by Raman Spectroscopy.* Laboratory Investigation, 2002. **82**(10): p. 1265-1277.
267. Kalkanis, S.N., et al., *Raman spectroscopy to distinguish grey matter, necrosis, and glioblastoma multiforme in frozen tissue sections.* Journal of Neuro-Oncology, 2014. **116**(3): p. 477-485.
268. Beljebbar, A., et al., *Ex vivo and in vivo diagnosis of C6 glioblastoma development by Raman spectroscopy coupled to a microprobe.* Analytical and Bioanalytical Chemistry, 2010. **398**(1): p. 477-487.
269. Daniel, A., et al., *Raman mapping of oral tissues for cancer diagnosis.* Journal of Raman Spectroscopy, 2014. **45**(7): p. 541-549.
270. Zoladek, A., et al., *Development of Raman Imaging System for time-course imaging of single living cells.* Spectroscopy, 2010. **24**: p. 521962.
271. Smith, R., K.L. Wright, and L. Ashton, *Raman spectroscopy: an evolving technique for live cell studies.* Analyst, 2016. **141**(12): p. 3590-3600.
272. Hatoum, A., R. Mohammed, and O. Zakieh, *The unique invasiveness of glioblastoma and possible drug targets on extracellular matrix.* Cancer Manag Res, 2019. **11**: p. 1843-1855.
273. Janeway, et al., *Immunebiology: the immune system in health and disease*. 6th ed. 2005, New York: Garland Science Publishing.
274. Olingy, C.E., H.Q. Dinh, and C.C. Hedrick, *Monocyte heterogeneity and functions in cancer.* Journal of Leukocyte Biology, 2019. **106**(2): p. 309-322.
275. Ahlers, J.D. and I.M. Belyakov, *Memories that last forever: strategies for optimizing vaccine T-cell memory.* Blood, 2010. **115**(9): p. 1678-89.

276. Bloch, O., et al., *Gliomas promote immunosuppression through induction of B7-H1 expression in tumor-associated macrophages.* Clin Cancer Res, 2013. **19**(12): p. 3165-75.
277. Mohme, M., et al., *Immunophenotyping of Newly Diagnosed and Recurrent Glioblastoma Defines Distinct Immune Exhaustion Profiles in Peripheral and Tumor-infiltrating Lymphocytes.* Clinical Cancer Research, 2018. **24**(17): p. 4187-4200.
278. Zhang, N. and M.J. Bevan, *CD8(+) T cells: foot soldiers of the immune system.* Immunity, 2011. **35**(2): p. 161-8.
279. Jermyn, M., et al., *Intraoperative brain cancer detection with Raman spectroscopy in humans.* Sci Transl Med, 2015. **7**(274): p. 274ra19.
280. He, Y., et al., *Ramanome technology platform for label-free screening and sorting of microbial cell factories at single-cell resolution.* Biotechnology Advances, 2019. **37**(6): p. 107388.
281. Surmacki, J.M., et al., *Raman micro-spectroscopy for accurate identification of primary human bronchial epithelial cells.* Scientific Reports, 2018. **8**(1): p. 12604.
282. Vargas-Obieta, E., et al., *Breast cancer detection based on serum sample surface enhanced Raman spectroscopy.* Lasers in Medical Science, 2016. **31**(7): p. 1317-1324.
283. Pyrgiotakis, G., et al., *Cell death discrimination with Raman spectroscopy and support vector machines.* Annals of biomedical engineering, 2009. **37**(7): p. 1464-1473.
284. Jolliffe, I.T. and J. Cadima, *Principal component analysis: a review and recent developments.* Philosophical transactions. Series A, Mathematical, physical, and engineering sciences, 2016. **374**(2065): p. 20150202-20150202.
285. Wold, S., K. Esbensen, and P. Geladi, *Principal component analysis.* Chemometrics and intelligent laboratory systems, 1987. **2**(1-3): p. 37-52.
286. Zhihua, Q., Z. Lan, and J. Huang, *Effective Linear Discriminant Analysis for High Dimensional, Low Sample Size Data.* Lecture Notes in Engineering and Computer Science, 2008. **2**.
287. Cristianini, N. and E. Ricci, *Support Vector Machines*, in *Encyclopedia of Algorithms*, M.-Y. Kao, Editor. 2008, Springer US: Boston, MA. p. 928-932.
288. Cortes, C. and V. Vapnik, *Support-vector networks.* Machine Learning, 1995. **20**(3): p. 273-297.
289. Awad, M. and R. Khanna, *Support Vector Machines for Classification*, in *Efficient Learning Machines: Theories, Concepts, and Applications for Engineers and System Designers*. 2015, Apress: Berkeley, CA. p. 39-66.
290. Trevethan, R., *Sensitivity, Specificity, and Predictive Values: Foundations, Pliabilities, and Pitfalls in Research and Practice.* Front Public Health, 2017. **5**: p. 307.
291. Hobro, A.J., et al., *Deconstructing RNA: optical measurement of composition and structure.* Physical Chemistry Chemical Physics, 2013. **15**(31): p. 13199-13208.
292. Ellis, D.I., et al., *Illuminating disease and enlightening biomedicine: Raman spectroscopy as a diagnostic tool.* Analyst, 2013. **138**(14): p. 3871-3884.
293. Tang, M., et al., *Distinguishing Different Cancerous Human Cells by Raman Spectroscopy Based on Discriminant Analysis Methods.* Applied Sciences, 2017. **7**(9): p. 900.
294. Hobro, A.J., et al., *Raman spectroscopy as a tool for label-free lymphocyte cell line discrimination.* Analyst, 2016. **141**(12): p. 3756-3764.
295. Pyrgiotakis, G., et al., *Cell death discrimination with Raman spectroscopy and support vector machines.* Ann Biomed Eng, 2009. **37**(7): p. 1464-73.
296. Varmuza, K. and P. Filzmoser, *Introduction to Multivariate Statistical Analysis in Chemometrics*. 2009, CRC Press: Boca Raton, FL.

297. Collin, M., N. McGovern, and M. Haniffa, *Human dendritic cell subsets.* Immunology, 2013. **140**(1): p. 22-30.
298. Mbongue, J.C., et al., *The Role of Indoleamine 2, 3-Dioxygenase in Immune Suppression and Autoimmunity.* Vaccines (Basel), 2015. **3**(3): p. 703-29.
299. Shipkova, M. and E. Wieland, *Surface markers of lymphocyte activation and markers of cell proliferation.* Clin Chim Acta, 2012. **413**(17-18): p. 1338-49.
300. Tamoutounour, S., et al., *CD64 distinguishes macrophages from dendritic cells in the gut and reveals the Th1-inducing role of mesenteric lymph node macrophages during colitis.* European Journal of Immunology, 2012. **42**(12): p. 3150-3166.
301. Tarique, A.A., et al., *Phenotypic, functional, and plasticity features of classical and alternatively activated human macrophages.* Am J Respir Cell Mol Biol, 2015. **53**(5): p. 676-88.
302. Castro, F., et al., *Interferon-Gamma at the Crossroads of Tumor Immune Surveillance or Evasion.* Front Immunol, 2018. **9**: p. 847.
303. Wang, X. and Y. Lin, *Tumor necrosis factor and cancer, buddies or foes?* Acta Pharmacol Sin, 2008. **29**(11): p. 1275-88.
304. Hassuneh, M.R., M. Nagarkatti, and P.S. Nagarkatti, *Role of interleukin-10 in the regulation of tumorigenicity of a T cell lymphoma.* Leuk Lymphoma, 2013. **54**(4): p. 827-34.
305. Jiang, T., C. Zhou, and S. Ren, *Role of IL-2 in cancer immunotherapy.* Oncoimmunology, 2016. **5**(6): p. e1163462.
306. Hu, X., et al., *IFN-γ Suppresses IL-10 Production and Synergizes with TLR2 by Regulating GSK3 and CREB/AP-1 Proteins.* Immunity, 2006. **24**(5): p. 563-574.
307. Ivashkiv, L.B., *IFNγ: signalling, epigenetics and roles in immunity, metabolism, disease and cancer immunotherapy.* Nat Rev Immunol, 2018. **18**(9): p. 545-558.
308. Kak, G., M. Raza, and B.K. Tiwari, *Interferon-gamma (IFN-γ): Exploring its implications in infectious diseases.* Biomolecular Concepts, 2018. **9**(1): p. 64.
309. Lees, J.R., *Interferon gamma in autoimmunity: A complicated player on a complex stage.* Cytokine, 2015. **74**(1): p. 18-26.
310. Oh, S.A., et al., *PD-L1 expression by dendritic cells is a key regulator of T-cell immunity in cancer.* Nature Cancer, 2020. **1**(7): p. 681-691.
311. Wu, A., et al., *Glioma cancer stem cells induce immunosuppressive macrophages/microglia.* Neuro Oncol, 2010. **12**(11): p. 1113-25.
312. Azambuja, J.H., et al., *Blockade of CD73 delays glioblastoma growth by modulating the immune environment.* Cancer Immunol Immunother, 2020. **69**(9): p. 1801-1812.
313. Fu, R., et al., *A ZEB1/p53 signaling axis in stromal fibroblasts promotes mammary epithelial tumours.* Nature Communications, 2019. **10**(1): p. 3210.

5. Appendix

5.1 Declaration of authors contribution

Enzymatic activity of CD73 modulates invasion of gliomas via epithelial-mesenchymal transition-like reprogramming

Julia Tsiampali[1], Silke Neumann[2], Beatriz Giesen[3], Katharina Koch[1,4], Donata Maciaczyk[2], Christoph Janiak[3], Daniel Hänggi[1] and Jaroslaw Maciaczyk[5,6]

[1] *Neurosurgery Department, University Hospital Duesseldorf, 40225 Duesseldorf, Germany*

[2] *Department of Pathology, University of Otago, 9016 Dunedin, New Zealand*

[3] *Institute of Inorganic Chemistry and Structural Chemistry, Heinrich Heine University Duesseldorf, 40225 Duesseldorf, Germany*

[4] *IUF - Leibniz Research Institute for Environmental Medicine, 40225 Duesseldorf, Germany*

[5] *Department of Neurosurgery, University Hospital Bonn, 53179 Bonn, Germany*

[6] *Department of Surgical Sciences, University of Otago, 9016 Dunedin, New Zealand*

Corresponding Author

Jaroslaw Maciaczyk (Jaroslaw.Maciaczyk@ukbonn.de)

Submitted to: Immune Checkpoint Inhibitor Therapy Issue, Pharmaceuticals, 23.09.2020
Journal Impact Factor (2018): 4.286

Contribution: 75%. Jaroslaw Maciaczyk, Silke Neumann and Julia Tsiampali designed the experiments. Julia Tsiampali, Katharina Koch and Beatriz Giesen performed the experiments and evaluated the data. Silke Neumann and Donata Maciaczyk assisted in data acquisition. JT, JM and SN wrote the manuscript. All authors commented on the manuscript.

Molecular monitoring of glioblastoma's immunogenicity using a combination of Raman spectroscopy and chemometrics

Chima Robert[1#], Julia Tsiampali[2#], Sara J. Fraser-Miller[1], Silke Neumann[3], Donata Maciaczyk[3], Sarah L. Young[4], Jaroslaw Maciaczyk[5,6#] and Keith C. Gordon[1#]

[1]*Dodd-Walls Centre for Photonics and Quantum Technologies, Department of Chemistry, University of Otago, Dunedin, New Zealand*

[2]*Neurosurgery Department, University Hospital Duesseldorf, 40225 Duesseldorf, Germany*

[3]*Department of Pathology, University of Otago, Dunedin, New Zealand*

[4]*School of Medical Sciences, Faculty of Medicine and Health, The University of Sydney, Sydney, Australia*

[5]*Department of Neurosurgery, University Hospital Bonn, 53179 Bonn, Germany*

[6]*Department of Surgical Sciences, University of Otago, Dunedin, New Zealand*

# equal contribution

Corresponding Authors

Keith C. Gordon (keith.gordon@otago.ac.nz)

Jaroslaw Maciaczyk (Jaroslaw.Maciaczyk@ukbonn.de)

Submitted to: Spectrochimica Acta Part A: Molecular and Biomolecular Spectroscopy, 23.08.2020.
Journal Impact Factor (2018): 2.931

Contribution: 75%. Jaroslaw Maciaczyk, Keith Gordon, Julia Tsiampali, Chima Robert designed the experiments. JT and CR performed the experiments and evaluated the data. Acquisition of Raman spectra was performed by Julia Tsiampali, Chima Robert and Sara Fraser-Miller. Silke Neumann, Sara Miller and Donata Maciaczyk assisted in data acquisition. JT, CR JM and CG wrote the manuscript. All authors commented on the manuscript.

5.2 Acknowledgment

I would like to express my sincere appreciation and gratitude to my supervisor Jarek Maciaczyk for his continuous support, motivation and guidance throughout my time at neurosurgery lab. I am grateful for the time and energy he put into supervising me through this entire process and especially for giving me the opportunity to perform part of the research in Dunedin.

I would like to thank Prof. Steiger and Prof. Hänggi for the chance to perform my PhD thesis at the department of neurosurgery and the Düsseldorf School of Oncology for my scholarship.

In addition, my special gratitude goes to my second supervisor Silke Neumann for the scientific guidance and support, especially while performing experiments in immunology and preparing the manuscripts. My sincere thanks goes also to Chima Robert, Sara Fraser-Miller and Keith Gordon at the University of Otago for our great collaboration and for the chance to learn and perform experiments with Raman spectroscopy in order to develop our project. A special thanks goes to Donata Maciaczyk for all the help and the great time both in Düsseldorf and in Dunedin. This work would not have been possible without them!

Many thanks to all my former and current lab colleagues Conny Uhlmann, Katharina Koch, Suad Yusuf, Philippe Aretz, Ann-Christin Nickel, Michael Hewera and Faye Petropoulou for the great atmosphere working together every day and the nice time supporting each other and making lots of jokes. A special thanks to Conny for the special support ☺

Finally, I would like to thank my family and friends for their never-ending love and support to achieve my goals. Σας ευχαριστώ πολύ για όλα! And my partner, Frederic Laprell, danke dass du immer für mich da bist.

Thank you all!

5.3 Abbreviations

ADO adenosine

ADP adenosine diphosphate

AIC 5-aminoimidazole-4-carboxamide

AMP 5′-adenosine monophosphate

APCP adenosine 5'-(α,β-methylene)diphosphate

APCs antigen presenting cells

AR adenosine receptor

ATP adenosine 5′-triphosphate

BBB blood-brain barrier

BTSCs brain tumour stem-cells

CARS Stokes Raman scattering

CAR-T-cell chimeric antigen receptor T-cell

cDCs classical dendritic cells

CDKN2A cyclin-dependent kinase inhibitor 2A

cDNA complementary desoxyribonucleic acid

CNS central nervous system

CRS Confocal Raman spectroscopy

CSCs cancer stem cells

CT computerized tomography

CTLA-4 receptor cytotoxic T-lymphocyte-associated protein

DAMPs damage-associated molecular patterns

DCs dendritic cells

DMEM Dulbecco's Modified Eagle's Medium

DMSO Dimethyl sulfoxide

ECs endothelial cells

EDTA ethylenediaminetetraacetic acid

EGFR epidermal growth factor receptor

EMT epithelial-to-mesenchymal transition

F12 Ham's F-12 Nutrient Mixture

FACS fluorescence-activated cell sorting

FBS fetal bovine serum

FSC-H/FSC-A forward scatter height and area

GABRA1 γ-aminobutyric acid type A receptor alpha-1 subunit

GBM glioblastoma

GPI glycosyl phosphatidylinositol

GSCs glioblastoma stem-cells

HDLA-DR human leukocyte antigen-DR isotype

HEK293T human embryonic kidney cells 293T

HIF hypoxia-inducible factor

HPLC high performance liquid chromatography

ICIs immune checkpoint inhibitors

IDH isocitrate dehydrogenase 1

IFNs interferons

IMP inosine monophosphate

LDA linear discriminant analysis

LPS lipopolysaccharide

MDSC myeloid-derived suppressor cells

MGMT O6-methylguanine-DNA methyltransferase

MHC major histocompatibility complex

MMP-2 matrix metalloproteinase-2

MRI magnetic resonance imaging

mRNA messenger ribunucleic acid

MTT thiazolyl blue tetrazolium bromide

MyD88 myeloid differentiation factor 88

MΦs macrophages

NaCl sodium chloride

NBT nitro blue tetrazolium chloride

NEFL neurofilament light

NLRP1 NACHT leucine-rich repeat protein 1

NLRs nod-like receptors

NT5E ecto-5'-nucleotidase

PAMPs pathogen-associated molecular patterns

PBS phosphate buffered saline

PCA principal component analysis

pDCs plasmacytoid DCs

PDGFRA platelet derived growth factor receptor alpha

PD-L1 programmed death-1 ligand and receptor

PEG Polyethylene glycol

PET positron emission tomography

PFS progression-free survival

PRRs pattern recognition receptors

PTEN phosphatase and tensin homolog

PTX pentoxifylline

RIPA radioimmunoprecipitation assay buffer

RPMI Roswell Park Memorial Institute

RS Raman spectroscopy

RT qPCR real time quantitative polymerase chain

SAH S-adenosyl homocysteine

shRNA short hairpin ribonucleic acid

SLC12A5 solute carrier family 12 member5

SNAIL snail family transcriptional repressor 1

SRS stimulated Raman scattering

SSC-H/SSC-A side scatter height and area

STAT3 signal transducer and activator of transcription 3

SVM support vector machine

SYT1 synaptotagmin-1

TAMs tumour-associated MΦs

TBST Tris-buffered saline with Tween20

TF1 neurofibromatosis Type 1

Tfh follicular helper T-cells

TGF-β transforming growth factor-β

Th helper T-cells

TLRs toll-like receptors

TME tumour microenvironment

TMZ temozolomide

TP53 tumour protein 53

Treg regulatory T-cells

TRIF toll/interferon response factor

TTFields tumour-treating fields

VEGF vascular endothelial growth factor

WT wild type

ZEB1 zinc finger e-box binding homeobox 1